UTILIZING MECHANISM-BASED PHARMACOKINETIC AND PHARMACODYNAMIC MODELS TO UNDERSTAND AND OVERCOME ANTIBIOTIC RESISTANCE

By

BENJAMIN MON WU

A DISSERTATION PRESENTED TO THE GRADUATE SCHOOL
OF THE UNIVERSITY OF FLORIDA IN PARTIAL FULFILLMENT
OF THE REQUIREMENTS FOR THE DEGREE OF
DOCTOR OF PHILOSOPHY

UNIVERSITY OF FLORIDA

2010

To my family and friends

ACKNOWLEDGMENTS

I would like to express my deepest appreciation to Professor Hartmut Derendorf for accepting me into his laboratory and his support and guidance throughout my graduate career. Professor Derendorf has given me a chance to express my potential as a graduate student which is one of the most important aspects of graduate school for me. His positive encouragement teaching style alone with decades of research experience helped me excel in my learning at the University of Florida. His research topics and vision for pharmaceutical research helped me orient my career focus.

I would also like to thank my supervisory committee members, Dr. Kenneth Rand, Dr. Charles Peloquin, and Dr. Tony Palmieri, for their support and discussions. They have generously provided support and collaboration. Despite their busy schedules, they always had their doors open for me and were willing to help me.

The day to day function of our program would not have been possible without the administrative staff of the Department of Pharmaceutics, especially Mrs. Patricia Khan, Mrs. Robin Keirnan-Sanchez, and Mrs. Sarah Scheckner .

Finally, I would like to thank all the graduate students and post-docs in the Department of Pharmaceutics for their friendship and scientific discussions.

TABLE OF CONTENTS

page

LIST OF TABLES

LIST OF FIGURES

Abstract of Dissertation Presented to the Graduate School
of the University of Florida in Partial Fulfillment of the
Requirements for the Degree of Doctor of Philosophy

UTILIZING MECHANISM-BASED PHARMACOKINETIC/PHARMACODYNAMIC MODELING TO UNDERSTAND AND OVERCOME ANTIBIOTIC RESISTANCE

By

Benjamin Mon Wu

December 2010

Chair: Hartmut Derendorf
Major: Pharmaceutical Sciences

The emergence of antimicrobial resistance poses a critical challenge to public health in the 21st century. The current practice to treat microbes relies on single minimum inhibitory concentration (MIC) data to define the optimal clinical dose. This over simplified approach disregards the adaptive nature of microbial response, which leads to emergence of drug resistant microbes over time. In order to overcome antimicrobial resistance, the time course relationships of drug and microbial behavior must first be delineated. In this dissertation, the development of novel mechanism-based pharmacokinetic/ pharmacodynamic (PKPD) models was described using new molecular and genetic findings. The resulting mathematical models provide insight into the complex PKPD relationships necessary to optimize antimicrobial treatments.

The two hypotheses tested were dormant and compensatory mutation hypotheses. A thorough model selection process identified the compensatory mutation model to the best model to describe the PKPD relationship. Dynamic kill-curve experiments were conducted for ciprofloxacin against a clinical isolate of *Pseudomonas aeruginosa* to further test the PKPD models. Aminoglycosides, but not most β-lactams, appeared to retain the bactericidal activities against the emerged resistant strains

following ciprofloxacin treatment. The induction of resistance was not limited to ciprofloxacin as shown with aztreonam.

The PD model was applied to a clinical study of ceftobiprole in healthy volunteers. The free fraction of drugs collected in several tissues in this study using microdialysis techniques were used to develop a novel population PBPK model. Target attainments using relevant tissue data were predicted for various dosing schemes. Model also implied one-hour intravenous infusion can produce similar PD effects as two-hour IV infusion. Scenarios of resistance were simulated by combining the PD model with the population PBPK model to explore dosing strategy in case of resistance development.

In summary, mechanism-based PKPD model was developed to test hypotheses, design laboratory experiments, and predict clinical drug resistance scenarios. Dynamic kill-curve revealed that aminoglycoside favorably suppress the resistant subpopulations emerged from ciprofloxacin treatment.

CHAPTER 1
INTRODUCTION TO ANTIMICROBIAL RESISTANCE

History of Antimicrobial Treatments and Resistance Classifications

The inadvertent discovery of the bactericidal activities of *penicillium notatum* against *staphylococcus aureus* by Alexander Fleming in 1928 has lead to a major revolution in the advancement of medical sciences.[1] In the following 80 years, major pharmaceutical companies have developed and deployed numerous new antimicrobial agents armed with different mode of actions to fight against infectious diseases.[2] At first, it appears that medical achievements had successfully conquered the debilitating effects of microbial infections. However, clinical observations quickly disclaimed the short-lived victory against the microbes. Through a range of highly adaptive mechanisms, microbes have consistently developed resistance to all the classes of antimicrobial drugs that they encountered.[3-12] Clinical observance of antimicrobial resistance occurs within a short period of time after the deployment of antimicrobial agents for public use; within three years for penicillin and within a year for methicillin (Table 1-1).[2]

The documented cases of untreatable infections due to multi-drug resistant characteristics are on the rise.[13] As observed for fluoroquinolone from 1990 to 2000, the trend of increased usage has been associated with increasingly resistant strains of *Pseudomonas aeruginosa*. This alarming correlation is exacerbated by a decreasing trend of new antimicrobials approved over the same period (Figure 1-1). The data suggests that the current antimicrobial dosing approach disregards the adaptive nature of microbes, thereby fostering resistance development. It would be imperative to further understand the drug-microbe interactions in order to explore new dosing strategies that

consider the emergence of resistance. To achieve this goal, our main approach uses mechanistic pharmacokinetic/pharmacodynamic (PK/PD) models to aid the understanding of antimicrobial resistance and explore new treatment strategies. Details of this approach will be discussed thoroughly in subsequent chapters.

Mechanisms of Antimicrobial Resistance

The common mode of antimicrobial actions can be divided into three major categories: (1) targeting microbial structural cell wall, (2) nucleic acid metabolism, and (3) protein synthesis.[14-17] The antimicrobial drugs target specific microbial traits, which spare the toxic effects on mammalian cells, and make them a relatively safe class of drugs to use. However, upon exposure to environmental challenges such as lack of nutrients or toxic agents, microbes have the ability to adapt by changing their intrinsic regulation or altering their genetic code to favor their survival. The four main adaptive mechanisms include: (1) reducing drug entry by increasing efflux pump activities, (2) changing membrane permeability, (3) directly altering the chemistry of the drugs or (4) promoting mutation at the drug binding sites.[4, 10, 11, 18-20] Besides the reactive defense mechanisms, microbes also have the intrinsic ability to deter drug actions. For example, macrolides are generally ineffective against gram-negative bacteria because their membrane morphology prevents drug entry.[21]

Once the antimicrobial resistance characteristics are developed, the genetic information can be transferred by genetic transfer to daughter cells or by mobile DNA transfer. Sharing genetic sequence is a common characteristic within a microbial community and it can be done using plasmid conjugation, bacteriophages (bacterial viruses) or transformation from nearby DNA.[14-17, 22] In summary, when challenged with antimicrobials, any given microbial population may use one or more of these strategies

to ensure the survivability of the microbial population as a whole. The mechanisms of resistance for each major class of antimicrobials are as follows:

Resistance to Cell Wall Inhibitors

The most apparent target against microbes is the structural cell wall, which is absent in the mammalian cells. The microbial cell wall forms by utilizing special sugar residues called peptidoglycan. These residues consist of a series of subunits of N-acetylglucosamine (NAG), and N-acetylmuramic acid (NAM) that make up the polymers capable of cross-linking to form the protective cell wall structure. Microbes are classified into gram-negative or gram-positive, depending on the thickness of the polymer structures that make up the peptidoglycan. Gram-negative bacteria with thin peptidoglycan and outer membrane will not retain crystal violet dye, while gram-positive bacteria with thick peptidoglycan will stain purple.[23]

The cell wall synthesis consists of several steps, and different antimicrobial agents have been developed to disrupt each step. First, precursors of peptidoglycan are synthesized in the cytoplasm. These precursors are then bound to lipids to facilitate the transportation across the cytoplasmic membrane. Once the residues reach the cell wall compartment, insertion and cross-peptide linkage are required to complete the cell wall formation.[23]

Antimicrobial drugs have been designed to target each of these different steps of cell wall maturation. There are currently limited numbers of antimicrobial drugs that target the precursor form of peptidoglycan. Among these, bacitracin and cycloserine prevent the precursors from reaching the cell wall compartment.[24] The majority of drugs, however, target the insertion and transpeptidation of peptidoglycan in the cell wall compartment. These drugs are mainly from the β-lactams and glycopeptides

classes. Once they cross the membrane via porin protein channels, these drugs inhibit cell wall synthesis by covalently binding to enzymes involved in the insertion and transpeptidation of peptidoglycan. A poorly assembled bacterial cell wall is readily lysed under normal osmotic pressure.[25]

Over time, microbes have developed resistance to β-lactams in several ways. The microbes can reduce the binding affinity of β-lactams to specific enzymes. They can also mutate a new form of peptidoglycan, or acquire a completely new form of peptidoglycan that β-lactams do not recognize. In addition, microbes can synthesize new enzymes that can hydrolyze the β-lactam rings. At the membrane level, up regulation of the efflux pump as well as alternation of the membrane protein that affects the ability of β-lactams to enter the cell through the porin channels, have also been observed.[14, 26]

Glycopeptides, such as vancomycin, disrupt the cell wall formation by binding directly to the D-Ala-D-Ala dipeptide terminus of peptidoglycan, thereby preventing the addition of new subunits.[27] Resistance to glycopeptides antimicrobials usually occurs through alteration of the terminus peptide; replacing D-Ala-D-Ala with D-Ala-D-Lac. For vancomycin, as many as six resistance subtypes of *enterococci* have been described.[28] Genes codes for this alteration are easily transferrable to other microbes through the plasmid pathway.[29] This poorly assembled cell wall will also lyse under normal osmotic pressure.

Resistance to Protein Inhibitors

Protein inhibitors include targeting microbial 30s and 50s ribosomal subunits and elongation factors.[30] Although the exact mechanisms of many protein inhibitors are unclear, microbial ribosomal subunits are different than the mammalian counterpart.

Aminoglycosides and tetracyclines are the classes of bactericidal and bacteriostatic antimicrobials that target 30s ribosomal subunits.[31, 32] Bacteriostatic antimicrobials targeting 50s ribosomal subunits include clindamycin, chloramphenicol and macrolides. Fusidic acid is a bacteriostatic agent that targets elongation factors to inhibit protein synthesis.

As seen with streptomycin resistance strains, microbes can alter the structure of the 30s ribosomal subunits to evade the cytotoxic effects streptomycin. The microbes can also develop resistance by producing enzymes that modify antimicrobial drugs through phosphorylation, adenylation or acetylation.[33-35] In addition, enhancement of efflux pump activities has shown to prevent the entry of chloramphenicol[36-38] and tetracyclines.[15] Linezolid, the only approved oxazolidinone that binds microbial ribosomal subunits has also been observed to have lowered activity due to the mutation of 23s rRNA subunits.[39]

Resistance to Nucleic Acid Inhibitors

Antimicrobial agents targeting DNA and RNA biosynthesis have shown to be effective against gram-negative and gram-positive bacteria. Generally, these nucleic acid inhibitors are divided into two classes – indirectly inhibiting DNA replication by targeting enzymes involving nucleotide formation or directly targeting nucleic acid.

The first category is sulfonamides, which are competitive inhibitors of dihydropteroate synthetase (DHPS), a critical enzyme involved in folate synthesis.[40] In addition, certain sulfonamides are also structural analogues for p-aminobenzoic acid. The maturation of purine and pyrimidine bases requires p-aminobenzoic acid as the substrate to donate carbon groups. Through competitive inhibition, sulfonamides disrupt further nucleotide production by interrupting the function of p-aminobenzoic acid.

Microbes have evaded such assault by producing alternative p-aminobenzoic acid that has little affinity for sulfonamides, thereby rendering the drug ineffective.[41-43]

The other classes of nucleic acid inhibitors include quinolones and rifamycins. Quinolones function by inhibiting DNA topoisomerases such as *gyrA, gyrB, parC and parE*[44]. Rifamycins inhibit nucleic acid synthesis through disabling RNA polymerase such as *rpoB.*[45] RNA polymerases and DNA topoisomerases are critical enzymes for transcription and translation. Similar to sulfonamide resistance mechanisms, microbes can mutate the RNA polymerases and DNA topoisomerases so that the antimicrobial agents can no longer bind or bind with reduced affinities for the new enzymes. Several clinical resistant strains of *Escherichia coli* have mutated gyrA that render fluoroquinolone ineffective.[44, 45]

Extensive studies have been conducted to study fluoroquinolone resistance. Besides mutating the drug binding sites, microbes can enhance efflux pump activities and alter the membrane permeability to prevent fluoroquinolone entry.[46] The resulting upregulation of efflux pump activities may explain the multidrug resistant characteristics.[47] Fluoroquinolone generally enter bacterial cells through porin channels, although some have shown to directly cross the lipid bilayers. Rearrangement of membrane proteins that alters the porin channels may also minimize fluoroquinolone entry.[48]

Recent Hypotheses for Antimicrobial Resistance: Dormant and Compensatory Mutation Hypotheses

In recent years, advancement in genetic and molecular techniques has provided additional insights into the adaptive nature of antimicrobial resistance. Even though various mechanisms of resistance have been studied for decades, the process required

to become a clinically relevant resistant strain was unknown. Two relatively new hypotheses have been emphasized within the last few years, which attempt to delineate the mechanisms involved in selection for resistant strains. The first is the Dormant hypothesis. In the example of tuberculosis infection, a biphasic killing was observed (Figure 1-2), characterized by a fast killing phase followed by a prolonged killing phase. It was hypothesized that the susceptible population can enter a dormant phase to escape drug killing; since antimicrobials only target dividing cells, this dormant population can evade antimicrobial killing.[49-53] During the dormant stage, cell replications are disabled through the production of intrinsic toxins that can shut down DNA and protein synthesis without inducing apoptosis. It is only when the microbes sense the clearance of drugs that they would upregulate an antitoxin to re-initiate the cell division.

The other hypothesis is the Compensatory Mutation hypothesis, which further explains the formation of genetic mutation discussed previously. The Compensatory mutation hypothesis states that there is fitness cost associated with genetic mutation. Studies have shown that bacterial fitness (defined by the bacterial growth rate without drugs relative to susceptible strain) reduces when resistance traits are acquired. In order for a particular resistant strain to be clinically relevant, it would need to restore the fitness while retraining the drug-resistance characteristics.[54-57] This sequential mutation process may account for the genetic mutations observed across different classes of antimicrobial agents. Details of these two hypotheses and how they contribute to the development of mechanism-based PKPD models are discussed in Chapter 3.

Specific Aims

Mathematical modeling of pharmacological responses provides: (1) quantitative approaches to determine optimal dosing strategies, (2) mechanism hypotheses testing incorporating system biology, (3) obtain information on the determinants of variability, and (4) provide a meaningful comparison of therapeutic products. This proposal seeks to utilize mechanism-based pharmacokinetics/pharmacodynamics (PK/PD) modeling and simulation to understand and overcome antimicrobial resistance.

While these independent molecular and genetic approaches are being used to study resistance, there is a lack of a discipline working on establishing the correlation between these hypotheses and the optimal clinical doses that also target resistant population. The mechanism-based modeling approach can provide quantitative insight that is urgently needed to link the newly proposed microbial behavior and dose optimization. In a time of few new antimicrobial candidates, the goal is to re-evalulate the dosing strategies of existing antimicrobials to better target both susceptible and resistant populations. The specific hypothesis behind this proposed research is that the current recommended antimicrobial doses do not consider the amplification of the resistant population. The insight gained from the final PK/PD model will be used to explore new dosing strategies that also target the resistant population. The specific aims of this dissertation are as follow:

Specific Aim 1

Develop mechanism-based PK/PD models mimicking the current hypotheses of antimicrobial resistance using extensive *in vitro* kill-curves of *E. coli 204* following ciprofloxacin treatment.

Specific Aim 2

Examine each model using criteria such as bootstrap statistics, visual predictive check, interpolation of sub-compartmental profiles and simulation of multiple dose scenarios.

Specific Aim 3

Utilize modeling and simulation techniques to design laboratory experiments that test the PKPD models and explore new sequential combination therapy.

Specific Aim 4

Develop a population physiologically based pharmacokinetic (PBPK) model for ceftobiprole in different tissues using microdialysis probes in healthy volunteers. Prediction of clinical target attainment with different dosing regimen will be assessed using Monte Carlo simulations. Bridging of the PBPK model with the mechanism-based PD model will be used to explore drug effects in relevant tissues in case of antimicrobial resistance development.

Table 1-1. Deployment of antimicrobial drugs and the subsequent clinical observation of drug resistance.[2]

Antibiotic	Year Deployed	Resistance Observed
Sulfonamides	1930s	1940s
Penicillin	1943	1946
Streptomycin	1943	1959
Chloramphenicol	1947	1959
Etracycline	1948	1953
Erythromycin	1952	1988
Vancomycin	1956	1988
Methicillin	1960	1961
Ampicillin	1961	1973
Cephalosporins	1960s	1960s

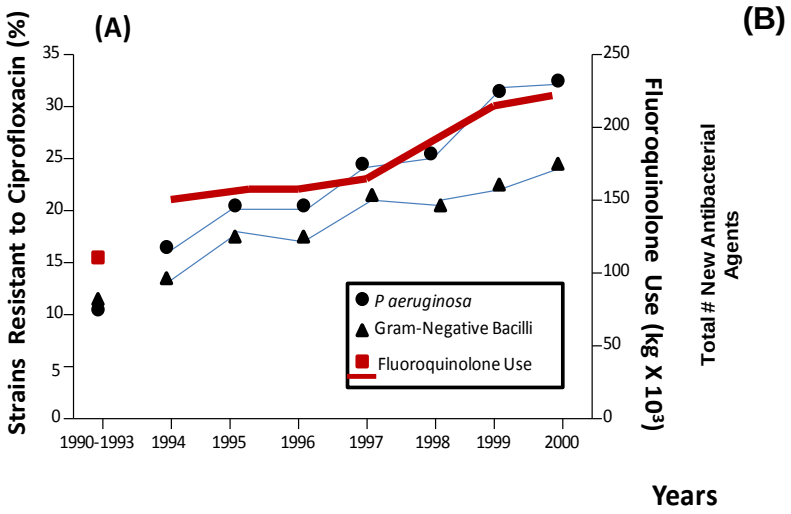

Figure 1-1. The parallel relationship of increasing *P. aeruginosa* isolates resistant to ciprofloxacin with increasing fluoroquinolone usage (A).[58] Over the same period, a trend of decreasing in the total number of newly approved antimicrobial agents was recorded (B).[59]

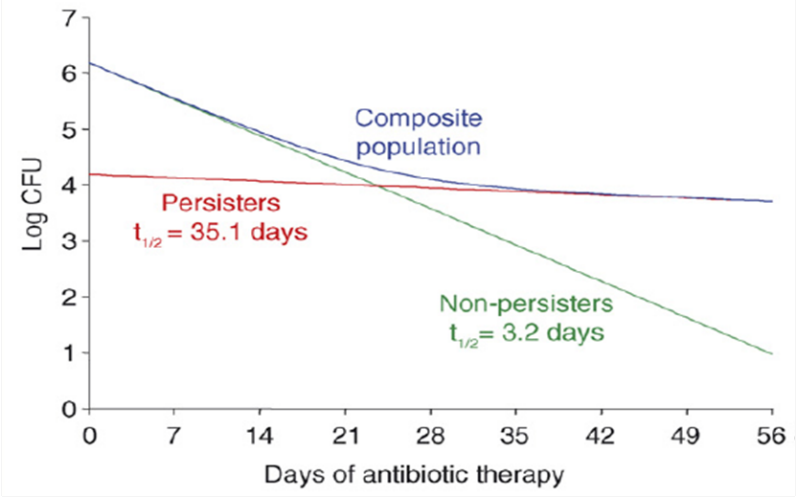

Figure 1-2. Baphasic killing of *mycobacterium tuberculosis* in murine infection model over the course of isoniazide treatment.[60]

CHAPTER 2
PRINCIPLES OF PKPD MODELING FOR ANTIMICROBIAL THERAPEUTICS

Application of PKPD Modeling in Antimicrobial Research

Mathematical modeling has been used in numerous therapeutic areas to gain insight into explaining complex dynamics, understand sources of variability, predict and optimize dosing regimen, quantitative approach to decision making, test new hypotheses, and answer specific questions. The success of overcoming a microbial infection depends on the understanding of the complex relationship between antimicrobial agent, host, and the microbes, making this field a suitable area for applied mathematical models. Pharmacokinetics and pharmacodynamics (PK/PD) modeling has been recognized to play major roles in the development of new antimicrobial agents, aid physicians in making decisions during the course of patient therapy, and understand complex dynamics, such as the emergence of antimicrobial resistant strains. The consequences of antimicrobial treatment failure can be life threatening, as well as create a more aggressive strain of microbes, resulting in a greater danger to public health. In this chapter, we will discuss how mathematical modeling can aid the field of antimicrobial therapy.

There has been great progress in PKPD modeling of antimicrobials over the years. For decades, the traditional PKPD model for dose selection in antimicrobial drug development was based on the relationship of drug kinetics to minimum inhibition concentration (PK-MIC), from which the maximum efficacy can be classified into either time-dependent or exposure (AUC or Cmax) dependent.[61] Screening across different classes of antimicrobials, one can determine which dosing approach would have the highest probability of success for a given mechanism of action, based on the PK-MIC

relationship. For example, most of the β-lactams are time-dependent, and keeping sufficient levels above MIC over the dosing period would be the main determinant of a successful outcome (Table 4-1). Although this approach provides physicians a readily available tool to make clinical decisions, it does not consider the complexity of drug-microbe relationship. In reality, the interactions of microbes with host immune and therapeutic agents are not a static process. The high replication rate of microbes often creates a heterogeneous population in the presence of environmental challenges, such as starvation and antimicrobials. Different concentrations of drugs may result in fostering the development of different subpopulations of microbes. The MIC model, often assessed at only a single time point, would not be able to capture the complex dynamic of microbial response. Because of an increase in the emergence of resistant strains shortly after the deployment of new antimicrobial agents, which has resulted in an increase in clinical failures, recent efforts have been focused on examining the entire time course of both drug and microbial response. *In vitro* models simulating the time course of clinical PK profiles, and the resulting microbial kill-curves, have now been widely used to better assess the PKPD relationships. Mathematical models can then be used to capture the PKPD relationship to aid the selection of optimal dose levels, route of administration, dosing frequency, and differentiation of antimicrobial candidate for a specific infection during drug development.

The following sections will discuss the important considerations of PKPD modeling, from both the MIC-based approach and the kill-curve approach.

Experimental Approaches for Studying Antimicrobial PKPD

MIC-Based PKPD Models

A physician, facing the challenge of selecting the best antimicrobial agent to treat a patient recently admitted into the emergency room, would appreciate the simple, fast, MIC-based approach. Laboratory tests screening the microbial isolate across a wide range of antimicrobials can readily identify which antimicrobial agent within a classification would be the most effective against the infection. This individualized treatment is further verified by numerous clinical observations of how to best dose the patient for that particular antimicrobial agent, whether it be time-dependent or concentration-dependent, as previously discussed. Table 4-1 shows the pattern of *in vitro* killing and the subsequent PKPD index used to aid dosing strategies.[62] When *in vitro* killing was observed to be time-dependent, keeping the drug plasma concentration above the MIC for a certain fraction of dosing interval may achieve the best killing activity.[63-66] When concentration-dependent killing is observed, it may be either the ratio of peak concentration to MIC (Cmax/MIC), or total exposure to MIC (AUC/MIC), that is critical to achieve target attainment[63, 66-68].

Although both drug potency and dosing strategy can obtained from such PKPD models, we now know that the over-simplified dosing scheme results in treatment failure, and foster the emergence of resistant populations. This concern is contributed to by inadequate information regarding both PK and PD parameters. The PK profiles obtained from these analyses are usually total plasma concentration, ignoring the protein binding and tissue distribution effects in the subjects. It is well accepted that only the free fraction of drugs is capable of exerting pharmacological effects. Upon entering the blood stream, drugs can readily bind to proteins such as albumin, α-, β-, or

γ-globulins, α1-acid glycoprotein, lipoproteins, and/or erythrocytes.[69-71] The binding process may be either linear or nonlinear. Hence, characterization of a range of drug concentration in relation to protein binding should be assessed. Most importantly, it is primarily the free fraction that crosses the membrane to infected tissues such as adipose tissue or, for skin infectious microbes, skeletal muscle. Using micro dialysis techniques to determine the profile of the free fraction of drug at the site of infection would be the most ideal method. Figure 4.1 shows the profiles of Ceftobiprole concentrations in different tissues.[72] Depending on which tissue profile is used, a different dosing regimen may result from the analysis. Hence, a PKPD relationship based on total plasma concentrations alone may not always represent the free fraction needed at the site of action for the PK-MIC relationship.

From a perspective of a PD profile, the single point MIC is highly empirical. The MIC value for a particular antimicrobial agent varies between laboratories because it is highly dependent on the dilution factors used, laboratory condition, and the interpretation of what constitutes no growth by the laboratory personnel. The rate of bactericidal or bacteriostatic effect with changing drug concentration is also unknown from such simplified analysis. As one can imagine, the same MIC value may result from different time course killing patterns, even though clinical outcomes may vary. Even without the dynamic kill-curve information, the inadequate MIC interpretations are sometimes revealed through post antimicrobial effects or suboptimal effects.[73]

One additional pitfall of the MIC approach for PKPD modeling is that only static drug concentrations are used. Using only static drug concentrations does not accurately reflect *in vivo* pharmacology, because it does not represent the PK profile of

orally administered drugs. As a result, the PKPD relationship cannot be thoroughly understood by using only the empirical value of the MIC approach.

Kill-Curve Based PKPD Models

The other popular modeling approach is to assess the PKPD of antimicrobial agents using *in vitro* kill-curves. This provides valuable time course evaluation of bacterial population dynamic in response to drugs. A mechanistic PKPD model can then be built to describe the relationship. Parameters such as bacterial growth rate, natural death rate, and the emergence of resistant strains within a population, can be estimated. In these *in vitro* experiments, the antimicrobial concentrations can be static[74-76] or dynamic[77-79], depending on the purpose of the study. The static kill-curve provides a quick view of the drug effects on specific strains of bacteria. However, even by capturing the dynamic microbial response, the static PK provides limited information. In order to mimic a clinically relevant scenario, the dynamic kill-curve should have drug concentration-time profiles resemble that of the free fraction of drugs in the site of infection in the relevant population.

Although the dynamic kill-curve has primarily been done using *in vitro* systems, similar approaches can be used for *in vivo* studies. The mouse thigh infection model has been widely used as the dynamic kill-curve evaluation.[80, 81] Although the variability of the PD data often increases with animal models compared to *in vitro* models, the incorporation of the immune system and the different nutrients available may provide additional valuable insight into the PKPD relationship.

Models of Antimicrobial Pharmacokinetic/Pharmacodynamic

Having established that the time kill-curve is a superior method for pharmacodynamic profiling of antimicrobial therapies compared to the arbitrary, single-point MIC method, this section will discuss the use of mathematical modeling in characterizing these time kill-curves.

Mathematical modeling of drug-response relationship provides a quantitative understanding of the complex dynamic relationships between drugs and microbial responses. This important tool benefits physicians by providing the ability to make pertinent predictions to specific questions regarding the safest and most effective dosing regimen. In the field of antimicrobial therapy, the mathematical modeling contains two major components. The first component is PK, which refers to the clinically relevant free fraction of drug kinetic at the effective site of action, and second, PD, which refers to the total bacterial cell count over a time period. Because the PD parameter is the bacterial count, it is impossible to conduct initial clinical trials in healthy volunteers to study the PKPD relationships. The PD is therefore often performed *in vitro;* using pertinent drug kinetics obtained from clinical studies to challenge bacteria in question, thereby allow a control study of the PKPD relationship. However, when interpreting the results, one must keep in mind that in vitro settings lack the affect that the immune system and various nutrients would have on the PD profile. In this section, we will discuss the important considerations in modeling antimicrobial drugs.

Modeling Constant Kill-Curve

An example of kill-curve profiles for bacteria exposed to constant drug concentrations over a period of time can be seen in Figure 4.3, showing the kill-curve profile of cefexime against *H. influenza.*[82] Modeling of this PKPD relationship can either

be described by a linear or nonlinear relationship. The idea is to capture the different growth rate between controls versus different levels of antimicrobial concentrations. If one wishes to assess the PKPD profile using a linear relationship, a minimum of three different drug levels should be used to assess the linearity relationship. When a linear relationship is assumed, the growth rate in the present of antimicrobial (kapp) can be described in equation 1:

$$kapp = ko - k1C \quad (2\text{-}1)$$

where ko is the growth rate of bacteria without drug treatment, k1 is a first-order inhibitory rate constant, and C is the drug concentration. If such a model is not sufficient to capture the data, a nonlinear, or saturable, process is assumed, requiring the use of equation 2:

$$kapp = ko - \frac{Ka*C}{1+Kb*C} \quad (2\text{-}2)$$

where ka is an equilibrium constant between the medium and the receptor sites at steady state, and kb is the affinity constant of drug to the receptor. Again, this simplified *in vitro* kill-curve approach does not reflect the dynamic profiles of drug concentrations. The following section shows how using a kill-curve system resembling an *in vivo setting* incorporates the mechanistic importance of such a complex relationship.

Modeling Dynamic Kill-curve

In order to build a relevant PK-PD model, the behavior of bacterial cell growth and degradation must first be described. In a most simplistic term, the natural self-replication and death of bacteria can be described using equation 2-3:

$$\frac{dN}{dt} = ks * N - kd * N \quad (2\text{-}3)$$

where N is the bacterial population with the initial count of N(0), k_s is the first order rate constant for bacterial synthesis, and k_d is the first order rate constant for bacterial death. This common structure to describe bacterial growth is also used to describe viruses and cancer cell population behavior. This basic model assumes bacteria are a homogenous population with the same growth and death rate constants, which we now know may not reflect the emergence of antimicrobial resistant strains.

Capacity limited growth.

In an *in vitro* setting where the kill-curves are produced, nutrient and space availability limits do not allow the bacteria to grow indefinitely. In order to describe this capacity limited growth in equation 4, we often see an additional term added to equation 1 known as the logistic growth function:

$$\frac{dN}{dt} = ks * N * (1 - \frac{N}{Nmax}) - kd * N \quad (2\text{-}4)$$

where N_{max} is the maximum number of bacteria growth. In this equation, as N approaches N_{max}, the growth term slows down and eventually reaches a steady state condition. The assumption of this growth model is that the maximum capacity is reached in a linear fashion. Depending on the experimental condition, it is sometimes preferable to use a nonlinear growth to describe the capacity limited growth. In this case, the first order synthesis rate is replaced with the new term in equation 2-5:

$$\frac{dN}{dt} = \frac{Vmax,g}{(N50+N)} * N - kd * N \quad (2\text{-}5)$$

where $V_{max,g}$ is the maximum growth rate and N_{50} is the number of bacteria at half of the maximum growth rate. In most situations, equation 2-3 or 2-4 is sufficient to describe the *in vitro* kill-curve behavior.

Drug effects

Antimicrobial drug actions are divided into two major categories; drug concentration-dependent killings or time-dependent killings. The concentration-dependent killing antimicrobials include aminoglycosides, quinolones, and metronidazole. Antimicrobials that exhibit time-dependent killing are mostly β-lactams, macrolides, oxazolidinones, and tetracyclines. Knowing these characteristics often can aid in the development of PKPD model. An antimicrobial drug with time-dependent killing, identified by the traditional PKPD indices of T>MIC, can often be best described by inhibition of k_s. Conversely, an antimicrobial drug with concentration-dependent killing, identified by AUC/MIC or C_{max}/MIC, can be best described by stimulation of k_d. As described by Czock and Keller 2007, a minimal change in rate of killing is often observed as drug concentration increase for time-dependent killing drugs. In contrast, the microbial kill rate increases substantially with increases in concentration for concentration-dependent killing. Antimicrobial drugs can reduce the overall bacterial population by inhibiting k_s, which limits growth, or by stimulating k_d , which enhances killing. A linear drug effect can be described by simply multiplying the free drug concentration (fC_p) by either k_s*N or k_d*N, and integrate the relationship over time. However, as is often the case, the drug effect is a nonlinear, saturable process. An example of direct drug effect on bacterial killing can be described by replacing the k_d with a modified Michaelis-Menten term ($Imax*fC_p/(IC_{50}+ fC_p)$), where Imax is the maximum drug effect and IC_{50} is the concentration at which half of the maximal drug effect is observed. As described previously,[83] MIC value can be related to this function by first integrating the equation:

$$\int_{No}^{Nt} \frac{1}{N} * dN = \int_0^t \left(ks - \frac{Imax*fCp}{IC50+fCp}\right) * dt \quad (2\text{-}6)$$

where t is the experimental incubation time for measuring MIC, Nt is the number of bacteria count at time t, and No is the initial inoculation count. Solving this equation, the MIC relationship can then be described as:

$$MIC = \left(\frac{d}{Imax-d}\right) * IC50 \quad (2\text{-}7)$$

where d is the ks-(lnNt-lnNo)/t. Although not as often done, the free drug fraction in these functions can be replaced with dose or AUC, yielding equation 2-8:

$$Effect = \frac{Emax*D}{ED50-D} \text{ or } \frac{Emax*AUC}{ED50-AUC} \quad (2\text{-}8)$$

This method is generally less informative than integrating concentration-time course, because it reflects only the single parameter used. If modeling of both the ks and k_d is desired, drug effects targeting k_s or k_d can also be described using equations 2-9 and 2-10:

$$\frac{dN}{dt} = ks * \left(1 - \frac{Imax*fCp}{IC50+fCp}\right) * N - kd * N \quad (2\text{-}9)$$

$$\frac{dN}{dt} = ks * N - kd * \left(1 + \frac{Smax*fCp}{SC50+fCp}\right) * N \quad (2\text{-}10)$$

where I_{max} and S_{max} represent maximum inhibitory or stimulatory rate and IC_{50} and SC_{50} represent the concentration of drug at half of the maximal effect.

In these saturable drug effects, the fitting of pharmacodynamic curves may be improved by incorporating an exponential term (hill factor (H), often denoted as gama (γ)) to fC_p and either IC_{50} or SC_{50} of the drug effect term. The addition of hill factor is strictly for the purpose of improving the fit of the curve, because, by itself, it has no biological meaning.

Application and Limitation of Antimicrobial PKPD Models

When these PKPD models are used to describe kill-curves of different drugs against specific bacteria, a quantitative comparison of drug effects can be evaluated. This is often first done using a static kill-curve model, in which the potency of the drugs (IC_{50} or SC_{50}), as well as the overall effects of the drugs (I_{max} or S_{max}), can be compared for the test article versus a standard treatment with equivalent MIC-fold exposure. For example, to compare a new antimicrobial to gentamicin for the treatment of pseudomonas aeruginosa infection, the initial free drug concentrations at 0.1, 0.5, 1, 2, 4, 8, 16X MIC can be compared. Assuming toxicity is not an issue for either, the PKPD relationship can be quantitatively compared through the modeling approach.

Likewise, an antimicrobial agent can be used to test across different species of Gram-negative and Gram-positive microorganisms to identify the relative effectiveness in each. Based on the mechanisms of action, it could be assumed that an agent that works on targeting the cell wall will not work as well in Gram-negative bacteria. However, the PKPD model can allow a quantitative distinction of a particular drug action across different species of bacteria.

There are several limitations that should be considered when interpreting PKPD models for antimicrobials. Different bacteria may have different growth behavior, especially when considering the presence of resistant populations. Such heterogeneous populations can result in different drug effects. As we observed with increased clinical usage of antimicrobial agents, the emergence of resistance strains has also increased. This additional phenomenon sometimes requires a more complex PD structure. Various attempts to use PKPD models to capture the complex relationship have been published.

Another limitation is the differences between *in vitro* and *in vivo* observations. In addition to lack of an immune system in the *in vitro* setting, the amount of nutrients available for bacterial growth is different. If the kill rate is dependent on bacteria growth rate, the comparison of drugs in an *in vitro* setting may be confounded. Likewise, if the emergence of resistance is fostered only through the artificial setting lacking the immunological component, the interpretation of the *in vitro* results should also be cautioned. In the following sections, we will discuss in detail the applications of PKPD models for antimicrobial agents, and the current modeling strategies to deal with resistant populations which may better explain certain kill-curve behaviors.

Modeling Complex Behavior

Using kill-curve data with only an empirical sigmoidal function may result in an over-simplified model. The complexity of the model greatly depends on the richness of the PD data, as well as the actual microbial behavior. Over the years, clinical observations have consistently shown that microbes have the ability to evolve and adapt in order to overcome drug challenges. This warrants using multiple populations to describe the kill-curve behavior. A dosing regimen that targets both susceptible and resistant populations may be a key to prevent the emergence of antimicrobial resistance. Complex modeling, such as those considering the multiple populations, have been demonstrated by Campion[84] and Jumbe[81] and others. A mechanistic model incorporating cell cycle is to evaluate inoculation effects is published by Bulitta.[85] In dept discussions of these topics will be covered in later chapters.

Clinical Applications

As briefly discussed above, to obtain data for modeling a dynamic PKPD relationship, relevant free fraction of drugs concentrations in human would first need to

be obtained. This information can then be used to conduct *in vitro* PD experiments for PKPD modeling. Many studies of antimicrobial agents have been studied using this approach.[71, 82, 86-88] The PK profiles of unbound antimicrobial concentrations were first studied in humans, then were mimicked in *in vitro* settings using continuous dilutions and replacement of fresh medium technique. The effects on the bacteria of interest can then be studied using both constant and dynamic kill-curves. For these kill-curves, generally a minimum of 3 dose levels, in addition to a growth control for each drug, are needed to obtain reliable PD parameter estimates. The frequency of the sampling time is also an important consideration to accurately obtain the curvatures of the PD profiles. In 24 hour experiment kill-curve experiments, it is frequently observed that a large segment of the kill-curve is void of samples due to logistic reasons.

Whenever possible, the PK profiles should be obtained at the site of actions. For cefpodoxime and cefixime, the free fraction of drugs in tissue was modeled using equations 11:

$$Ct = \frac{TD*fu*F*D*ka}{(ka-ke)Vd} * \left(e^{-ke(t-tlag)} - e^{-ka(t-tlag)}\right)(1 - e^{-kat}) \quad (2\text{-}11)$$

where TD is the tissue partition coefficient ($AUC_{tissue}/AUC_{plasma}$), fu is the unbound fraction in plasma, F is the bioavailability of the drug, D is the dose, k_e is the elimination rate constant, k_a is the absorption rate constant, V_d is the volume of distribution, and t_{lag} is the absorption lag time for the tissue. Once the PK is modeled in such a way, which takes into consideration free fraction and tissue concentrations, the profile can be simulated *in vitro* to evaluate PD behavior.

For a clinical trial, when the data are modeled with a population approach, the variants from the model can be used to predict therapeutic outcome using the Monte

Carlo statistical approach[89-91]. Typically 1,000 to 10,000 subjects can be simulated to display the population distribution using model estimated parameters and population variance. For a time-dependent drug where *in vivo* data show that the time of drug concentration above MIC for at least 50% of dosing interval is required to achieve efficacy can now be assess in a more meaningful population approach. If the objective of the study is to have 95% of the population achieved this T>MIC of 50% dosing interval, Monte Carlo simulation will allow such assessment at different dose levels or dosing intervals.

Conclusions

The best PKPD modeling is rooted in both the data collected and the understanding of the biological process. The results of model prediction cannot be stronger than the premises. Hence, thoughtful studies to obtain the most clinically relevant data are first needed. For studying the PKPD of antimicrobials, knowing the dynamic profiles of free fraction of drug concentrations at the site of action is important. The in vitro kill-curves appear to be superior to the PK-MIC approach. The dynamic kill-curve model allows the field of antimicrobial modeling to progress from empirical to mechanistic, thus providing a greater insight into the drug-response relationship as compared to the limited MIC approach. The examples above have shown the versatility of PKPD model in aiding different areas of antimicrobial research. Whenever possible, the model should make biological sense and concur with laboratory data in order to confirm the model's validity. As we improve and explore molecular and genetic techniques to evaluate a specific question about drug-microbial response, the PKPD models can be refined and modified to incorporate the new findings. Hence, PKPD

modeling for antimicrobials will remain an important tool and will integrate well with other functional areas.

Table 2-1. MIC-based PKPD index.[62]

Antimicrobial agent	Bactericidal pattern of in vitro activity	PK-PD measure(s)
Aminoglycosides	Concentration dependent	AUC_{0-24}:MIC, C_{max}:MIC
β-Lactams		
Penicillins	Time dependent	T>MIC
Cephalosporins	Time dependent	T>MIC
Carbapenems	Time dependent	T>MIC
Monobactams	Time dependent	T>MIC
Clindamycin	Time dependent	AUC_{0-24}:MIC
Glycopeptides/lipopeptides		
Daptomycin	Concentration dependent	AUC_{0-24}:MIC, C_{max}:MIC
Oritavancin	Concentration dependent	T>MIC, C_{max}:MIC
Vancomycin	Time dependent	AUC_{0-24}:MIC
Macrolides and clindamycin		
Azithromycin	Time dependent	AUC_{0-24}:MIC
Clarithromycin	Time dependent	AUC_{0-24}:MIC
Teilithromycin	Concentration dependent	AUC_{0-24}:MIC
Metronidazole	Concentration dependent	AUC_{0-24}:MIC, C_{max}:MIC
Oxazolidinones		
Linezolid	Time dependent	AUC_{0-24}:MIC
Quinolones	Concentration dependent	AUC_{0-24}:MIC, C_{max}:MIC
Tetracyclines		
Doxycycline	Time dependent	AUC_{0-24}:MIC
Tigecycline	Time dependent	AUC_{0-24}:MIC

NOTE. AUC_{0-24}:MIC, the ratio of the area under the concentration-time curve at 24 h to the MIC; C_{max}:MIC, the ratio of the maximal drug concentration to the MIC; T>MIC, duration of time a drug concentration remains above the MIC.

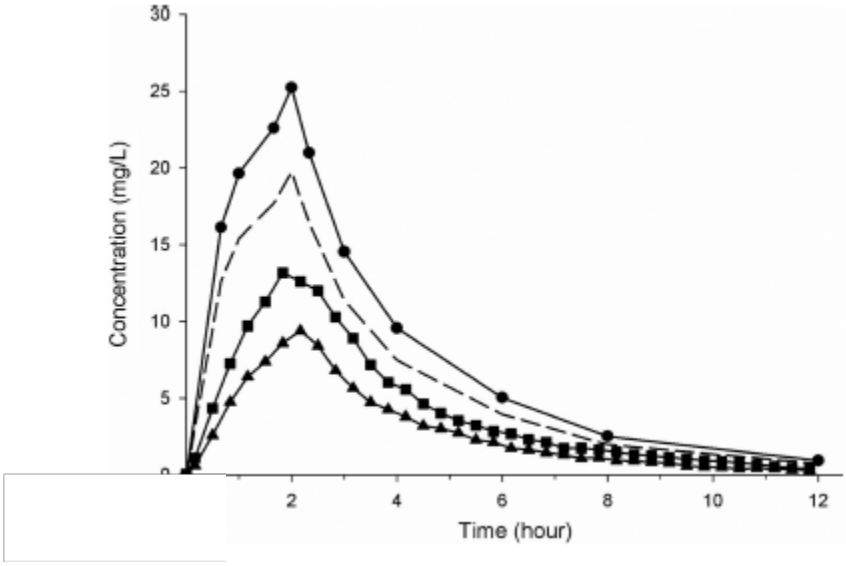

Figure 2-1. Mean (n=12) of total plasma ceftobiprole concentrations (circles), calculated unbound plasma ceftobiprole concentrations (dashline) and unbound ceftobiprole concentrations sampled from skeletal muscle (squares) and subcutaneous adipose tissue (triangles) using microdialysis probes in healthy volunteers.[72]

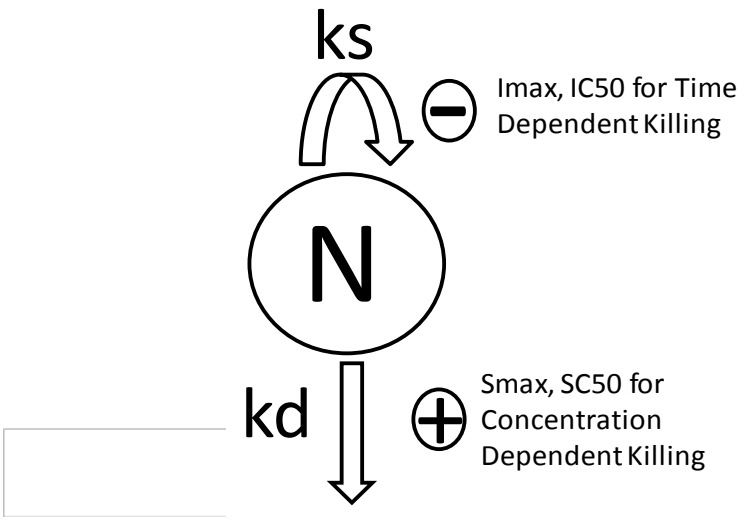

Figure 2-2. Basic structure of PKPD model for antimicrobial agents inhibiting the first order growth rate constants (k_s) or stimulating the first order degradation rate constants (k_d) of microorganisms.

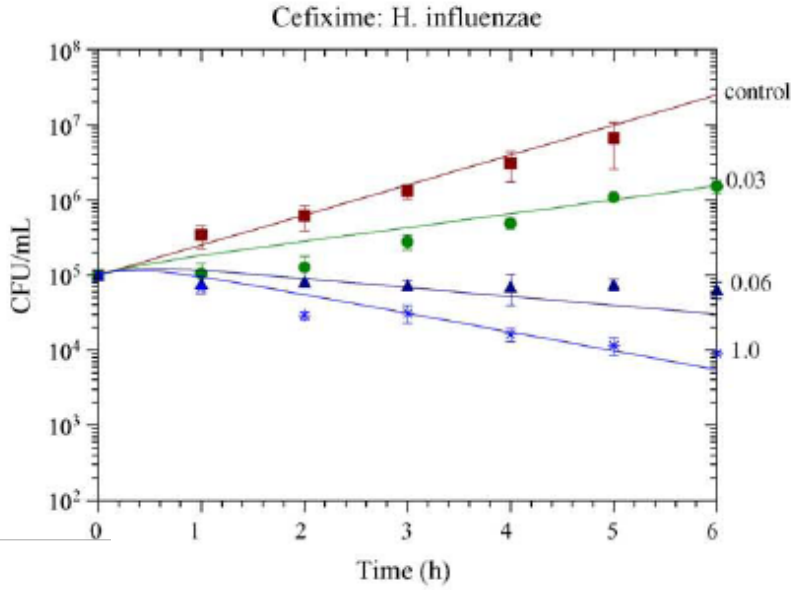

Figure 2-3. Example of *in vitro* static kill-curve.[92]

CHAPTER 3
NOVEL MECHANISM-BASED PHARMACOKINETIC/PHARMACODYNAMIC MODELS FOR EMERGED ANTIBIOTIC RESISTANCE

Theory

The major factor contributing to clinical failure in treating antimicrobial infection is that the current dosing strategy disregards the adaptability of microbes. Treatments usually impose inadequate pressure against the resistant population, which results in the promotion of a more virulent strain. The main determinants of resistance emergence over the course of antimicrobial therapy are not well understood. Over the years, the evaluation of microbial susceptibility has improved from point estimates (MICs) to complete time-course approach (dynamic kill-curves). However, recent advancements in molecular and genetic research have provided additional insights in explaining the microbial kill-curve relationships. With the aid of these new findings, new PKPD models can be developed to bridge basic science research to optimal dosing strategies.

Currently there are two major competing hypotheses in the literature claiming to explain the process by which microbes develops resistance over the course of antimicrobial therapy. The first hypothesis is the phenotypic variant hypothesis, often referred to as the dormant or persistent population hypothesis, in the literature. This hypothesis emphasizes the importance of an endogenous toxin-antitoxin regulation system that can favorably shut down cell divisions temporarily in the presence of antimicrobial drugs.[50, 51, 53, 93, 94] The idea is depicted in Figure 3-1. For the susceptible population, upon binding of an antimicrobial agent, the biosynthesis processes of microbes are disrupted, leading to microbial cell death. The persister population, however, has up-regulated endogenous toxins that can shut down cell replication

without inducing apoptosis. Since antimicrobial agents bind only dividing cells, the dormant variant escapes the cytotoxic effects of drugs. Alternatively, the ineffectiveness of drug actions may be explained by a tolerance mechanism. In this case, the drug is able to bind the dormant population but exert no effect on it due to the tolerance induced from endogenous toxins.[50, 51, 53]

A list of endogenous toxins responsible for this mechanism is summarized in Table 3-1. Toxins such as RMF, UmuDC, SulA, RelE and HipA can inhibit translation, replication, or septation when produced. Their toxic effects can be reverse upon the upregulation of antitoxins. Within the last several years, many of these inhibitory proteins have been extensively studied.[53, 60, 94, 95]

For example, by using an inducible promoter (pBAD) for the RelE gene, the ability of *E. coli* to shut down cell divisions within 30 minutes of activating RelE expression (Figure 3-2). Three hours after inducing the RelE gene, the microbes were exposed to lethal doses of cefotaxime, ofloxacin, or tobramycin that target DNA gyrase, cell wall synthesis, or protein synthesis respectively. A significantly higher survival rate in the RelE induced microbes was observed when compared to that of the non-RelE induced strain. It was only when the antitoxins expression for RelE (RelEB) was induced that microbial cell divisions could be resumed[51]. This molecular evidence supports the presence of persister cells that may explain the biphasic kill-curves, incomplete killings, and latent infections.[60]

The second hypothesis is the Compensatory Mutation hypothesis. The importance of “mutation and fitness” concept was proposed to describe the sequential process in developing antimicrobial resistance. Mutation events result in developing

resistance characteristics that are often accompanied with a fitness cost (Figure 3-3). Fitness is defined as the microbial grow rate *in vitro* compared to that of the susceptible strain. A higher fitness cost results in a lower growth rate of the microbes. In order for a mutated resistant strain to be clinically relevant, additional mutations (compensatory mutations) are needed to restore the fitness. This new population would have similar growth characteristics as that of the susceptible strain but with increased MIC due to their drug-resistance characteristics. This hypothesis emphasizes that genetic changes rather than phenotypic changes are responsible for the emergence of antimicrobial resistance.[54-57, 96-102]

Using mechanism-based models is one of the approaches used to test these hypotheses. Although in reality, both dormant and compensatory mutation resistant mechanisms could occur simultaneously, the predominant mechanisms may be favorably described by a hypothesis-specific model. While these independent molecular and genetic approaches are being used to study emergence of resistance, there is a lack of discipline establishing the correlation between these hypotheses to optimize antimicrobial doses. Because the development of resistant strains was not considered in the dosing, drug exposure may result in fostering the selection of resistant populations. A PKPD model can reveal important insights into the recently proposed antimicrobial resistance behavior with clinically relevant drug kinetics. Anticipating that few new antimicrobials will be available in the next few years, this approach is important to maximize the efficacious potential of current drugs. Refinement of dosing strategies specifically targeting the drug-induced resistant population may lead to successful treatment. In this study, we developed novel mechanism-based PKPD models to

distinguish between competing hypotheses for resistance emergence during drug treatment, using extensive *in vitro* dynamic kill-curve data of ciprofloxacin and *E. coli*.

Model Descriptions

In order to develop complex mechanism-based PKPD models, a rich dataset with a wide range of dosing groups with frequent sampling in order to capture the time-course of drug-microbe dynamics were needed. In this section, the dynamic kill-curves used for the model development were obtained from a previous publication[103] using GetData Graph Digitizer 2.24. Details of the *in vitro* dynamic kill-curve experiments were described by previously.[103] Briefly, a two-flask system with a constant pump was used. Flask 1 contains the Ca^{2+} and Mg^{2+} Mueller-Hinton broth. Flask 2 contains bacteria with or without antimicrobials in the Mueller-Hinton broth. The bacteria were initially incubated for 18 hours to reach an exponential growth rate, prior to diluting them to 10^6 CFU/mL for the experiment. Ciprofloxacin was then added to Flask 2 to test the drug effects. *E coli* 204 were subjected to ciprofloxacin treatment at 0.0, 0.1, 0.2, 0.5, 1.0, 2.0, 4.0, 8.0, 16.0, 32.0 and 125 times the MIC. A group without ciprofloxacin was used as the control. An automated pump was used to remove and replace the Flask 2 medium with fresh broth at a rate of 7 mL/hr. By maintaining a constant volume of 40 mL in the flask, the clinical half-life of 4 hours was simulated. Series of samples were taken throughout a 48 hour period for colony counting. The kill-curve for each dose group ended when the microbial growth reached approximately 10^{11} CFU/mL.

Four models were used to describe the emergence of antimicrobial resistance. The first model is a commonly used model from the literature.[104] The other three are novel PKPD models describing the Dormant hypothesis, Compensatory Mutation hypothesis, and a combination of these two hypotheses. Graphical descriptions of the

models are shown in Figure 3-4 to Figure 3-7. Estimates of model parameters for each model were computed using data from all 11 dose groups fitted simultaneously using Adapt II software.[105] A proportional error model with maximum likelihood was used for all models.

Model 1 assumes the total microbial population consists of susceptible (S) and resistant (R_{fit}) populations. Each subpopulation exhibits its own first order growth rate constant (k_s or k_{ss}), and degradation rate constant (k_d or k_{dd}). The susceptible population is converted to the resistant population with a rate constant of k_c. Ciprofloxacin stimulates the killings of microbes by enhancing the kill rate constants (k_d and k_{dd}). The stimulatory drug function is described by S_{max}*C/(SC_{50}+C) or denoted as H(C(t)) in Figure 3-4. This model does not include the current in-depth knowledge of microbial resistance behaviors as discussed above. The equations describing Model 1 are:

$$\frac{dS}{dt} = ks * s - kd * (1 + Emax, s) * S - kc * S \qquad \text{IC} = 10^6 \text{ CFU/mL} \quad (3\text{-}1)$$

$$\frac{dRfit}{dt} = kss * Rfit - kdd * (1 + Emax, Rfit) * Rfit + kc * S \qquad \text{IC} = 0 \text{ CFU/mL} \quad (3\text{-}2)$$

Where, $Emax, S = \left(\frac{Smax, S*C}{SC50, S+C}\right)$ and $Emax, Rfit = \left(\frac{Smax, Rfit*C}{SC50, Rfit+C}\right)$.

Model 2 describes the Dormant hypothsis. The only observable population is the susceptible subpopulation where the cell division occurs. In the absence of drug treatments, transfer between the susceptible (S) and dormant (D) compartments occurs randomly, with a rate constant of k_e. The addition of ciprofloxacin promotes the conversion of S to D compartment as well as stimulates the killing of the S population. Since antibiotics target only dividing cells, no drug action is imposed on the D population. It is assumed that once the antimicrobial pressure is reduced to a certain

level, D population can initiate cell division through upregulation of antitoxins and be converted back to the S population. The equations describing Model 2 are:

$$\frac{dS}{dt} = ks * s - kd * (1 + Emax, s) * S - ke * (1 + Emax, D) * S + ke * D \qquad \text{IC} = 10^6 \text{ CFU/mL} \quad (3\text{-}3)$$

$$\frac{dD}{dt} = ke * (1 + Emax, D) * S - ke * D \qquad \text{IC} = 0 \text{ CFU/mL} \quad (3\text{-}4)$$

where $Emax, S = \left(\frac{Smax,S*C}{SC50,S+C}\right)$ and $Emax, D = \left(\frac{Smax,D*C}{SC50,D+C}\right)$.

Model 3 describes the Compensatory Mutation hypothesis, where R is a mutated population with no significant growth rate. The subsequent compensatory mutation restores the microbial fitness while retraining the resistance characteristics. As a result, the R population is converted to an important contributing population (R_{fit}). The Compensatory Mutation hypothesis assumes the fitness is fully restored. Hence, the R_{fit} population exhibits the same growth rate and degradation rate constants as those of the S population (same k_s and k_d). The mutation process is described by an arbitrary k_c rate constant. Although the S and R_{fit} population have the same fitness, their responses to drug actions are different. The equations describing Model 3 are:

$$\frac{dS}{dt} = ks * s - kd * (1 + Emax, s) * S - kc * S \qquad \text{IC} = 10^6 \text{ CFU/mL} \quad (3\text{-}5)$$

$$\frac{dR}{dt} = kc * s - kc * R \qquad \text{IC} = 0 \text{ CFU/mL} \quad (3\text{-}6)$$

$$\frac{dRfit}{dt} = ks * Rfit + kc * R - kd * (1 + Emax, Rfit) * Rfit \qquad \text{IC} = 0 \text{ CFU/mL} \quad (3\text{-}7)$$

where $Emax, S = \left(\frac{Smax,S*C}{SC50,S+C}\right)$ and $Emax, Rfit = \left(\frac{Smax,Rfit*C}{SC50,Rfit+C}\right)$.

Model 4 is a combination of both dormant and compensatory mutation hypotheses. Modifications to Models 2 and 3 were done to evaluate the multiple mechanisms simultaneously while adhering to parsimony principle. The equations describing Model 4 are:

$$\frac{dS}{dt} = ks * S + ke * D - kd * (1 + Emax, s) * S - ke * (1 - Emax, D) - kc * S \qquad \text{IC} = 10^6 \text{ CFU/mL} \quad (3\text{-}8)$$

$$\frac{dD}{dt} = ke * (1 + Emax, D) * S - ke * D \qquad \text{IC} = 0 \text{ CFU/mL} \quad (3\text{-}9)$$

$$\frac{dRfit}{dt} = ks * Rfit + kc * S - kd * Rfit \qquad \text{IC} = 0 \text{ CFU/mL} \quad (3\text{-}10)$$

where $Emax, S = \left(\frac{Smax, S*C}{SC50, S+C}\right)$ and $Emax, D = \left(\frac{Smax, D*C}{SC50, D+C}\right)$.

Results

The ADAPT II estimates for Models 1-4 are tabulated in Tables 3-2 to 3-5. The tables show the final model output values with %CV associated for the parameter estimates. The observed versus the model predicted profiles are shown in Figures 3-8 to 3-11. The symbols are the observed microbial count and the lines are the model predictions.

Model 1 has the most parameters (9 total). The degradation rate constants for susceptible and resistant populations were slightly lower than the respective growth rate constants. The higher synthesis rate explains the exponential microbial growth observed in the control group. The conversion rate between the two populations was relatively small, showing k_c of 0.119/hr. The overall drug effects of the susceptible population was approximately three-fold higher than that of the resistant population ($S_{MAX,S}$ = 0.1 versus $S_{MAX,R}$ = 0.0342). The potency of the drug was slightly better in the resistant population compared to the susceptible population (0.192 versus 0.249 µg/mL). The variance of the proportional error was reasonable at 0.198. The model parameter estimates from ADAPT II revealed a good %CV (below 50%). Visual inspection of the observed versus predicted results implies adequate fitting of the control and most dose groups.

Model 2 also describes the observed data reasonably well (Figure 3-9). Model 2 has 7 parameters with a growth and degradation rate constants similar to that of Model 1, enabling capture of the exponential growth of the control (k_d slightly lower than k_s). In the absence of drug concentrations, minimal distribution between susceptible and dormant compartment occurs (ke = 0.108/hr). This conversion is greatly enhanced in a drug concentration dependent manner, showing $S_{max,D}$ of 3.61 and $SC_{50,D}$ of 0.263 µg/mL. The variance of the proportional error was 0.212. The %CVs of the parameter estimates were slightly higher in Model 2 than in Model 1. However, all results were within a reasonable range.

Model 3 also consists of only 7 parameters. It appears that Model 3 has the best model fitting, as shown in Figure 3-10. The same k_s and k_d for the susceptible and resistant populations reveals a similar growth rate for the resistant population and the control group. The overall drug effects of the susceptible population were more than five-fold higher than that of the resistant population with restored fitness ($S_{MAX,S}$ =1.02 versus $S_{MAX,D}$ = 0.193). The %CV estimates of the third model were the lowest out of all four models, showing estimates mainly below 20%. The proportional error was comparable to previous models.

Model 4 consists of components of Models 2 and 3. Model 4 has the poorest fitting (Figure 3-11), despite having 9 parameters. In addition, the k_s value was 6 fold higher than the k_d values. The %CVs for the parameters were not estimated by ADAPT II. It appears that the PKPD model cannot describe the dual mechanisms using the richest kill-curve data set.

Model Selections and Discussions

Several model selection criteria were implemented to select the best model. These evaluations include (1) available literature data to support the hypotheses (2) objective function and Akaike criteria of the model output (3) visual inspections of observed versus predicted plots (4) biological meaning of the model output (5) subcompartmental profile analysis (6) simulation of multiple dose scenarios (7) model stability via bootstrap statistics and (8) model predictability via simulation of visual predictive checks. The last three assessments are discussed in Chapter 4 as part of model validation steps.

For criterion one, a wealth of data have been published in the literature to support both dormant and compensatory mutation hypotheses. The molecular and genetic approaches to study antimicrobial resistance are important and insightful. However, studying an isolated pathway sometimes limits the ability to assess its contribution to the overall clinical observations. The kill-curve data offers meaningful drug-microbial dynamic relationships. For selecting a PKPD model, it was assumed that both hypotheses are relevant contributors to the mechanisms of antimicrobial resistance based on the literature support.

For each model to reach its final stage, objective functions and Akaike criteria were compared. However, they were not used to evaluate model fitting across models due to the fundamental differences of these models. For each model, the parsimonious modeling principle was applied while capturing the highlight of the hypothesis.

The subcompartmental profiles for Dormant and Compensatory mutation models are shown in Figures 3-12 to 3-13. The drug concentrations are shown in dash lines and microbial populations are shown in solid lines. In Figure 3-12, the dynamic profiles

of susceptible and dormant populations are shown as dark and light green lines over the 2 day treatment period. The simulation shows that as ciprofloxacin is administered, the susceptible population decreases in a dose dependent manner, while the dormant population increases. Although the model predicted an increase in dormant population after drug exposure, the proportion of dormant population appear to be larger than what was observed in the laboratory settings. According to the literature, dormant population exceeding the susceptible population, as indicated in the simulation, had not previously been observed.

The Compensatory Mutation hypothesis on the other hand suggests that following the exposure to ciprofloxacin, the susceptible population is reduced to a minimal level. The resistant population without fitness increased slightly in the presence of the drug but due to the lack of fitness, the population becomes insignificant. However, the resistant population, with fitness restored appears to dominate the overall population in the regrowth phase. This model suggests that re-exposure to the same drug would have reduced effects because of the dominant R_{fit} population. Simulations of multiple doses are presented in Chapter 4.

In conclusion, while most of the criteria cannot concretely distinguish among models, the sub-compartmental profile simulation revealed that the Dormant Model requires a huge portion of the susceptible population be converted to the dormant population in order to describe the dynamic kill-curves. The Compensatory Mutation hypothesis provided the best explanation of the drug-microbe dynamic. It suggests that a resistant population emerged after undergoing multiple mutations. Experimental designs, along with the results of multiple doses used to confirm the prediction of loss

drug effects from the Compensatory Mutation Model are shown in chapters 5 and 6. The MIC dynamic will also be assessed over time to confirm the validity of selecting the Compensatory Mutation Model.

Table 3-1. Endogenous toxin-antitoxin (TA) molecules identified to disable and reinstate microbial replications in gram-negative and gram-positive bacteria.

TA Family (locus)	Toxin	Antitoxin	Target	Phyletic Distribution
ccd	Ccdb	CcdA	DNA replication	Gram-neg
relBE	RelE	RelB	translation	Gram-neg/pos, Archaea
parDE	ParE	ParD	DNA replication	Gram-neg/pos
higBA	HigB	HigA	unknown	Gram-neg/pos
mazEF	MazF/Pemk	MazE/Peml	Translation	Gram-neg/pos, Archaea
phd/doc	doc	Phd	Translation	Gram-neg/pos, Archaea
vapBC/vag	VapC	VapB	unknown	Gram-pos

Table 3-2. Model 1 parameter estimates (literature PKPD model).

Parameter	Model Estimates	%CV
k_s (/hr)	5.92	14.4
k_d (/hr)	5.79	15.0
k_c (/hr)	0.119	14.8
$S_{MAX, S}$	0.100	20.0
$SC_{50, S}$ (µg/mL)	0.249	20.7
k_{ss} (/hr)	3.06	0.873
k_{dd} (/hr)	2.93	1.15
$S_{MAX, R}$	0.0342	15.8
$SC_{50, R}$ (µg/mL)	0.192	44.7
Proportional Error	0.198	6.71

K_s and k_{ss} = growth rate constants of susceptible and resistant populations; k_d and k_{dd} = degradation rate constants of susceptible and resistant populations; k_c = conversion rate constant from susceptible to resistant population; $S_{max,S}$ and $S_{max,R}$ = overall drug effects on stimulating the k_d or k_{dd}; $SC_{50,S}$ and $SC_{50,R}$ = potency of drug on stimulating the k_d or k_{dd}.

Table 3-3. Model 2 parameter estimates (Dormant PKPD model).

Parameter	Model Estimates	%CV
k_s (/hr)	0.921	66.1
k_d (/hr)	0.709	88.5
k_e (/hr)	0.108	15.5
$S_{MAX, S}$	0.188	42.4
$SC_{50, S}$ (µg/mL)	0.0588	56.4
$S_{MAX, D}$	3.610	21.1
$SC_{50, D}$ (µg/mL)	0.263	31.4
Proportional Error	0.212	6.78

K_s = growth rate constant of susceptible population; k_d = degradation rate constant of susceptible population; k_e = conversion rate constant between susceptible and dormant populations; $S_{max,S}$ and $S_{max,D}$ = overall drug effects on stimulating the k_d or conversion of susceptible to dormant population; $SC_{50,S}$ and $SC_{50,D}$ = potency of drug on stimulating the k_d or conversion of susceptible to dormant population.

Table 3-4. Model 3 parameter estimates (Compensatory Mutation PKPD model).

Parameter	Model Estimates	%CV
k_s (/hr)	0.813	14.5
k_d (/hr)	0.660	18.3
k_c (/hr)	0.172	10.7
$S_{MAX, S}$	1.020	18.9
$SC_{50, S}$ (µg/mL)	0.358	14.6
$S_{MAX, R}$	0.193	21.3
$SC_{50, R}$ (µg/mL)	0.113	31.6
Proportional Error	0.220	0.210

K_s = growth rate constants of susceptible or resistant with fitness populations; k_d = degradation rate constants of susceptible or resistant with fitness populations; k_c = conversion rate constant from susceptible to resistant population; $S_{max,S}$ and $S_{max,R}$ = overall drug effects on stimulating the k_d of susceptible and resistant with fitness populations; $SC_{50,S}$ and $SC_{50,R}$ = potency of drug on stimulating the k_d of susceptible and resistant with fitness populations.

Table 3-5. Model 4 parameter estimates (dormant and compensatory mutation combined PKPD model).

Parameter	Model Estimates	%CV
k_s (/hr)	0.142	NA
k_d (/hr)	0.0235	NA
k_e (/hr)	0.088	NA
k_c (/hr)	0.00326	NA
$S_{MAX, S}$	28.60	NA
$SC_{50, S}$ (µg/mL)	0.374	NA
$S_{MAX, D}$	4.230	NA
$SC_{50, D}$ (µg/mL)	0.2680	NA
Proportional Error	0.231	NA

K_s = growth rate constant of susceptible population; k_d = degradation rate constant of susceptible population; k_e = conversion rate constant from susceptible to dormant population; k_c = conversion rate constant from susceptible to resistant population; $S_{max,S}$ and $S_{max,D}$ = overall drug effects on stimulating the k_d and conversion of susceptible to dormant population; $SC_{50,S}$ and $SC_{50,D}$ = potency of drug on stimulating the k_d of susceptible and conversion of susceptible to dormant population; NA = not available from ADAPT II output.

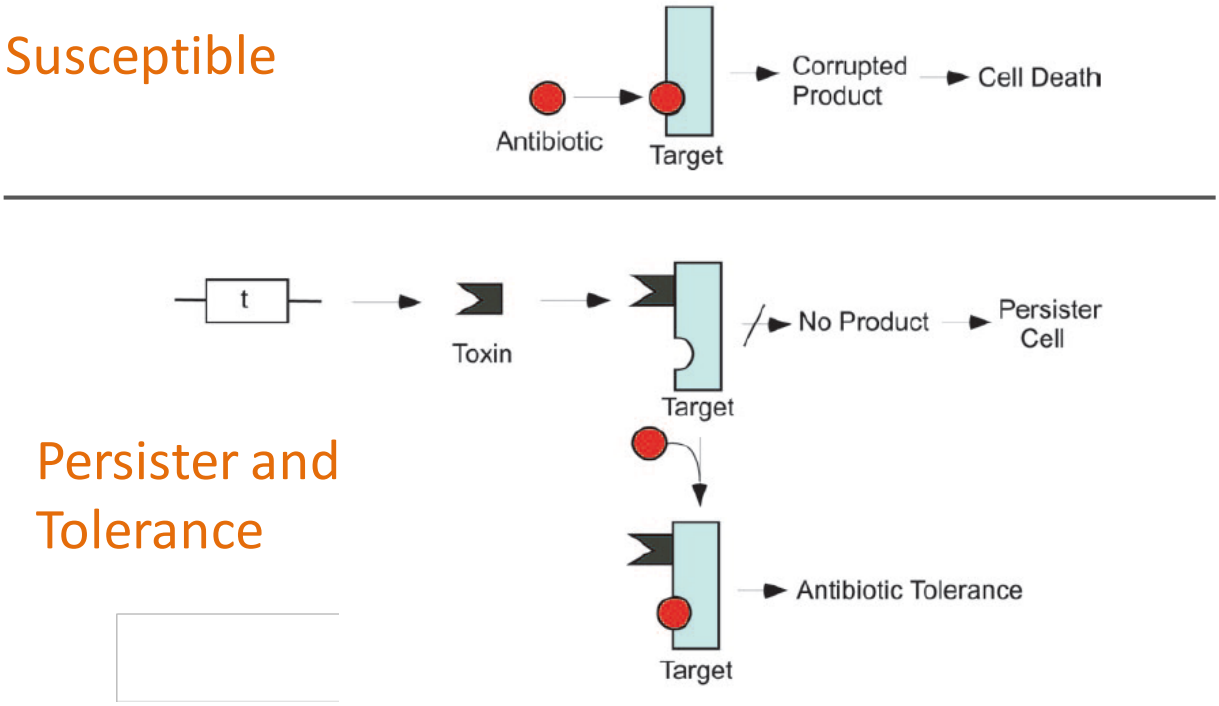

Figure 3-1. Dormant hypothesis: Upregulation of endogenous toxins in the presence of antimicrobial agents prevents drug binding or tolerance to evade drug killings.[51]

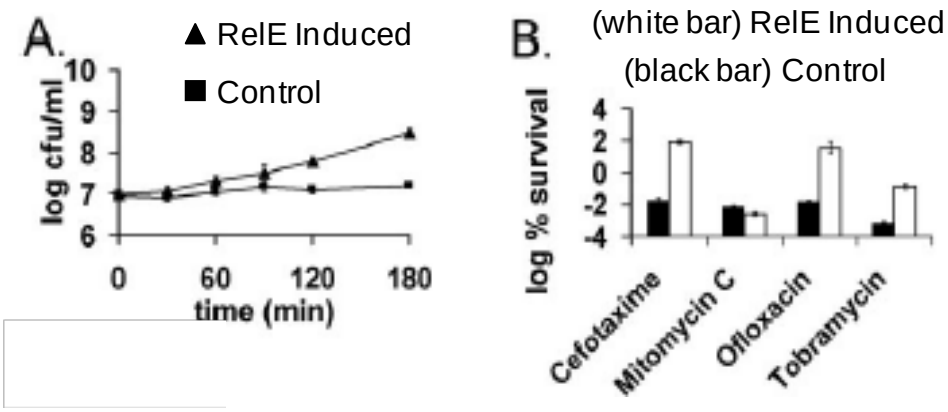

Figure 3-2. (A) *In Vitro* growth rate of control (triangle) and RelE induced (square) *E. coli* populations. The growth of RelE induced group showed growth retardation within 30 minutes. (B) Treatment with lethal doses of cefotaxime, mitomycin C, ofloxacin and tobramycin three hours after RelE induction showing greater survival rate (black bar) compared to the control (white bar).[51]

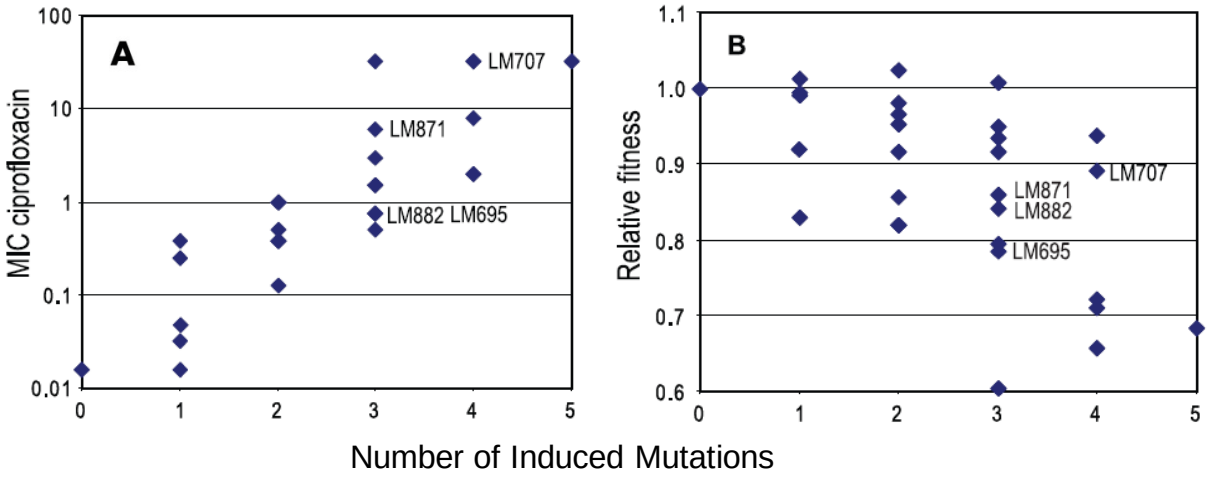

Figure 3-3. Compensatory mutation hypothesis: Increase number of mutations leads to increase in drug resistance (A). However, the relative fitness decreases as the number of mutations increases (B).[57]

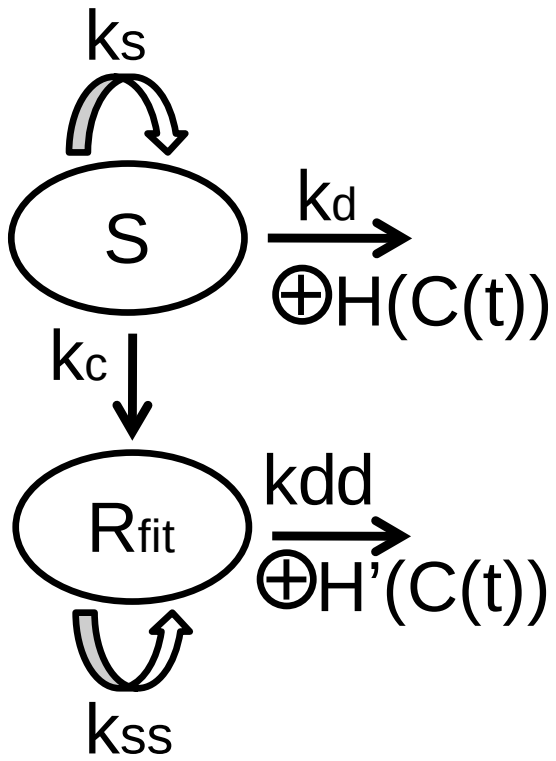

Figure 3-4. Literature PKPD model: Susceptible (S) and resistant (R_{fit}) population with independent growth rate constants (k_s and k_{ss}) and degradation rate constants (k_d and k_{dd}). Susceptible organisms can be converted to resistant ones with the rate constant of k_c. Drug effects are Hill functions denoted as H(C(t)) that work by stimulating the degradation rate constants of S and R_{fit} populations.

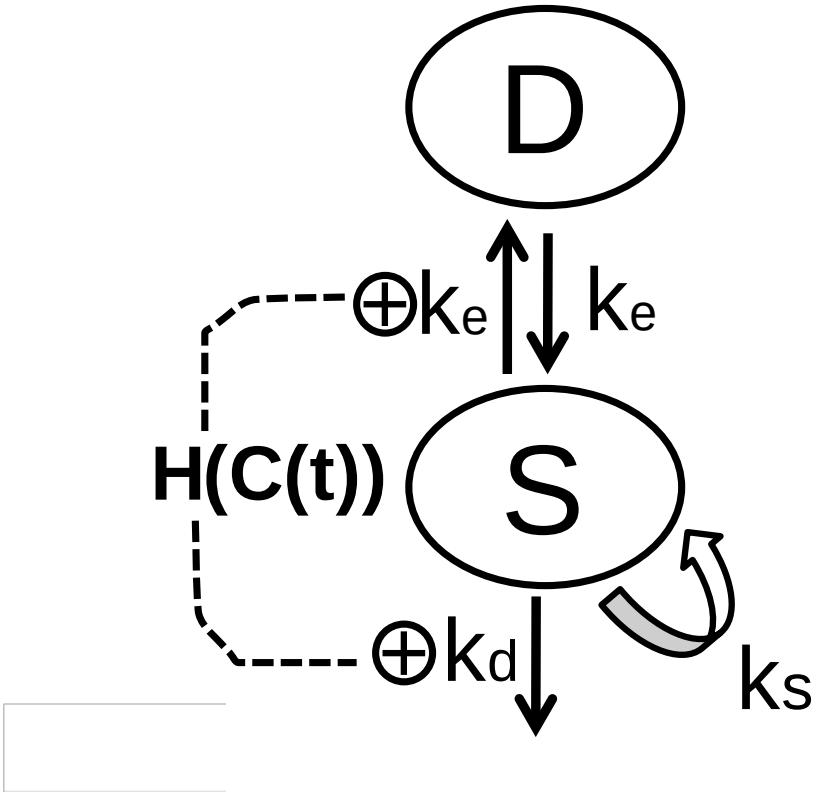

Figure 3-5. PKPD model based on Dormant hypothsis: The susceptible population (S) has the growth and degradation rate constants of k_s and k_d and has nonspecific switching (k_e) between the susceptible and dormant (D) populations. Drug effects denoted as (H(c(t)) stimulate the degradation rate constant of S and conversion of S to D.

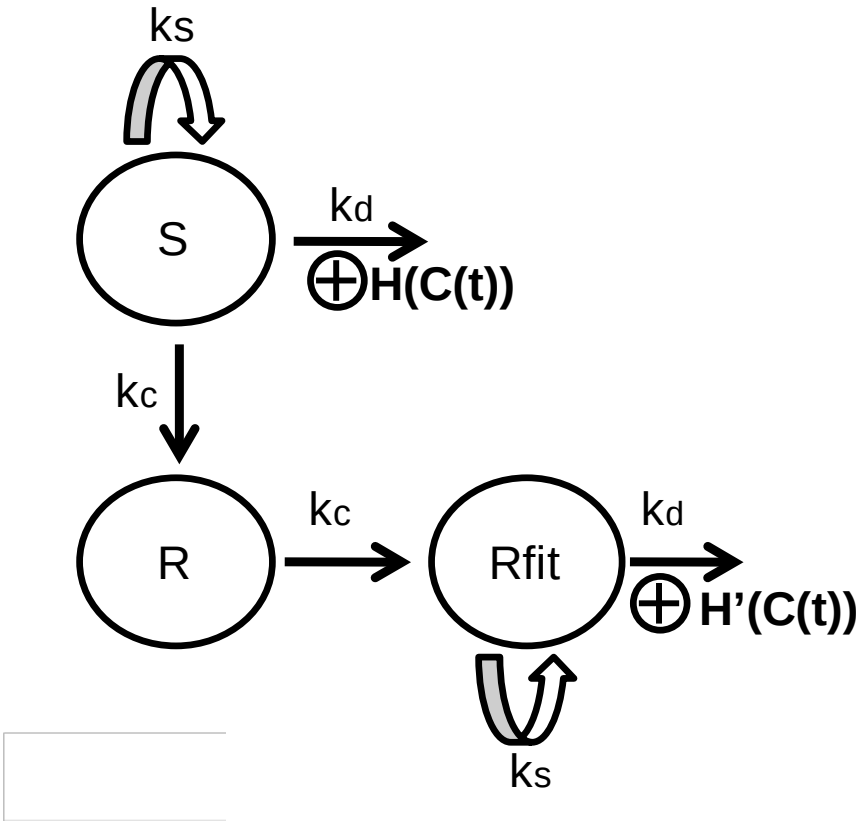

Figure 3-6. PKPD model describing Compensatory Mutation Model: The susceptible population (S) is converted to a resistant population without fitness (R) with the rate constant of k_c. The R population undergoes compensatory mutation with the rate constant of k_c to restore the fitness to become resistant with fitness population (R_{fit}). The S and R_{fit} have the same growth and degradation rate constants (k_s and k_d) but different drug effects.

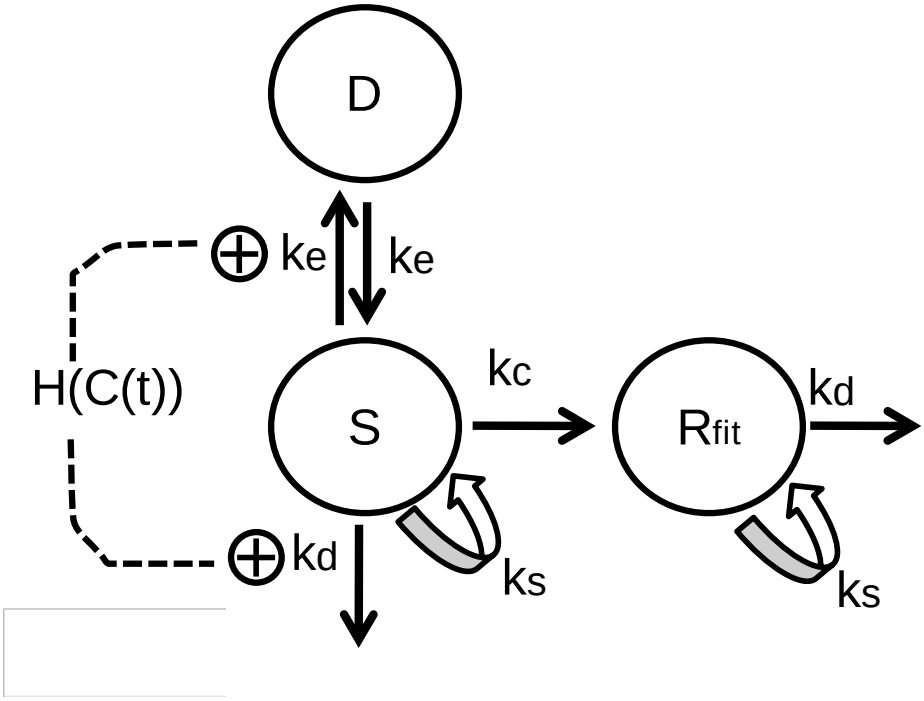

Figure 3-7. PKPD model describing both dormant and compensatory mutation hypotheses: Susceptible population (S) can be converted to dormant population (D) with a rate constant of k_e or resistant population (R_{fit}) with the rate constant of k_c. The S and R_{fit} population exhibit the same growth and degradation rate constants (k_s and k_d). The drug stimulates the k_d of S and conversion S to D.

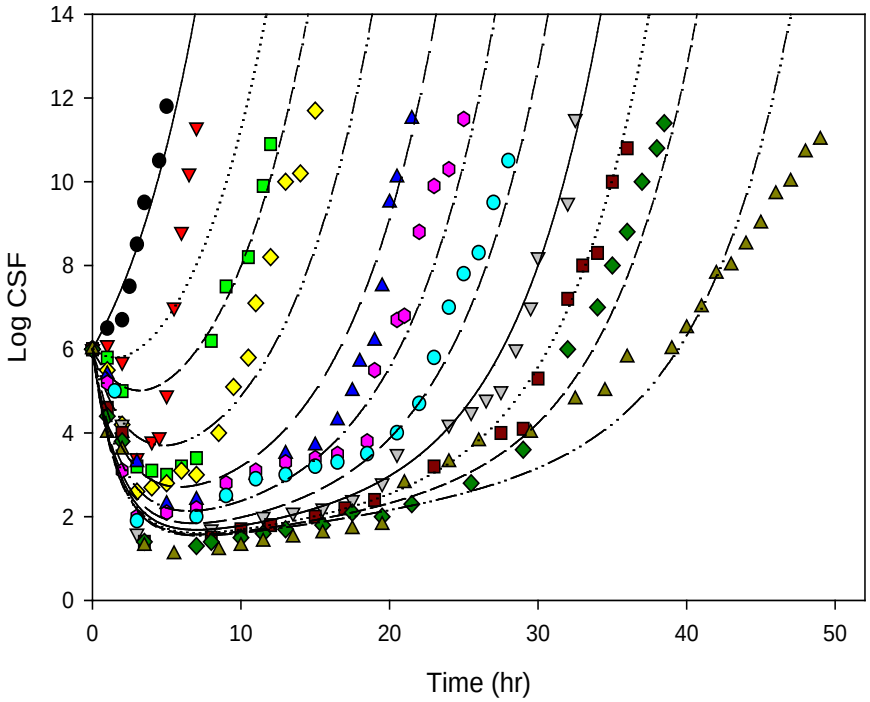

Figure 3-8. Observed (symbol) versus model predicted (line) values from Model 1 (literature PKPD model).

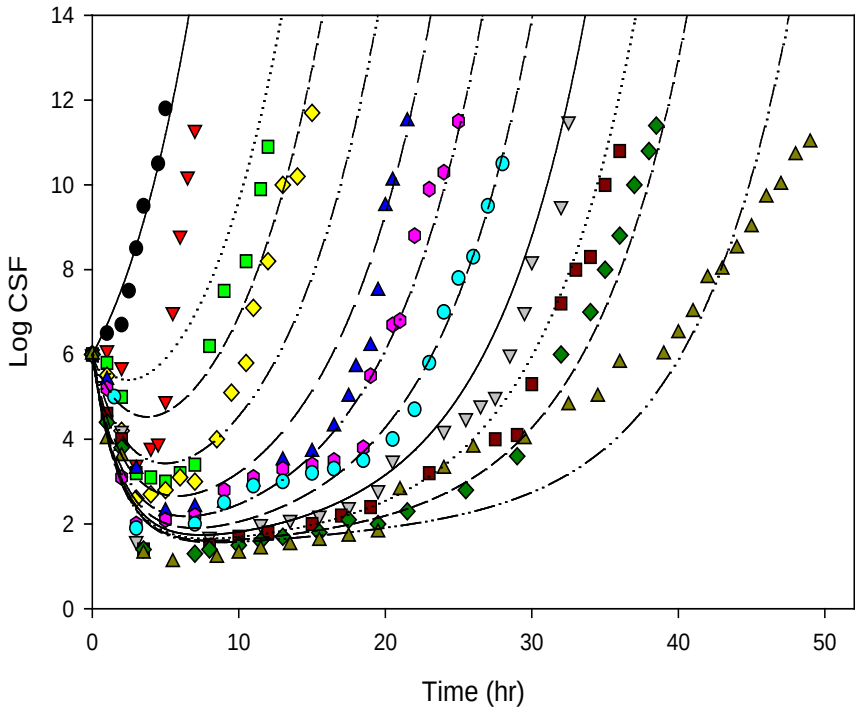

Figure 3-9. Observed (symbol) versus model predicted (line) values from Model 2 (dormant PKPD model).

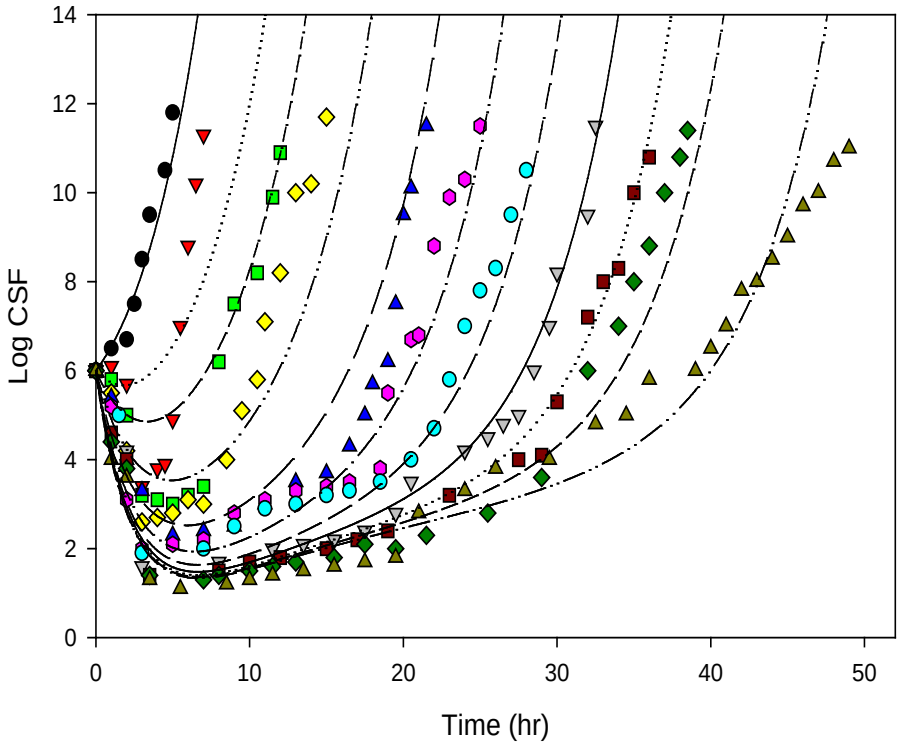

Figure 3-10. Observed (symbol) versus model predicted (line) values from Model 3 (compensatory PKPD model).

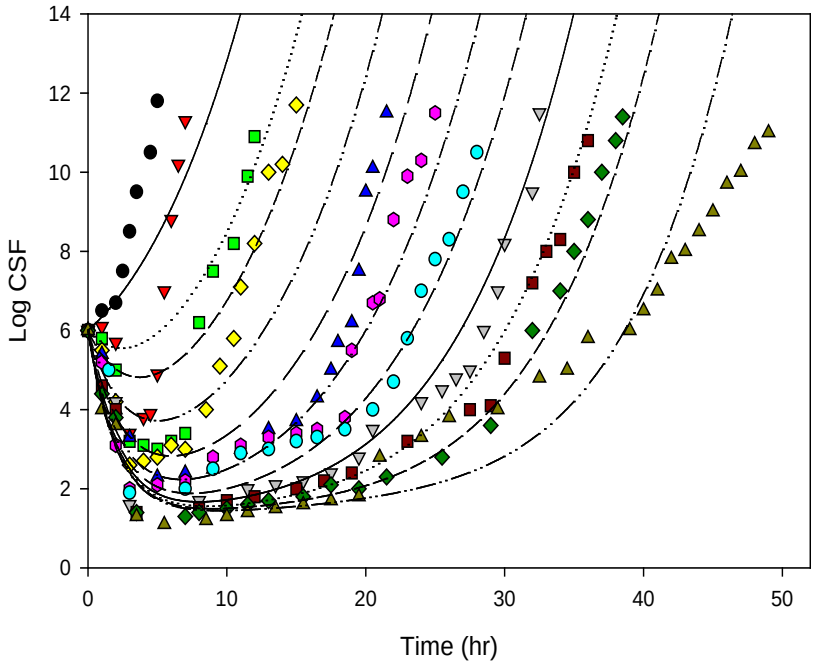

Figure 3-11. Observed (symbol) versus model predicted (line) values from Model 4 (dormant and compensatory mutation combined PKPD model).

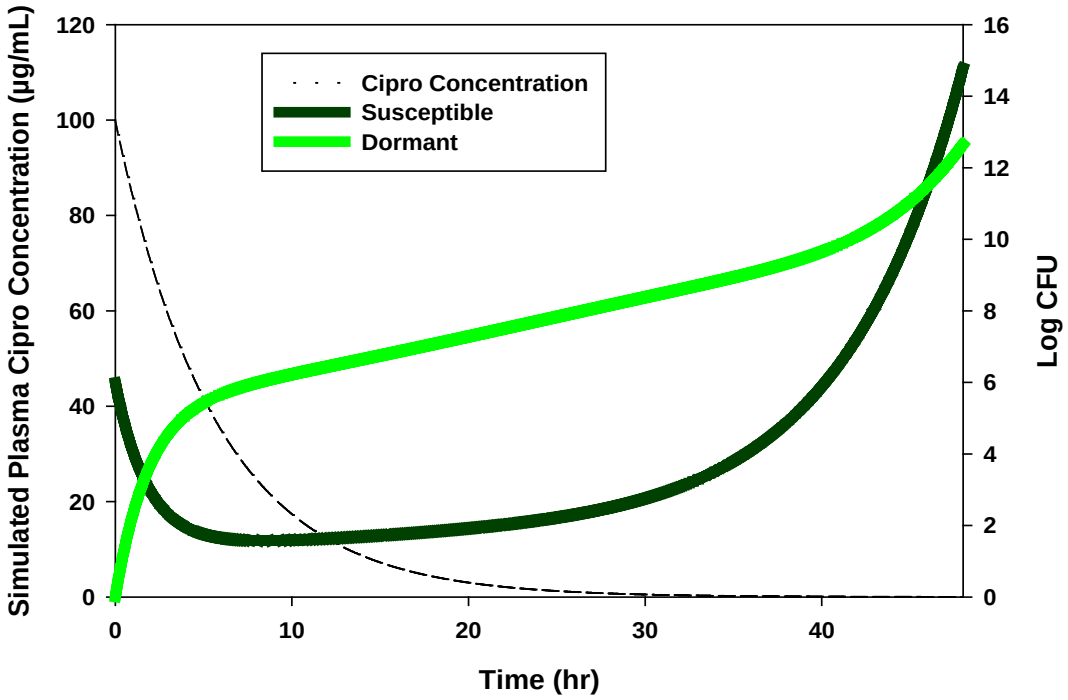

Figure 3-12. Subcompartmental profiles of Model 2 (dormant PKPD model): Dashline indicates ciprofloxacin concentrations, dark and light green lines indicate susceptible and dormant *E.coli* populations.

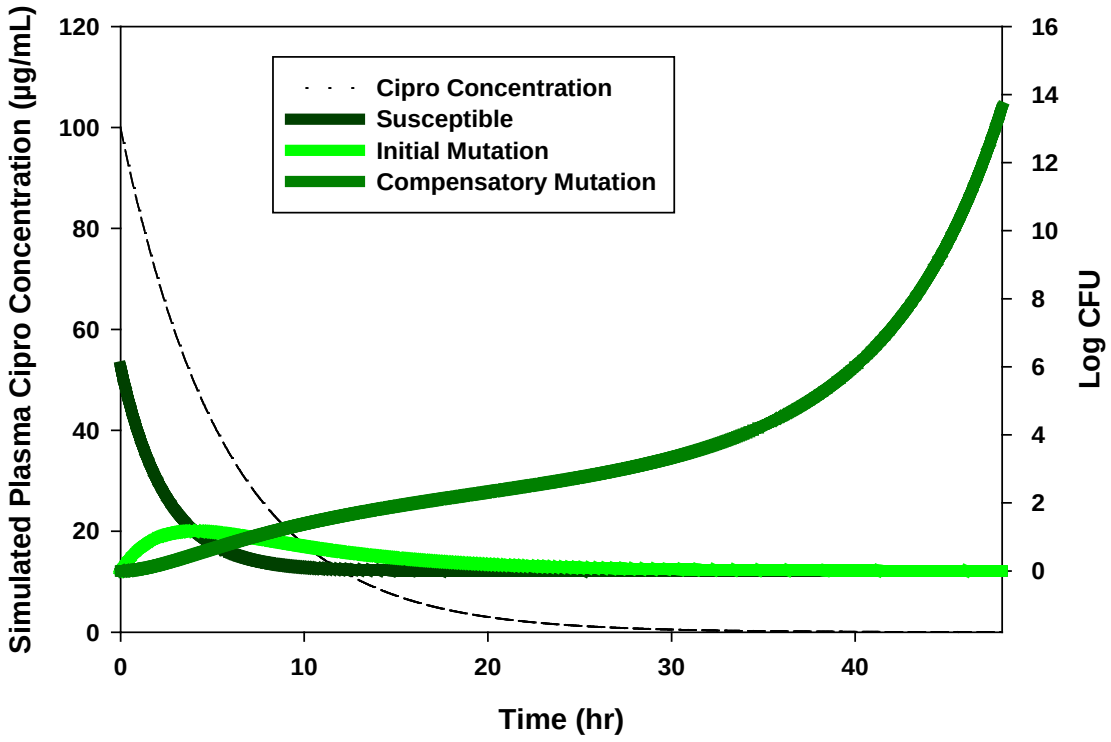

Figure 3-13. Subcompartmental profiles of Model 3 (compensatory mutation PKPD model): Dashline indicates ciprofloxacin concentrations; dark, light, and median dark green lines indicate susceptible, resistant, resistant with fitness *E. coli* populations, respectively.

CHAPTER 4
MODEL VALIDATION AND PREDICTIONS

Model Validation Using Bootstrap Statistics

Model Validation Approaches

The common model validation approaches include testing the model fitting or predictions using either an independent dataset or subsets of the original data that was not included in the model development. When these approaches are not feasible, bootstrap statistics are routinely used for model validation. The four antimicrobial resistance models described in Chapter 3 were developed using rich, dynamic kill-curve data published over 20 years ago[103]. The laboratory conditions and experimental procedures greatly affect the growth and degradation rates of microbes. Hence, the model validation approach to generate an independent dataset for modeling introduces inter-laboratory and inter-occasion variability that would be difficult to resolve. The "leave-some-out" approach from the original dataset was not preferred because the complex mechanism-based PKPD models require extensive data points. Thus, to validate the PKPD models, bootstrap statistics of a 1000-run-each were performed.

NONMEM VI with FOCE interactions was used to generate 1000 new datasets, with each dataset equivalent in size to the original dataset. Model fittings were performed for the datasets, and statistical summaries (mean and 90% confidence interval) for these are tabulated in Tables 4-1 to 4-4. The model estimates of the original dataset presented in Chapter 3 were compared with the bootstrap statistics. In addition, the bootstrap success rates for the models, defined by PDx-POP software for consistency, are shown in the footnotes of the summary tables.

Bootstrap Statistics Comparisons

As described in Chapter 3, Model 1 is the literature model. Model 2 is the Dormant hypothesis model. Model 3 is the Compensatory Mutation hypothesis model. Model 4 describes the combination of Models 2 and 3. All models, except for model 4, showed that the model estimates from the original dataset were comparable to that of the bootstrap means, and are mostly within the 90% confidence interval. Model 4 serves as an example that the wellness of model prediction cannot be determined based solely on evaluating the comparison between observed and predicted outcomes. The model estimates for Model 4 were not in agreement with the bootstrap statistics; the confidence intervals were large, and parameters such as SMAX,S exhibited a large difference between the model estimate and bootstrap mean (28.6 versus 12.4). Not surprisingly, the bootstrap success rate was the lowest for Model 4 (61.8%).

The bootstrap statistics for Models 1-3 were all reasonable, with the Compensatory Mutation Model having the highest success rate (83.9% versus 78.5% and 71.3%) and smallest confidence interval range. Although model selection cannot be based on bootstrap statistics alone, these analyses provide valuable information regarding model stability and precision.

Model Predictions

Visual Predictive Check

Model predictability was evaluated using visual predictive checks (VPC) and multiple dose simulations. Visual predictive checks have been routinely used to evaluate model performance. Using the model parameters and error variances estimated from the final model, 1000 outputs were generated using NONMEM VI. The 90^{th} percentiles of the profile distributions were computed for each model to evaluate

the distribution of the observed data within this range. To compare among the models, the percent of observed data points outside the 90th percentile were also calculated. In general, if the percentage of observed data is grossly greater than 10% outside the 90th percentile distribution, the model is considered to have undesirable VPC outcome. The results of the visual predictive checks for the models are shown in the footnotes of Tables 4-1 to 4-4.

In comparison, the lowest percentage of observed data outside the 90th percentiles infers best model performance. The VPC rankings for the four models, from best to worst, are: Model 4 (7.3%), Model 3 (8.3%), Model 1 (9.4%), and Model 2 (11.4%). This VPC analysis reveals the importance of not depending on a single criterion in model selection, because Model 4 performed inadequately with bootstrap statistics. Among the other models (Models 1-3), both the VPC and bootstrap statics show reasonable values. Based on these results, Models 1-3 were subject to further testing, but Model 4 was discarded.

PKPD Multiple Dose Simulations

Ciprofloxacin is administered as twice-a-day dose. The PKPD model predicted that in an *in vitro* setting, the drug effect after the first dose is greatly reduced due to the emergence of resistance. Since Model 1 does not consider the emergence of resistance, it was not used for multiple dose simulation. The multiple dose PKPD profiles for Models 2 and 3 are simulated in Figures 4-1 to 4-2. The PK profiles show the free fraction of ciprofloxacin concentrations in the plasma after a 200 mg b.i.d. dose for five doses. The corresponding PD profiles for each subpopulation are shown for comparison (susceptible and dormant subpopulation for Model 2, and susceptible, resistance, with and without fitness, subpopulation for Mode 3). In addition, the total

populations in Model 3 (sum of all three subpopulations) are shown as a comparison to the susceptible population from Model 2.

In both Models 2 and 3, significant losses of drug activities were predicted by the model. While a noticeable drug effect was predicted for Model 2 for all subsequent ciprofloxacin doses, Model 3 predicted a loss of killing effect after the first dose. The dormant population was predicted to increase after the initial ciprofloxacin exposure, which is consistent with the hypothesis that microbes self-induce toxins to inhibit cell divisions when they sense a harmful substance in their environment. However, the proportion of the dormant population was predicted to be too large. There has not been any literature publication indicating that the dormant population is comparable to, or larger than, the susceptible population. Hence, the sub-compartmental simulation revealed that the Dormant Model did not have the biological support published in the literature.

On the other hand, the Compensatory Mutation Model appeared to provide reasonable explanation for each subpopulation. Following the initial dose of ciprofloxacin, the susceptible population was reduced to a negligible level within 12 hours. Over the next 24 hours, a resistant population without fitness developed, but failed to contribute as a significant population. However, the resistant population with fitness was responsible for lack of drug efficacy and regrowth in the later dosing period. This model suggests that the subsequent doses of ciprofloxacin have minimal effects on microbial killing. This explanation was consistent with the available data in the literature. Other published multiple dose *in vitro* kill-curves, shown in Figure 4-3, where the same doses of ciprofloxacin 200 mg were administered to *P. aeruginosa,* also

showed the loss of drug effects by the second dose. In Dudley's study, the MIC increased over the course of ciprofloxacin therapy. Because, according to the Dormant hypothsis, it is a phenotypic variant, it has been suggested that the MIC may not differ once the microbes resume cellular activities following the elimination of drugs. Dudley's experiment further confirms the Compensatory Mutation Model as the superior model to explain emerged antimicrobial resistant pattern.

Table 4-1. Comparison of model estimates with bootstrap mean and 90% confidence intervals (CI) for Model 1 (literature PKPD model). Bootstrap success rate and visual predict checks shown as the percentage of observed data outside the 90% confidence interval are presented.

Parameter	Model Estimates	%CV	Bootstrap Mean	Bootstrap 90% CI
k_s (/hr)	5.92	14.4	5.80	3.18-8.77
k_d (/hr)	5.79	15.0	5.64	3.13-8.65
k_c (/hr)	0.119	14.8	0.126	0.0916-0.176
$S_{MAX, S}$	0.100	20.0	0.120	0.0765-0.190
$SC_{50, S}$ (µg/mL)	0.249	20.7	0.32	0.107-0.753
k_{ss} (/hr)	3.06	0.873	2.97	1.88-4.29
k_{dd} (/hr)	2.93	1.15	2.79	1.72-4.02
$S_{MAX, R}$	0.0342	15.8	0.0559	0.0392-0.0969
$SC_{50, R}$ (µg/mL)	0.192	44.7	0.114	0.029-0.256
Proportional Error	0.198	6.71	0.188	0.157-0.215
Bootstrap Success Rate: 78.5%				
Visual Predictive Check: % Observation outside 90% CI = 9.4%				

K_s and k_{ss} = growth rate constants of susceptible and resistant populations; k_d and k_{dd} = degradation rate constants of susceptible and resistant populations; k_c = conversion rate constant from susceptible to resistant population; $S_{max,S}$ and $S_{max,R}$ = overall drug effects on stimulating the k_d or k_{dd}; $SC_{50,S}$ and $SC_{50,R}$ = potency of drug on stimulating the k_d or k_{dd}.

Table 4-2. Comparison of model estimates with bootstrap mean and 90% confidence intervals (CI) for Model 2 (Dormant PKPD model). Bootstrap success rate and visual predict checks shown as the percentage of observed data outside the 90% confidence interval are presented.

Parameter	Model Estimates	%CV	Bootstrap Mean	Bootstrap 90% CI
k_s (/hr)	0.921	66.1	1.05	0.811-1.52
k_d (/hr)	0.709	88.5	0.805	0.603-1.17
k_e (/hr)	0.108	15.5	0.124	0.0835-0.183
$S_{MAX, S}$	0.188	42.4	0.225	0.116-0.365
$SC_{50, S}$ (µg/mL)	0.0588	56.4	0.0751	0.0140-0.164
$S_{MAX, D}$	3.610	21.1	3.23	1.33-4.91
$SC_{50, D}$ (µg/mL)	0.263	31.4	0.346	0.0979-0.894
Proportional Error	0.212	6.78	0.198	0.159-0.233
Bootstrap Success Rate: 71.3%				
Visual Predictive Check: % Observation outside 90% CI = 11.4%				

K_s = growth rate constant of susceptible population; k_d = degradation rate constant of susceptible population; k_e = conversion rate constant between susceptible and dormant populations; $S_{max,S}$ and $S_{max,D}$ = overall drug effects on stimulating the k_d or conversion of susceptible to dormant population; $SC_{50,S}$ and $SC_{50,D}$ = potency of drug on stimulating the k_d or conversion of susceptible to dormant population.

Table 4-3. Comparison of model estimates with bootstrap mean and 90% confidence intervals (CI) for Model 3 (Compensatory Mutation PKPD model). Bootstrap success rate and visual predict checks shown as the percentage of observed data outside the 90% confidence interval are presented.

Parameter	Model Estimates	%CV	Bootstrap Mean	Bootstrap 90% CI
k_s (/hr)	0.813	14.5	0.819	0.654-0.941
k_d (/hr)	0.660	18.3	0.664	0.538-0.771
k_c (/hr)	0.172	10.7	0.325	0.166-0.565
$S_{MAX, S}$	1.020	18.9	1.364	0.890-2.087
$SC_{50, S}$ (µg/mL)	0.358	14.6	0.346	0.215-0.542
$S_{MAX, R}$	0.193	21.3	0.215	0.163-0.269
$SC_{50, R}$ (µg/mL)	0.113	31.6	0.139	0.0636-0.365
Proportional Error	0.220	0.210	1.04	0.812-1.237
Bootstrap Success Rate: 83.9%				
Visual Predictive Check: % Observation outside 90% CI = 8.3%				

K_s = growth rate constants of susceptible or resistant with fitness populations; k_d = degradation rate constants of susceptible or resistant with fitness populations; k_c = conversion rate constant from susceptible to resistant population; $S_{max,S}$ and $S_{max,R}$ = overall drug effects on stimulating the k_d of susceptible and resistant with fitness populations; $SC_{50,S}$ and $SC_{50,R}$ = potency of drug on stimulating the k_d of susceptible and resistant with fitness populations.

Table 4-4. Comparison of model estimates with bootstrap mean and 90% confidence intervals (CI) for Model 4 (Combined PKPD model). Bootstrap success rate and visual predict checks shown as the percentage of observed data outside the 90% confidence interval are presented.

Parameter	Model Estimates	Bootstrap Mean	Bootstrap 90% CI
k_s (/hr)	0.142	0.139	0.0556-0.417
k_d (/hr)	0.0235	0.0447	0.0101-0.227
k_e (/hr)	0.088	0.0845	0.0179-0.182
k_c (/hr)	0.00326	0.0234	0.0001-0.0471
$S_{MAX, S}$	28.60	12.4	1.01-44.3
$SC_{50, S}$ (µg/mL)	0.374	0.291	0.0109-0.515
$S_{MAX, D}$	4.230	3.74	0.139-8.933
$SC_{50, D}$ (µg/mL)	0.2680	2.51	0.0991-16.4
Proportional Error	0.231	0.189	0.157-0.218
Bootstrap Success Rate: 61.8%			
Visual Predictive Check: % Observation outside 90% CI = 7.3%			

K_s = growth rate constant of susceptible population; k_d = degradation rate constant of susceptible population; k_e = conversion rate constant from susceptible to dormant population; k_c = conversion rate constant from susceptible to resistant population; $S_{max,S}$ and $S_{max,D}$ = overall drug effects on stimulating the k_d and conversion of susceptible to dormant population; $SC_{50,S}$ and $SC_{50,D}$ = potency of drug on stimulating the k_d of susceptible and conversion of susceptible to dormant population; NA = not available from ADAPT II output.

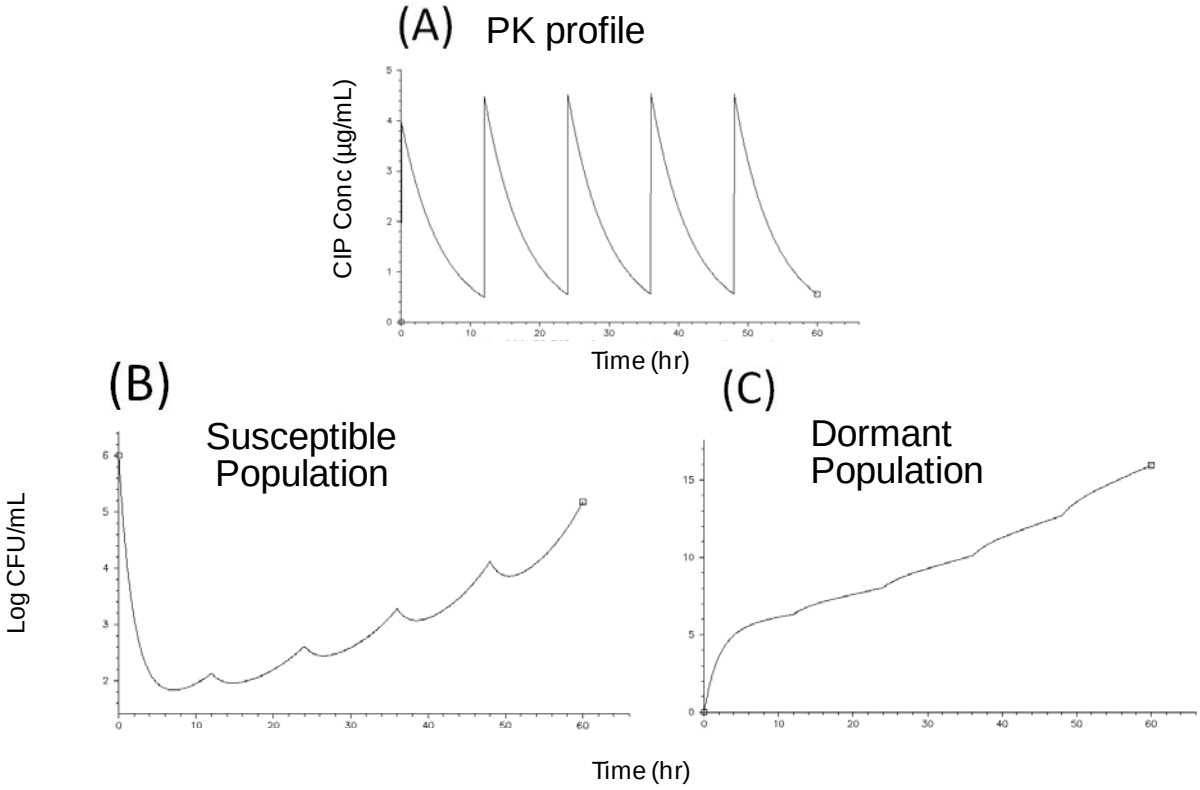

Figure 4-1. Subcompartmental simulation of the dormant PKPD model following 5 b.i.d. IV doses of 200 mg ciprofloxacin in *E.coli*.

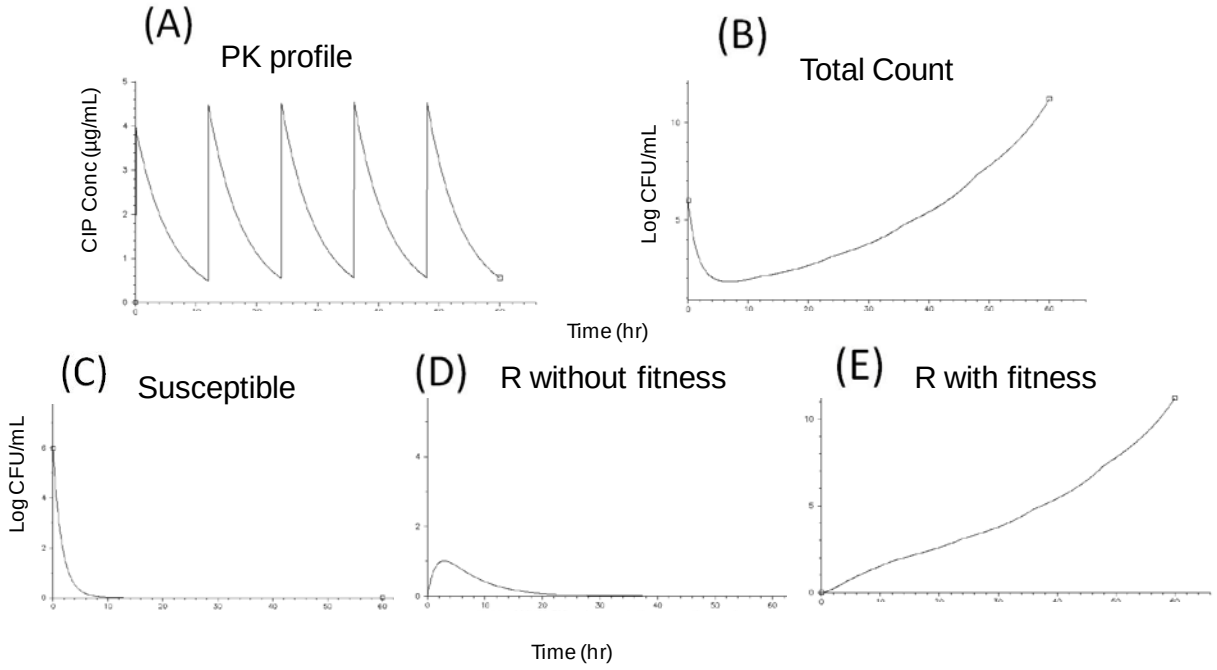

Figure 4-2. Subcompartmental simulation of the Compensatory Mutation PKPD model following 5 b.i.d. IV doses of 200 mg ciprofloxacin in *E.coli*.

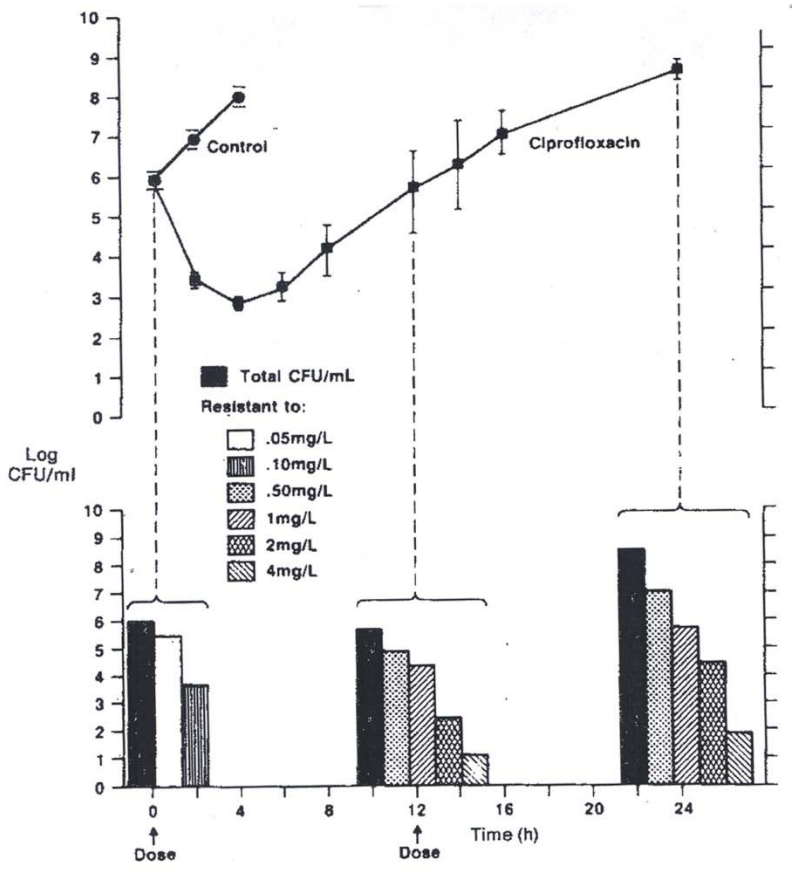

Figure 4-3. MIC distribution for *P. aeruginosa* following 200 mg ciprofloxacin b.i.d. dose.[106]

CHAPTER 5
UTILITIES OF MODELING AND SIMULATION IN DESIGNING EXPERIMENTS

Introduction

Regardless of the mechanisms of actions of antimicrobial classes, microbes have been able to consistently develop resistance to new drug treatments within a few years after their implementations[58, 107, 108] The major factors contributing to this predicament include lack of understanding of the underlying mechanisms of antibacterial resistance and the use of sub-optimal pressure specifically against the resistance population. The evaluation of antimicrobials and microbial survival response has evolved from point estimates (minimum inhibitory concentrations) to complete time course approach (bacterial kill-curve) to reveal the drug-bacterial killing relationships.[87, 92, 109, 110] However, it is only within recent years that the emphasis has shifted towards molecular and genetic approaches to understanding the mechanisms of resistance with additional insight on how to interpret the bacterial kill-curve relationships. It is with these new experimental findings that we propose a new mathematical model to bridge basic science research to relevant clinical usage. In this chapter, we use the Compensatory Mutation hypothesis[54-57, 99, 101, 102, 111-113] as the foundation for the mechanism-based pharmacokinetic/pharmacodynamics (PK/PD) model. The importance of the fitness concept and genetic mutation relationship were proposed to describe antimicrobial resistance. As the microbes undergo life cycle division every 20 min, selection for drug resistance mutants occurs within a short period of time following treatment. However, mutation is often associated with a fitness cost (the rate of cell division is reduced). It is only after multiple mutations that a drug resistant trait is acquired while further mutations occur and the mutated population becomes clinically relevant. It is this new

compensated mutation population that explains the observed rising MIC over the time course of antimicrobial treatment.[106]

We believe a quantitative modeling approach can provide the urgently needed link between the newly proposed microbial behavior and clinical dose optimization needed to better protect against infections. In the absence of adequate new antimicrobials available in the next few years, we believe our approach has great potential to revive some older antimicrobials rendered useless due to resistance. The occurrence of resistance may be related to misuse of antimicrobials that foster selection of resistance populations since this population was not considered when the clinical dosage was selected. In this study, we utilized a semi-mechanism-based pharmacokinetic/pharmacodynamic (PK/PD) model to explore combination therapy that considers the emerged resistance population following ciprofloxacin treatment.

Pharmacokinetic/pharmacodynamic model descriptions

Details of the *in vitro* procedures have been published before.[103, 114] Extensive *in vitro* kill-curve data suitable for complex mechanistic modeling were obtained using GetData Graph Digitizer 2.24 software. Briefly, a two flask system with ciprofloxacin was used against *Escherichia coli* 204 (*E. coli* II), ranging from 0.0, 0.1, 0.2, 0.5, 1.0, 2.0, 4.0, 8.0, 16.0, 32.0 and 125 times the minimum inhibitory concentration (MIC) of 0.08 ug/mL. The flask containing bacteria and drug was inoculated with 18 h-cultured bacteria followed by 2 h incubation. Ciprofloxacin was injected at the 20th hour. The inoculum size at the time of treatment was approximately106 colony forming units (CFU)/mL and the experiments ended when the total bacterial growth reached $\sim 10^{11}$ CFU/mL for each dose group. A clinical half-life of 4 h for ciprofloxacin was established

in an *in vitro* kill-curve system by replacing 7 mL/h of fresh media in a constant 40mL flask. The mono-exponential decline rate was described as:

$$\frac{dC}{dt} = -kel * C \qquad \textit{Initial Condition = DOSE} \qquad (5\text{-}1)$$

where k_{el} rate constant is fixed to 0.175 h^{-1}. A graphical description of the semi-mechanism-based PD model is shown in Fig. 5-1 and the respective differential equations are included below.

$$\frac{dS}{dt} = ks * S - kd * (1 + Emax, S) * S - kc * S \qquad \textit{IC} = 10^6 \textit{CUF/mL} \qquad (5\text{-}2)$$

$$\frac{dR}{dt} = kc * S - kc * R \qquad \textit{IC} = 0\ \textit{CFU/mL} \qquad (5\text{-}3)$$

$$\frac{dRfit}{dt} = ks * Rfit + kc * R - kd * (1 + Emax, Rfit) * Rfit \qquad \textit{IC} = 0\ \textit{CFU/mL} \qquad (5\text{-}4)$$

where the stimulatory function for susceptible population is described as:

$$Emax, S = \frac{Smax,s*C}{SC50,s+C} \qquad (5\text{-}5)$$

and for R_{fit} population as:

$$Emax, Rfit = \frac{Smax,Rfit*C}{SC50,Rfit+C} \qquad (5\text{-}6)$$

The model describes the Compensatory Mutation hypothesis, where S is the susceptible population, R is the mutated population with reduced fitness characteristic (negligible growth and degradation) and R_{fit} is the resistance population after second mutation that restores fitness while retaining drug resistance characteristics. The model assumes the fitness is fully restored, showing the R_{fit} population exhibiting the same growth and degradation rate constant (k_s and k_d) as those of the S population. The multiple mutation process is described by an arbitrary k_c rate constant. Ciprofloxacin has independent nonlinear killing effect on both S and R_{fit} population.

A total of 10 ciprofloxacin-treated groups and one control treated group were modeled simultaneously with the PK/PD model described above using ADPT II[105]. A total of 44 differential equations (sets of equations 5-1 to 5-4) were written to describe the eleven treatment groups. A proportional error model with maximum likelihood estimator in ADAPT II was implemented. Standard goodness of fit criteria used to obtain the final model included model convergence, Schwartz Criterion, Akaike Information Criterion, residuals versus predicted concentrations and time, and visual inspection.

Exploratory mechanism-based combination therapy

The final model output was tabulated in previous chapter (Table 3-4). The use of mechanism-based PKPD models to design and predict outcome of combination therapy is shown in Figure 5-1. Antibiotic resistance is associated with increased MIC following drug treatment. Although MIC distribution over time was not assessed in the current study, a reduction in drug effects indirectly infers a rise of MIC during the drug exposure period. Using the time course relationship of sub-compartmental analysis from Section 2.2, additional simulations were explored to assess the feasibility of combination therapy. Figure 5-4 shows the proposed combination therapy approach using the mechanism-based PK/PD model. It simulates scenarios where a second drug is inhibiting the production of bacterial synthesis with IC_{50} set at 0.1, 1, and 10 ng/mL using Eq. (5-7).

$$Kmax, S = \frac{Imax * C}{IC50 + C} \quad (5\text{-}7)$$

where K_{max} is the inhibitory equation on the synthesis rate constant of R_{fit} population. I_{max} is the maximum inhibitory effect, which was fixed to the maximum of 1 in the

simulation. IC_{50} represents the drug potency. Provided the reduction of the ciprofloxacin response after the initial dose, an antimicrobial drug from a different class that exhibits an alternative pharmacological action given as the second dose has greater beneficial effects compared to continuing ciprofloxacin mono-therapy at the same or elevated (3X) dose.

Discussion

The semi-mechanism-based PK/PD model mimicking the compensatory antimicrobial resistance hypothesis appears to describe the effects of eleven ciprofloxacin dose groups simultaneously reasonably well. The model captures the multiple step process needed for bacteria to develop into a clinically relevant resistant population. The resistance without fitness compartment (R) explains the findings that mutated bacteria often lead to lower bacterial growth. Subsequent mutations that retain the drug resistance characteristics while acquiring the restoration of fitness from the clinically resistant populations that should be the target of interest. In theory, the second clinical dose would render diminished drug response with increased MIC. This phenomenon was observed previously[106] using a multiple dose *in vitro* kill-curve system of ciprofloxacin against *P. aeruginosa*. Their findings show that bacterial killing at the second dose (12 hr) did not show an apparent reduction as compared to the first dose. In addition, the profiles of MIC distributions at 12 h were shown to increase by a large degree compared to the initial drug exposure. This multiple dose profile appears to be explainable by our compensatory PK/PD model. The multiple dose simulation from the model also did not show an apparent bacterial killing profile at a second dose given at 12 h compared to the initial drug exposure. In our simulation, a three-fold increase in ciprofloxacin dosing only slightly increased bacterial killing (Figure 5-2). This lead us to

explore novel dosing schemes using bacterial behavior information extracted from the PK/PD model.

In general, a higher initial dose may result in a more pronounced pharmacodynamic effect, assuming maximum effects have not been reached. However, higher doses increase the risks of toxicity to patients. Hence, an alternative class of antimicrobials with a different mode of pharmacological action may be more effective against the merged resistant population. At various potency levels (IC_{50}), the model suggests a second drug with different pharmacological actions given at a subsequent dose may be more beneficial than continuation of ciprofloxacin where the bacterial have already evolved to successfully resist and grow with comparable fitness as that of the parent population.

In conclusion, this paper demonstrates a novel semi-mechanism-based PK/PD model that describes the complex mechanisms of antimicrobial resistance using findings from recent basic science research. The microbial behavior extracted from the developed model was used to propose a study design for future experiments, predicting a different class of drug at a subsequent dose may result in superior killing of the resistant population compared to a continued treatment with ciprofloxacin.

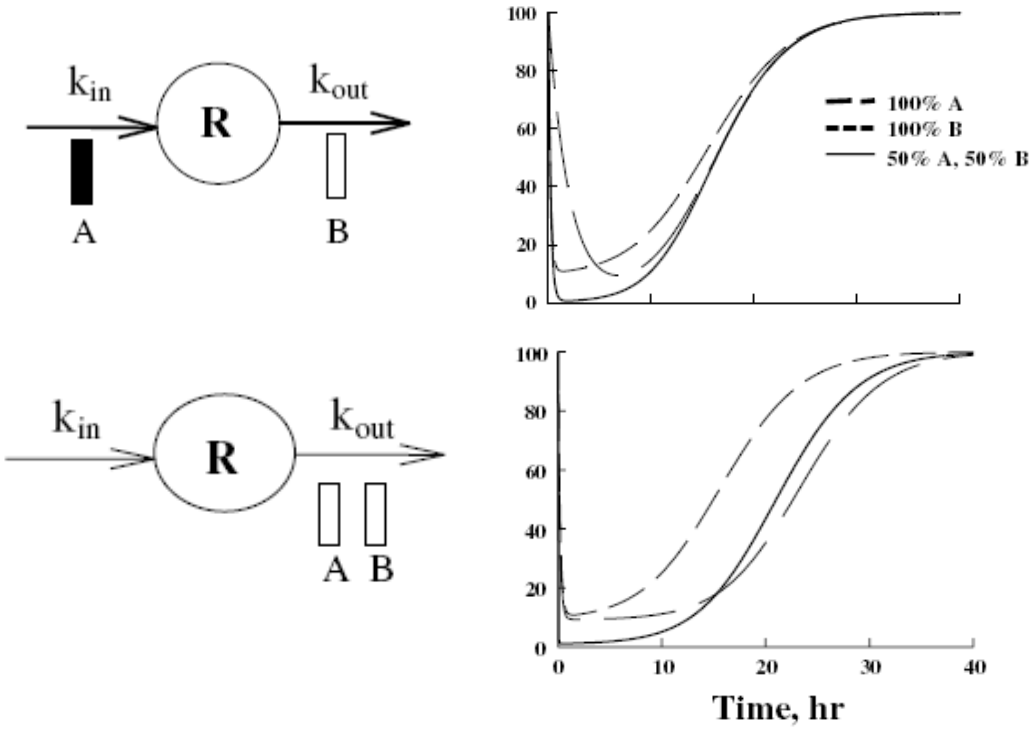

Figure 5-1. Use of mechanism-based PKPD models for combination therapy[115].

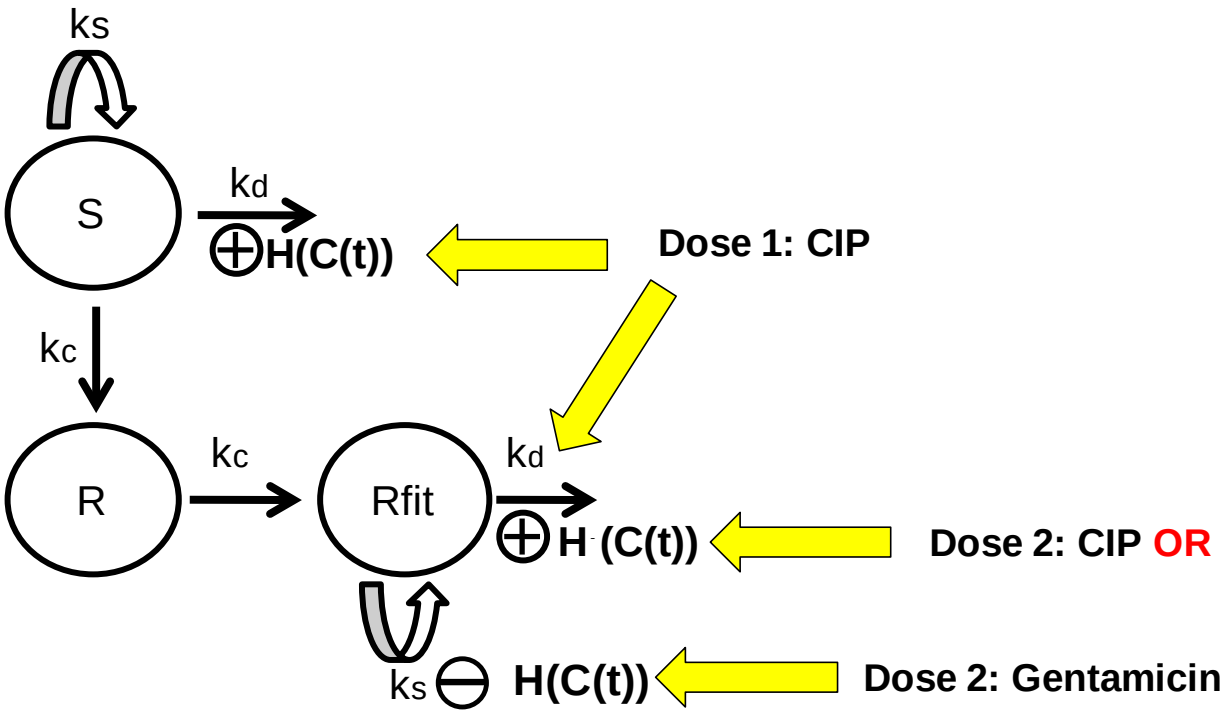

Figure 5-2. Utilizing the compensatory mutation PKPD model to design combination therapy for *in vitro* dynamic kill-curve experiments.

ID	Dose 1	Dose 2
(A)	200 mg CIP	200 mg CIP
(B)	200 mg CIP	600 mg CIP
(C)	200 mg CIP	Low Dose X
(D)	200 mg CIP	Mid Dose X
(E)	200 mg CIP	High Dose X

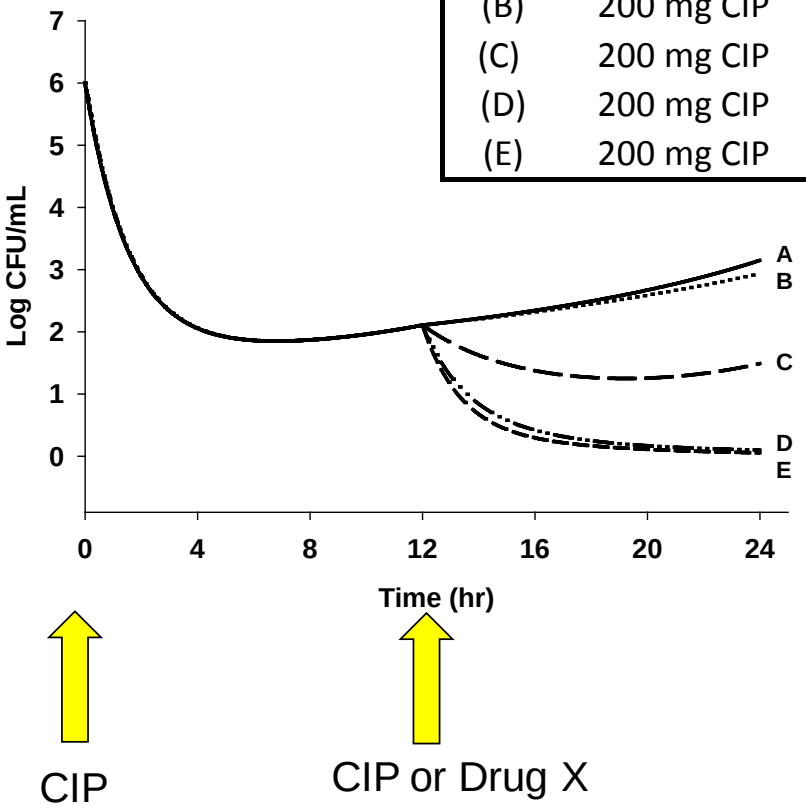

Figure 5-3. Model anticipated kill-curve profiles following 200 mg of ciprofloxacin at first dose then 200 mg ciprofloxacin at second dose (A), or 3-fold higher of ciprofloxacin at second dose (B), or gentamicin at low (C), mid (D), or high (E) at second dose.

CHAPTER 6
PKPD MODEL CONFIRMATION USING DYNAMIC KILL-CURVE EXPERIMENTS

Introduction

Pseudomonas aeruginosa is infamous for being highly adaptive to their environment, as well as for imposing a significant public health threat. Within the field of infectious agents, *P. aeruginosa* has one of the largest genome, with the number of genes being 1.3-fold more than that of *Eschericia coli*, 2.2-fold more than that of *staphylococcus aureus*, and 3.3-fold more than that of *Haemophilus influenza.*[116] The large genome increases the ability to produce a large number of functional proteins and intricate defense systems within a short period of time. The well-known antimicrobial resistant mechanisms of *P. aeruginosa* include (1) decreasing membrane permeability (2) enhancing efflux pump systems such as the mexAB-oprM, mexXY-oprM, mexCD-oprJ and mexEF-oprN[117], (3) altering drug binding sites[118, 119] and (4) modifying drug properties.[118, 120-130] In reality, the phenotypic expression of resistance is likely a combination of all mechanisms working simultaneously.

Given the adaptability of *P. aeruginosa* following antimicrobial administration, it is not surprisingly that the tradition antimicrobial treatment approach, which relies on single MIC time point (AUC/MIC, Cmax/MIC, or T>MIC), is bound to be ineffective over time. Therefore, *in* vitro dynamic kill-curve and MIC dynamics were utilized in our experiments to more thoroughly elucidate the time-course of the PKPD relationship involving the emergence of resistance. The objectives of the studies are to characterize the emergence of ciprofloxacin resistance strain using a clinical isolate of *P. aeruginosa,* and, once the resistance emerged, explore different treatment options to overcome the recalcitrant population. The experiments were designed using predictions from the

compensatory mutation PKPD model discussed in Chapter 5. Hence, the kill-curve data also serves as a confirmatory experiment for the PKPD model.

Material and Methods

Study Conduct

The clinical strains of *pseudomonas aeruginosa* used in the dynamic kill-curve and MIC assays are considered biohazard level 2. All experiments were conducted in a microbiology lab using the standard operating procedure (SOP) approved by the department of Environmental Health and Safety at the University of Florida. The MIC procedures were conducted in compliance with the Clinical and Laboratory Standards Institute (CLSI) approved standard methods. Sterile techniques and proper disposal of biohazard materials were practiced throughout the experiments.

Antimicrobial Drug Preparations

Ciprofloxacin (CAS 85721-33) was purchased from Sigma-Aldrich (St. Louis, MO). The original stock solution of 40 µg/mL was prepared by dissolving 20 mg of ciprofloxacin in 500 mL of purified water using heat and a sonicator.

Ceftriaxone (CAS 104376-79-6) was purchased from Sigma-Aldrich (St. Louis, MO). The stock solution of 1650 µg/mL was prepared by dissolving 16.5 mg in 10 mL of purified water.

Gentamicin (CAS 1405-41-0) was purchased from Sigma-Aldrich (St. Louis, MO) in the form of 50 mg/mL of deionized water. The stock solution of 1000 µg/mL was prepared by diluting 1 mL of the 50 mg/mL solution with 50 mL of purified water.

Aztreonam (CAS 78110-38-0) was purchased from MP Biomedicals (Irving, CA). The stock solution of 5000 µg/mL was prepared by dissolving 10 mg in 2 mL of DMSO.

Microbial Strain

A clinical strain of *pseudomonas aeruginosa* isolated from a patient at Shands Hospital at the University of Florida, was used throughout the experiments. The same microbe isolate was subcultured on agar plates throughout the kill-curve experiments to maintain the cell line.

Sterile Broth and Saline Preparation

A Mueller-Hinton broth (Becton Dickinson BBL) was prepared according to the manufacturer's instructions. Dissolved solution was autoclaved at 121°C for 15 minutes, then cooled to room temperature prior to use. Normal saline was prepared by dissolving 9 g of sodium chloride in 1 L of double distilled water. The saline solution was then autoclaved at 121 °C for 20 minutes.

Pre-Resistance Strain Determination

An agar solution was prepared by mixing 38g of agar powder in 1 L purified water. The agar solution was autoclaved at 121 ºC for 15 minutes then cooled to 45-50 ºC. Two dose levels of ciprofloxacin were prepared for the pre-resistant strain experiment: 0.563 mg/mL and 1.688 mg/mL of ciprofloxacin were prepared in purified water, and 1 mL was spiked into 375 mL agar solution to obtain 1.5 and 4.5 ug/mL of ciprofloxacin concentration in the agar solution. A control of the agar group without ciprofloxacin was included. The ciprofloxacin containing agar solutions were poured into sterile petri dishes in triplicates to a 4 mm depth, and cooled to room temperature to form agar plates. Aliquots of 150 µL of 10^8 CFU/mL bacteria were dispensed into tissue culture flasks containing 15 mL Mueller-Hinton broth to achieve the initial inoculation of 10^6 CFU/mL. For bacterial cell plating, five aliquots (10 µL each) from each group were

pipetted onto the ciprofloxacin containing agar plates and dried at room temperature prior to being incubated at 37 ºC for 16-20 hours for colony counting.

Dynamic Kill-Curves

Two dynamic kill-curves were performed using sequential dosing scheme of two doses. Experiment 1 consists of 4 groups. Group 1 received saline dose as control at time 0 and 12 hours. Group 2 received 200 mg ciprofloxacin as the first dose then 200 mg ciprofloxacin again as the second dose. Group 3 received 200 mg ciprofloxacin as the first dose then increase to 600 mg ciprofloxacin as the second dose. Group 4 received 200 mg ciprofloxacin the first dose then switch to 2 g of Ceftriaxone as the second dose. Each group was performed in triplicates.

Experiment 2 consists of 4 groups with 2 doses at 0 and 12 hours. Group 1 is the control. Group 2 received 200 mg ciprofloxacin as the first dose then 200 mg ciprofloxacin again as the second dose. Group 3 received 200 mg ciprofloxacin as the first dose then switch to 7 mg/kg gentamicin as the second dose. Group 4 received 2 g aztreonam for both doses.

The day before the experiment, *P. aeruginosa* were removed from a fridge and plated on agar plates in a 37 ºC incubator to obtain the exponential growth prior to the experiment. An aliquot of bacteria was then diluted in sterile saline to 10^8 CFU/mL using a calibrated turbidity meter. Aliquots of 150 µL of 10^8 CFU/mL bacteria were dispensed into 25 mL canted neck Tissue Culture Flasks containing 15 mL of Mueller-Hinton broth, to achieve the initial inoculation of 10^6 CFU/mL. The bacteria and broth solution were incubated at 37 ºC for two hours prior to adding any drugs.

The drug profiles in the experiments were determined by clinical dose, protein binding, and clinical half-life information. To obtain the initial free fraction of

ciprofloxacin concentrations (C_O) of 1.5 and 3 µg/mL, equivalent to 200 mg and 600 mg IV bolus doses in humans, 0.563 and 1.125 mL of stock solution was spiked in cell culture flasks containing 15 mL of bacteria containing broth solutions. To obtain the free fraction of ceftriaxone with a C_O of 40 µg/mL after clinical dose of 2 g IV bolus dose, a 0.364 mL of stock solution was spiked into a cell culture flask containing15 mL of bacteria containing broth. To obtain the free fraction of gentamicin C_O of 20 µg/mL after clinical dose of 7 mg/kg or 490 mg IV dose for a 70 kg person, a 0.3 mL of stock solution was spiked into the cell culture flask containing 15 mL of broth and bacteria. To obtain the free fraction of aztreonam with Co of 40 µg/mL after clinical dose of 2 g IV bolus dose, a 0.12 mL of stock solution was spiked into cell culture flask containing 15 mL broth and bacteria.

For each flask, a 5 mL syringe with a 0.22 µm filter (Millipore Cat. SLGV033NS, Billerica, MA) was attached. The dilution of drug concentrations were done manually with a syringe by drawing out appropriate sample volumes, then replacing the same amount with fresh broth every 2 hours to mimic clinical half-life. The 0.22 µm filters selectively remove the drug without significantly changing the bacterial population within the system. Each test group was performed in triplicate. Bacterial count was taken at 0, 2, 4, 6, 10, 12, 14, 16, 18, 22, and 24 hours post initial drug administration. For each bacteria cell count, 20 µL of sample was removed from the flask and appropriate dilutions in saline (ranging from 1 to 9-fold dilutions) were performed in Corning Costar 96 Cell culture plates (Sigma-Aldrich, CLS3596, St. Louis, MO). The diluted samples were then aliquotted in 4 replicates (10 µL each) onto agar plates. Agar plates containing 5% sheep blood were purchased from Remel (Lenexa, KS). The samples

were dried at room temperature then incubated at 37 ºC for 16-20 hours for colony count. For each group, mean and standard deviation of the bacterial count was calculated for plotting with SigmaPlots 11.0 (San Jose, CA).

MIC Determination

Minimum inhibition concentration (MIC) for ciprofloxacin was determined using an E-strip test. Aztreonam was determined using a disk-MIC test. The E-strip contains a gradient of ciprofloxacin ranging from 0.002 to 32 µg/mL. The E-strip method is superior to the dilution method because the MIC value is independent of the dilution factors. The disk-MIC test measures only the diameter of the area without growth, so the results are shown as a percentage change relative to the pre-dose level. The samples for the MIC test were a combination of various colonies from the triplicate plating for each group so that only one MIC reading per group was obtained. For both techniques, lawns of bacteria were platted on agar plates and the E-strip or disk was placed in the center of the plate, then incubated at 37 ºC for 14 hours for MIC determination. For the first ciprofloxacin and ceftriaxone kill-curve experiments, MIC was determined at 0, 6, 12, and 24 hours. For the second ciprofloxacin, gentamicin, and aztreonam experiments, MIC was determined at 0, 6, 12, 16, 18 and 24 hours during the treatment period and 48, 72, and 96 hours for post-antimicrobial-effect analyses.

Results

Pre-Resistance Strain

No visible colony was observed on either the 200 or 600 mg groups after overnight incubation. The control, without drug added in the agar solution, showed an abundance

of colonies after overnight incubation. The control samples were not diluted and the colonies were too dense for cell counting.

Ciprofloxacin and Ceftriaxone Kill-Curves

The kill-curve profiles, after ciprofloxacin and ceftriaxone treatments, are shown in Figure 6-1. The control showed an exponential growth rate reaching approximately 10^{11} CFU/mL by hour 12. The microbial concentration approximates the maximum growth within the system and no further bacterial count was performed after the 12^{th} hour. All groups exposed to 200 mg of ciprofloxacin at the first dose exhibited an approximate 2-log kill profile. The mean and standard deviation of all three groups were comparable for all time points in the first 12 hour period. At the second dose, the 200 mg ciprofloxacin dose showed no apparent killing effect. Furthermore, increasing the ciprofloxacin dose to 600 mg at second dose only slightly lowered the growth rate; no log-kill was observed. Switching from ciprofloxacin to ceftriaxone at second dose also did not show significant killing activities (Figure 6-1).

The MICs of ciprofloxacin taken throughout the kill-curve experiment are shown in Figure 6-2. All bacteria have a similar pre-dose MIC of 0.13 µg/mL. After 6 hours of 200 mg ciprofloxacin exposure, a significant increase in MIC was observed for all dose groups. The MIC values stay high throughout the treatment period and were approximately 4 µg/mL at the end of the 24 hour experiment.

Cross-Resistance Evaluations with Automated MicroScan

MicroScan analysis determines the susceptibility of a particular microbe to an array of antimicrobial agents. From the first kill-curve experiment, the 0 and 12 hour samples were submitted for MicroScan analysis at the Clinical Microbiology Laboratory at the University of Florida. Drugs that the particular clinical isolate of *P. aeruginosa* are

pre-resistance to are tabulated in Table 6-1. It appeared that *P. aeruginosa* is pre-resistance to many β-lactams, DNA inhibitor, antifolate, and tetracycline. Drugs belong to the susceptible and intermediate resistance classes are tabulated in Table 6-2. The drug class that appears to maintain effectiveness against the *P. aeruginosa* isolate is the aminoglycosides. The second kill-curve experiment evaluates the effects of gentamicin following the emergence of resistance.

Ciprofloxacin, Gentamicin, and Aztreonam Kill-Curves

The kill-curve profiles of the control group and drug treated groups are shown in Figure 6-3. The control group reached maximum growth of approximately 10^{11} CFU/mL. In this experiment, Groups 2 and 3 received ciprofloxacin as the first dose then ciprofloxacin at the same dose again or switch to 7 mg/kg gentamicin. Bacterial cell count was performed on only one of these two groups after the initial ciprofloxacin dose due to comparable values observed in the first kill-curve experiment. The 200 mg ciprofloxacin again showed no apparent drug effect after the second dose. However switching to gentamicin at the second dose achieved the necessary log-kill. This reduction of bacterial count is consistent with the MicroScan output that *P. aeruginosa* remained susceptible to gentamicin after ciprofloxacin exposure. The group that received aztreonam as the first and second dose showed the same loss of drug effect as observed for ciprofloxacin. However, the rate of growth after the second exposure was lower than that of ciprofloxacin or the control group.

The percentages of MIC changed from baseline for aztreonam are shown in Figure 6-4. By the 24^{th} hour, the MIC increased more than 25% from the baseline level. The MIC correlated with the same reduced drug effects as observed in the kill-curve experiment.

In this kill-curve experiment, MIC values were obtained for ciprofloxacin during the drug exposure period and continued for another 3 days in order to assess the post-antimicrobial effects. The MIC also showed a noticeable increase 6 hours after the initial ciprofloxacin exposure and increased 5-6 fold by 24 hours. By the second day after drug exposure, the MIC values had gradually been reduced to the pre-dose level (Figure 6-5). However, the E-strip test showed a heterogeneous *P. aeruginosa* population at 3 days post-dose, with colonies growing in the higher drug concentration zone (Figure 6-6). This laboratory observation indicates that new strains of *P. aeruginosa,* with higher MICs had emerged after ciprofloxacin treatment and remained within the population for days after drug had cleared.

Discussions/Conclusions

The first experiment examined the presence of a pre-resistance strain of *P. aeruginosa* to ciprofloxacin. If the particular clinical isolate is pre-resistance to ciprofloxacin, then the previous model found in the literature (Model 1 discussed in Chapter 3), which modeled two populations independently may be sufficient. However, since a pre-resistant population was not present, a new PKPD model capable of capturing the emergence of resistance over the course of drug treatment is warranted.

As described in Chapter 5, the compensatory mutation PKPD model was used to design kill-curve experiments that evaluate the emergence of resistant characteristics. Using the single dose data, the model predicted a loss of drug effect once the microbes were exposed to 200 mg ciprofloxacin *in vitro*. This was confirmed by the multiple dose kill-curve experiment; Once the resistance is developed, increasing the second ciprofloxacin dose by three-fold was insufficient to exhibit the same log-kill profile as observed after the first dose. Hence, the kill-curve confirms the model predictions. In

addition, the increase in MICs further supports the compensatory mutation PKPD model; Dormant hypothsis model claims the phenotypic variance may not change the MIC once the cellular activities resume after drug exposure.

Table 6-2 shows the alarming trend of several classes of susceptible antimicrobials to become resistant following exposure to ciprofloxacin. Most of these appear to be β-lactams. As observed from the kill-curve experiment, this particular clinical *P. aeruginosa* isolate was intermediately resistant to ceftriaxone prior to ciprofloxacin exposure, and advanced to fully resistant following ciprofloxacin exposure. The majority of clinical isolates of *P. aeruginosa* are pre-resistant to ceftriaxone. Ceftriaxone would not be a drug of choice for patients infected with *P. aeruginosa*.

Consistent with the pre-resistance strain experiment, the clinical isolate was susceptible to ciprofloxacin prior to drug exposure. Although a significant loss of drug effect was observed after ciprofloxacin treatment, the MicroScan results showed that clinical isolate was only an intermediate resistant strain after ciprofloxacin exposure.

The MicroScan also revealed that a microbe population with susceptible status prior to ciprofloxacin treatment was converted to full resistance after ciprofloxacin exposure. This proved true for several antimicrobials commonly prescribed for *P. aeruginosa* infections, including cefepime, imipenem, and piperacillin/tazobactam. These findings suggest β-lactams should be avoided once ciprofloxacin treatment fails. Aminoglycosides such as amikacin, gentamicin, or tobramycin, which were shown by MicroScan to retain susceptible status before and after ciprofloxacin exposure, should be used instead. The second kill-curve introducing gentamicin at the second dose

further confirms the effectiveness of this sequential dosing approach once ciprofloxacin resistance has emerged.

Beta-lactams and quinolones primarily enter the bacterial cell wall through the porin channels, which are located at the outer membrane of *P. aeruginosa* and are permeable to small aqueous compounds. Several porin channels have been identified. The most common, OprD, appears to be associated with imipenem resistance when it is altered. Since different antimicrobial agents may utilize different porin channels for cell entry, alteration of a particular porin channel may explain drug-specific failure, despite coming from the same class of antimicrobials. A strain that relies on altering membrane proteins may not be effective against aminoglycosides, which cross the outer membrane through lipopolysaccharide (LPS) uptake, rather than porin channels. Inevitably, *P. aeruginosa* can still prevents aminoglycoside entry through alteration of the LPS binding site[131].

The induction of drug resistance by ciprofloxacin is not class dependent. Treatment with a β-lactam such as aztreonam also showed a similar development of resistance as that observed with ciprofloxacin. This increase in response failure is also accommodated by the increase in aztreonam MIC. Besides reducing membrane permeability, β-lactams are often ineffective against *P. aeruginosa* because of their ability to upregulate the gene ampC, which codes for β-lactamase[132]. For other classes of antimicrobial agents, *P. aeruginosa* can also inactivate the drug product through phosphorylation, acetylation, or adenylation.

Post-antimicrobial evaluation reveals that the absence of drug influence leads to a reversal of the MIC values to approximately the pred-dose level. However, the visible

emergence of colonies with acquired resistance and restored fitness as described by the Compensatory Mutation hypothesis remain long after drug exposure. This observation suggests that once *P. aeruginosa* are exposed to ciprofloxacin, a biological memory is retained throughout the subpopulation that may render future treatment more difficult. If these characteristics were not recognized and the same fluoroquinolone or β-lactams were used to treat re-infection, treatment failure may occur. It appeared that aminoglycosides would be a preferred option for treating resistance that emerged from ciprofloxacin treatment.

The dose dependency of resistance emergence was not evaluated in this study. The 200 mg ciprofloxacin used to foster resistance development is considered a low clinical dose. It would be informative for future studies to evaluate the different initial dose levels on the development of resistance. In addition, it would be useful to evaluate the initial inoculation effects on the emergence of resistance in order to better understand the PKPD relationship. The relationship of each antimicrobial agent with a particular microbe species is difficult to predict and is currently not well understood. Future experiments extending this kill-curve approach to study emergence of resistance will provide important insight into drug-microbial resistance dynamic.

Table 6-1. The susceptibilities of *P. aeruginosa* used in the *in vitro* dynamic kill-curve before and after 200 mg ciprofloxacin treatment determined by MicroScan Gram Neg BP Combo 34 panel (list of pre-resistance antimicrobial agents).

Antimicrobial Agent	*P. aeruginosa* QC BREAKPOINT (ATCC 27853)	0 HR PREDOSE	12 HR CIPRO	SUSCEPTIBLE (S), INTERMEDIATE (I), RESISTANCE (R)
Beta-Lactams (2nd generation cephalosporin)				
Cefoxitin	>16	>16	>16	Pre-Resistance
Cefuroxime	>16	>16	>16	Pre-Resistance
Cefotetan	>32	>32	>32	Pre-Resistance
Cefazolin	>16	>16	>16	Pre-Resistance
Beta-Lactams (penicillin)				
Ampicillin	>16	>16	>16	Pre-Resistance
Ampicillin/Sulbactam	>16	>16	>16	Pre-Resistance
Beta-Lactams (carbapenem)				
Ertapenem	≤2 - >4	>4	>4	Pre-Resistance
DNA Inhibitor				
Nitrofurantoin	>64	>64	>64	Pre-Resistance
Polyketide				
Tetracycline	8	>8	>8	Pre-Resistance
Antifolate				
Trimethoprim/Sulfamethoxazole	8	>2	>2	Pre-Resistance
Carboxypenicillin				
Ticarcillin/K Clavulanate	≤16	≤16	≤16	Pre-Resistance

Table 6-2. The susceptibilities of *P. aeruginosa* used in the *in vitro* dynamic kill-curve before and after 200 mg ciprofloxacin treatment determined by MicroScan Gram Neg BP Combo 34 panel.

Antimicrobial Agent	*P. aeruginosa* QC BREAKPOINT (ATCC 27853)	0 HR PREDOSE	12 HR CIPRO	SUSCEPTIBLE (S), INTERMEDIATE (I), RESISTANCE (R)
Piperacillin/Tazobactam	≤16	≤16	64	S to R
Beta-Lactams (carbapenem)				
Meropenem	≤4	≤4	≤4	S TO S
Imipenem	≤4	≤4	>8	S TO R
Beta-Lactams (3rd generation cephalosporin)				
Ceftriaxone	8-64, BP >32	32	>32	I TO R
Cefotaxime	≤8	16	32	I TO R
Ceftazidime	≤8	4	16	S TO I
Beta-Lactams (4th generation cephalosporin)				
Cefepime	≤8	≤8	>16	S TO R
Beta-Lactams (monobactam)				
Aztreonam	≤8	≤8	>16	S TO R
Aminoglycosides				
Amikacin	≤16	≤16	≤16	S TO S
Gentamicin	≤4	≤4	≤4	S TO S
Tobramycin	≤4	≤4	≤4	S TO S
Fluoroquinolone				
Ciprofloxacin	≤1	≤1	2	S TO I
Levofloxacin	≤2-4	≤2	≤2	S TO S

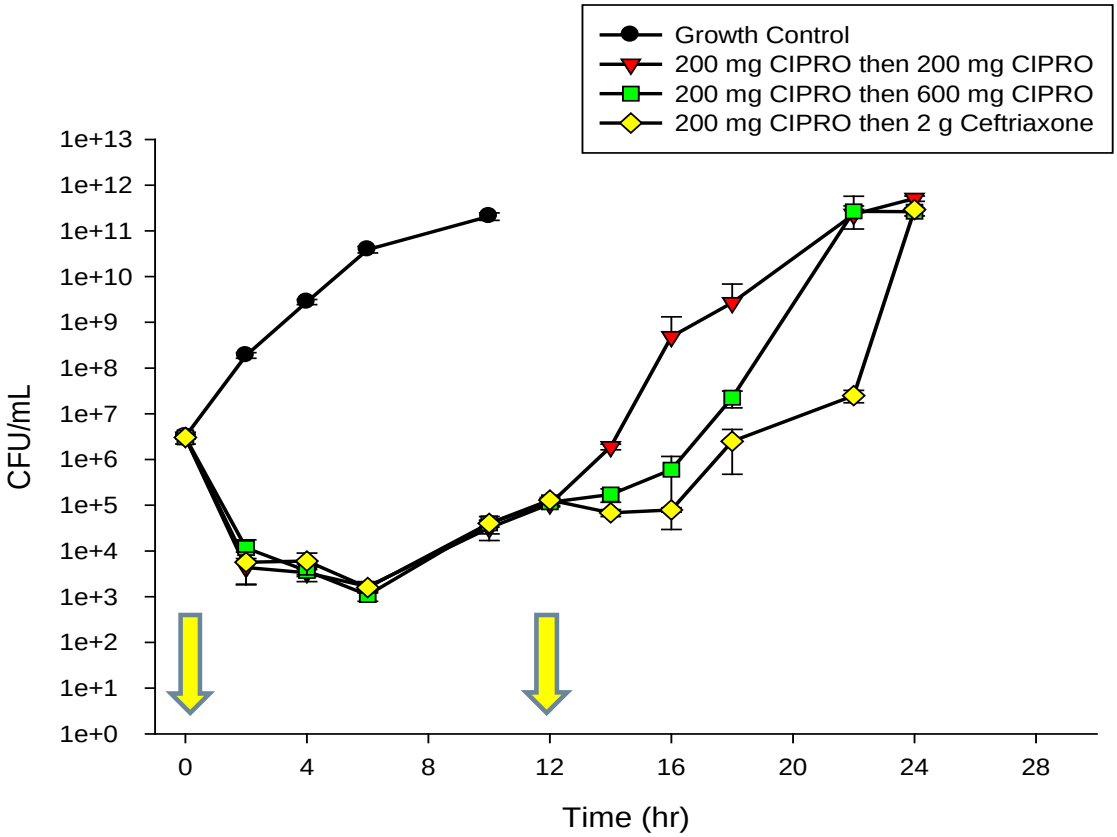

Figure 6-1. *In vitro* dynamic kill-curves involving saline control, ciprofloxacin and ceftriaxone. Arrows indicate dosing.

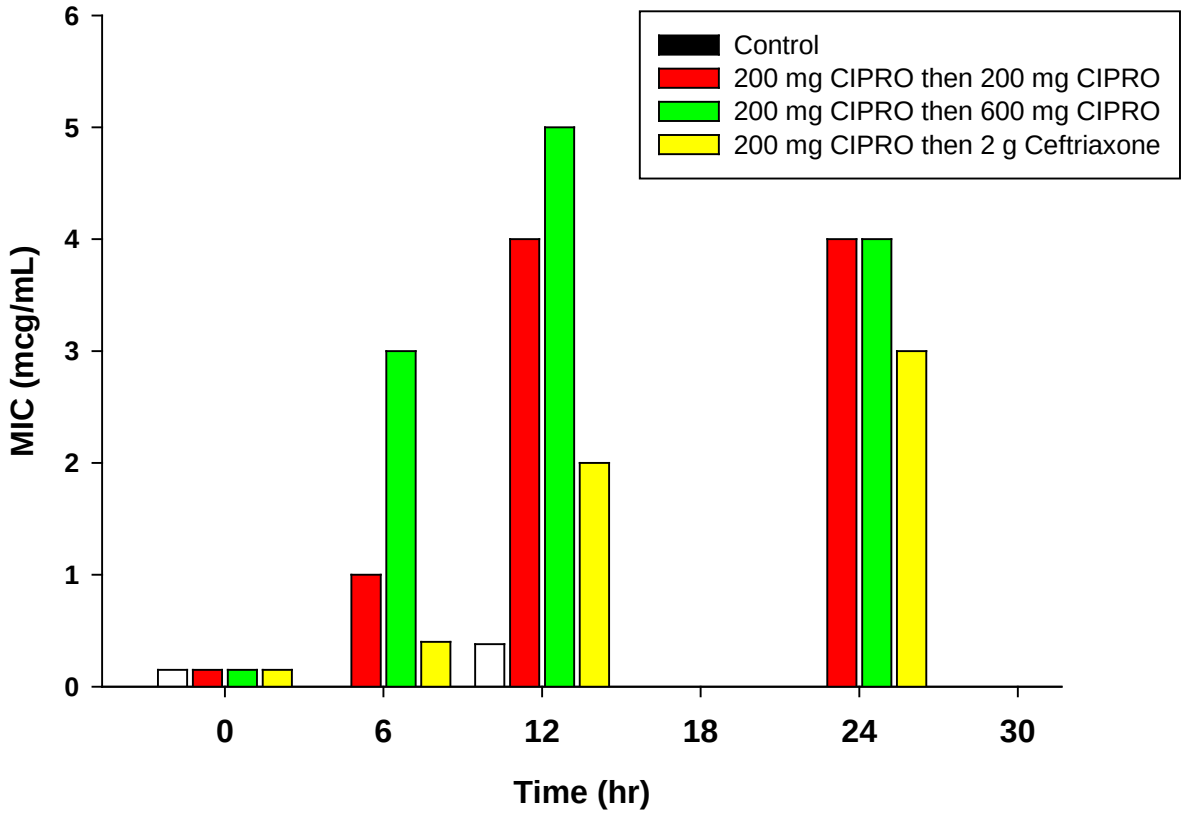

Figure 6-2. Ciprofloxacin MIC dynamics corresponding to the kill-curve experiment in Figure 6-1.

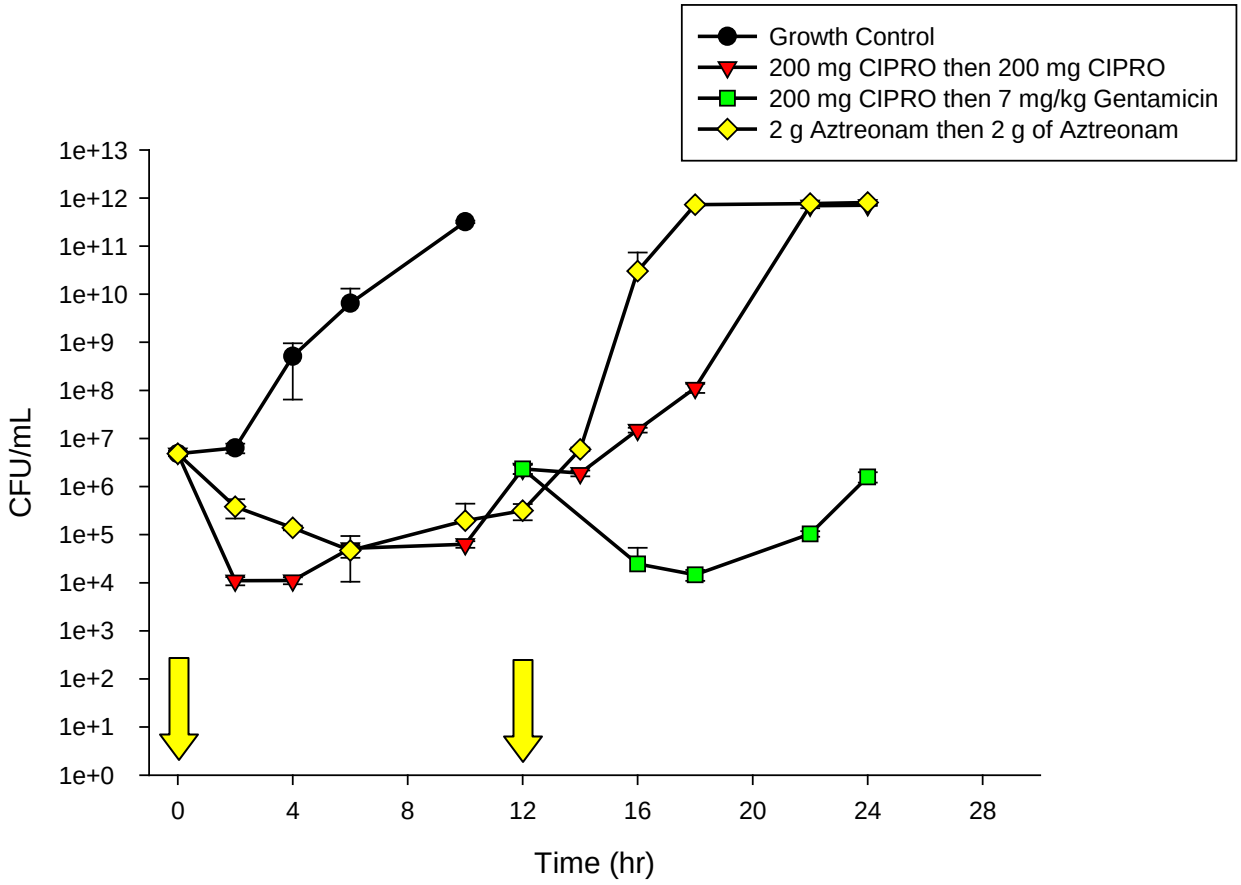

Figure 6-3. *In vitro* dynamic kill-curves involving saline control, ciprofloxacin, gentamicin, and aztreonam. Arrows indicate dosing.

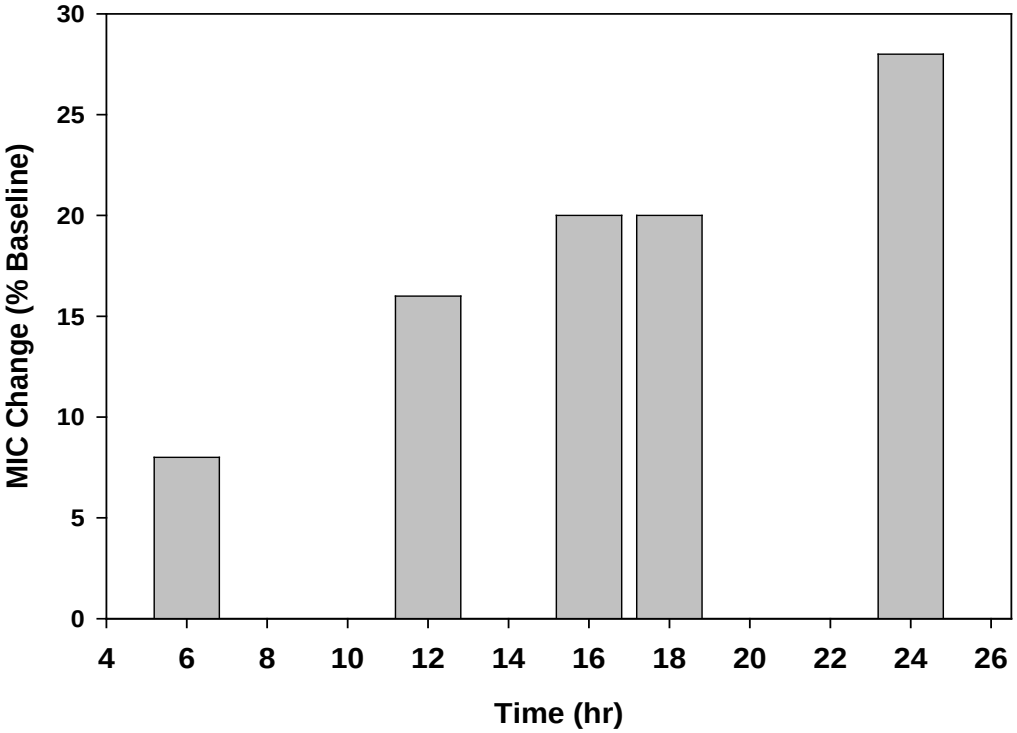

Figure 6-4. Aztreonam MIC dynamic corresponding to the kill-curve experiment in Figure 6-3.

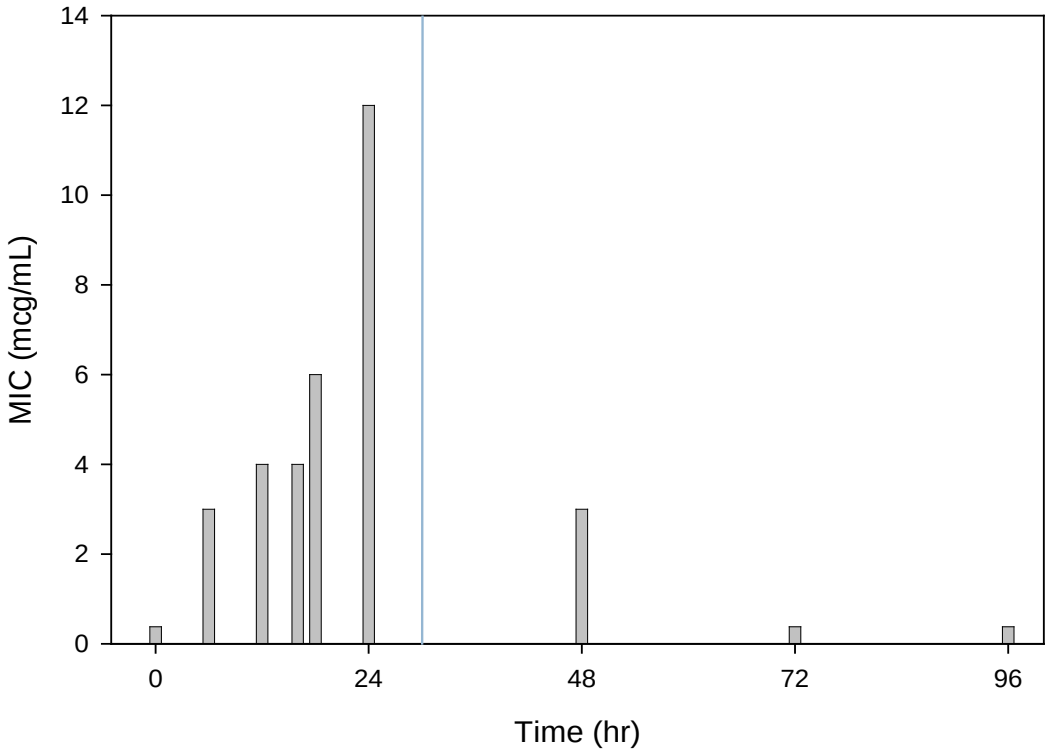

Figure 6-5. Ciprlfoxacin MIC dynamic corresponding to the kill-curve experiment in Figure 6-3. The line after 24 hour separates the dosing period and the post antibiotic period.

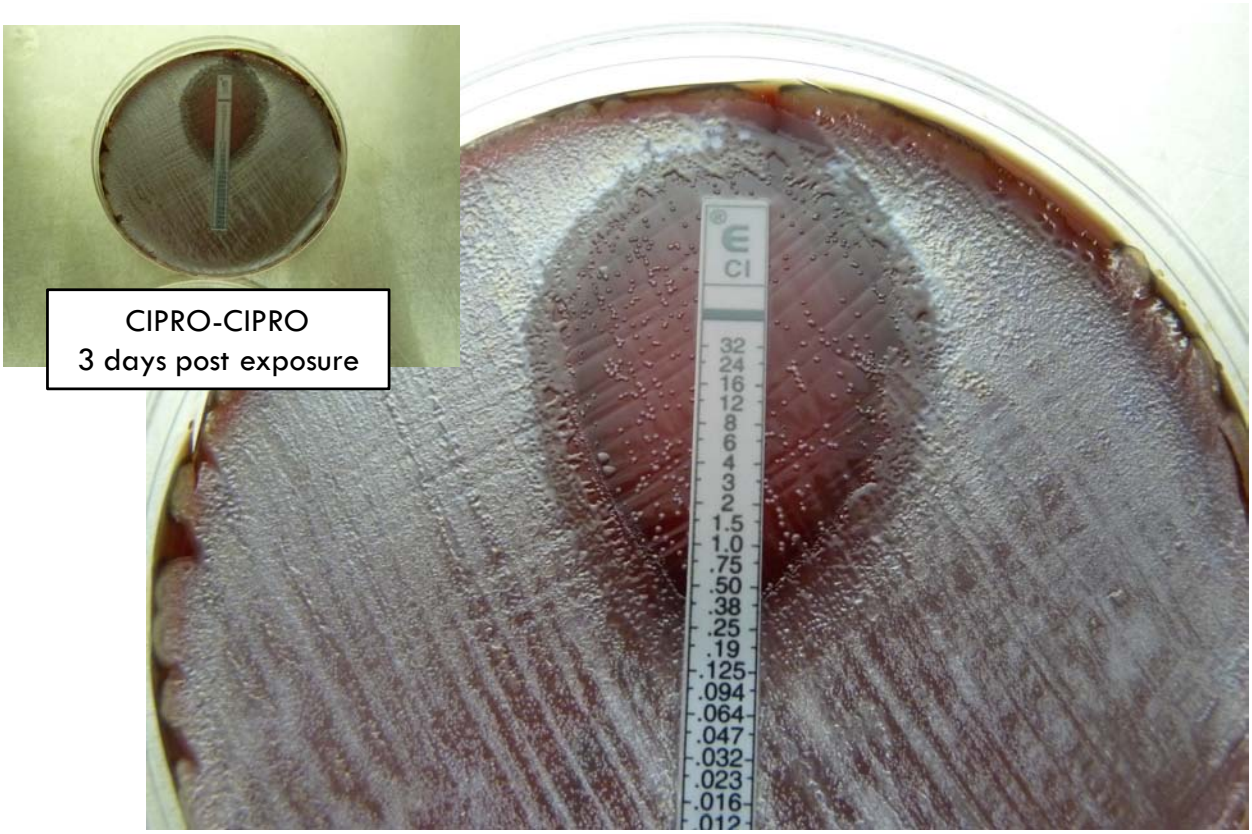

Figure 6-6. Ciprofloxacin E-strip test for MIC determination 3 days post the last ciprofloxacin exposure (96 hr). Visible colony growth was observed in the high ciprofloxacin concentration zone, which was not present in the pre-treatment samples. The overall MIC was recorded as 0.38 µg/mL.

CHAPTER 7
POPULATION PHYSIOLOGICALLY-BASED PHARMACOKINETIC MODEL OF CEFTOBIPROLE IN HEALTHY VOLUNTEERS

Introduction

Methicillin-resistant Staphylococcus aureus (*MRSA*) are resistant to most of the currently available β-lactam antimicrobials[133-136]. Ceftobiprole is a 5th generation cephalosporin for treating skin and soft tissue infections caused by either gram-negative or gram-positive bacteria. It has bactericidal properties against *MRSA* because of its resistant characteristics to staphylococcal β-lactamase. Ceftobiprole target *MRSA* by binding to PBP2a, which is encoded by the *mecA* gene of β-lactam-resistant *MRSA*[137, 138]. It is also effective against *S. pneumoniae* and *P. aeruginosa*[139]. Moreover, ceftobiprole is well tolerated and has reported only minor adverse effects; nausea, vomiting and headaches in clinical trials[140, 141].

It's a common practice to measure and use total plasma concentrations for PK or PKPD evaluations. However this approach, though convenient, ignores the following two important facts: (1) The free fraction of the drug is responsible for the observed pharmacological response. Therefore measuring free drug concentrations is more meaningful than using total drug concentrations in plasma. (2) The measured drug concentrations in plasma may not always represent drug concentrations at the site of action. For drugs like ceftobiprole, used for treating skin and skin structure infections, the time-course of free drug concentrations at target sites can be measured using microdialysis technique. For ceftobiprole, two microdialysis probes placed onto skeletal muscle and subcutaneous adipose tissue provided accurate representation of the drug's availability at its target site in humans.

Traditionally, physiologically-base pharmacokinetic (PBPK) models are developed in animals for extrapolation to predict human exposure. It is possible to predict human tissue concentrations of a drug by utilizing the known physico-chemical characteristics of the drug and available animal data. However it is advisable to use information on human tissue distribution, if available, for building a reliable PBPK model. Microdialysis, though not suitable for all tissues in clinical settings, is ideal for measuring drug distribution in adipose and muscle tissues. It also provided an unique opportunity for population PBPK model to gain insights into the population variance which is informative in predicting population target attainment rate. In this paper, we describe a population PBPK model for ceftobiprole using microdialysis data from muscle and adipose tissues and free drug concentrations measured in plasma. The Pop-PBPK model was then employed to assess the drug's exposures at the target sites using different dosing strategies.

Method

Study Design

The details of the study design have been previously published[72]. The study was conducted at the General Clinical Research Center at Shands Hospital at University of Florida (Gainesville, FL). The age of the subjects (6 males and 6 females) ranged from 20 to 34 years and no subject received any other drug treatment for at least a week prior to the study. Subjects received single dose of 500 mg ceftobiprole infused intravenously over 2 hours. Microdialysis samples were collected from skeletal muscle and subcutaneous adipose tissue according to a previously developed method[142]. Briefly, the microdialysis probes implanted into subcutaneous adipose and muscle tissues were perfused with lactated Ringer's solution at a flow rate of 1.5 µL/min.

Dialysate samples were collected at pre-dose, every 20 min for 12 hours after the start of infusion and at 16 and 24 hours post dose. Retrodialysis was performed according to Stahle et al 1991[143] as a calibration measure to calculate true tissue interstitial fluid (ISF) concentrations of Ceftobiprole. Samples were collected without anesthetics to prevent drug-drug interactions. Blood samples were collected into EDTA containing tubes at predose, 40 min, and 1, 1.6, 2, 2.3, 3, 4, 6, 8, 12, 16, and 24 hours after the start of infusion for plasma Ceftobiprole concentration determination. Additional blood was samples were collected at 2 and 12 hours for protein binding determination. A validated high performance liquid chromatography with UV detection method with a limit of quatitation (LOQ) of 0.1 µg/mL was used to determine drug concentrations from the microdialysis samples. A validated liquid chromatography tandem mass spectrometry with a LOQ of 0.05 µg/mL was used to determine total plasma drug concentrations. The noncompartmental parameters published previously are shown in Table 7-1 for comparisons.

PBPK Model

Individual tissue volumes and blood flow were used for building the PBPK model. The physiological parameters for cardiac output, blood perfusion and organ weights for both male and females were obtained from Williams and Leggett (1989)[144] and the relevant values used in the model are summarized in Table 7-2. The body surface for each subject was first calculated using DuBois & DuBois method[145]: BSA (m^2) = 0.20247 x Height $(m)^{0.725}$ x Weight $(kg)^{0.425}$. Individual blood perfusion rate were then calculated as $BSA_i/BSA_{average}$*organ $mass_{average}$*blood $perfusion_{average}$*60 mins/1000. Individual cardiac output was calculated as $BSA_i/BSA_{average}$*blood $flow_{average}$*60 mins/1000 (Table 7-3). Assuming the density of the tissue and blood to be 1 kg/m^3,

individual organ mass were calculated as $BSA_i/BSA_{average}$*organ $mass_{average}$ (Table 7-4). All values were then converted to plasma flow to match the free drug concentrations in plasma. The plasma flow rates and tissue weights obtained from the literature for males and females are shown in Figure 7-2. Subject-specific plasma flow rates and tissues weight were calculated as discussed above and presented in Figure 7-3.

A diagrammatic representation of the PBPK model is shown in Figure 7-1. The cardiac output distributes plasma to muscle, subcutaneous (S.C.) adipose tissue, kidneys, and remainders (the rest of the body besides the ones aforementioned) with the organ specific plasma flow rates (QM, QF, QK, and QR, respectively). The QR is calculated as plasma flow of cardiac output minus the sum of plasma flow rate from other compartments (QM+QF+QK). Similarly, the remainder volume is calculated as total body volume minus other tissue volumes used for the PBPK model. The outflow of plasma from the compartments becomes the input of the plasma compartment. Ceftobiprole is predominantly cleared by the kidneys (80%)[146], hence, it was assumed to be cleared only from the kidney compartment. The equations used for the PBPK model are listed below:

$$\frac{dFP}{dt} = \left(\sum \frac{QT*CT}{KpT} - QCO * FP\right)/Vp \qquad \textit{IC = 500 mg } IV_{inf} \textit{ over 2 hr} \quad (7\text{-}1)$$

$$\frac{dM}{dt} = \left(QM * FP - QM * \frac{M}{KPM}\right)/VM \qquad \textit{IC = 0} \quad (7\text{-}2)$$

$$\frac{dF}{dt} = \left(QF * FP - QF * \frac{F}{KPF}\right)/VF \qquad \textit{IC = 0} \quad (7\text{-}3)$$

$$\frac{dK}{dt} = \left(QK * FP - QK * \frac{K}{KPK}\right)/VK \qquad \textit{IC = 0} \quad (7\text{-}4)$$

$$\frac{dR}{dt} = \left(QR * FP - QR * \frac{R}{KPR}\right)/VR \qquad \textit{IC = 0} \quad (7\text{-}5)$$

where dFP/dt, dM/dt, dF/dt, dK/dt, and dR/dt describe the time courses of unbound ceftobiprole concentrations in plasma, skeletal muscle, subcutaneous adipose tissue, kidney, and remainder compartments, respectively, CO is the cardiac output, and Q, V, and K_P are the plasma flow, tissue volume, and partition coefficient for the tissues. The partition coefficient in this case isn't a true measurement of ceftobiprole partition into tissue sites due to insufficient knowledge of protein binding and other biochemical factors occurring between plasma and tissue sites.

The population PBPK model was developed using Monolix software (INRIA, France). The estimated model parameters were tissue partition coefficients, ceftobiprole clearance, inter-subject variabilities (ω) and residual errors (σ). Intersubject variabilities were initially added to all parameters and then any estimates less than 10^{-5} were removed from the final model. Addition of inter subject variability on parameters that failed to improve VPCs were excluded. The final model included ω on volumes of plasma, skeletal muscle, subcutaneous adipose tissue, and kidneys, and on partition coefficient of skeletal muscle, subcutaneous adipose tissues, kidneys, and remainders, and on the clearance parameters (a total of 9 ω for the final model). Residual error was defined by a proportional error model in the final PBPK model. In Monolix, a random seed and automatic iteration design was selected. The visual predictive check was produced from 1000 simulations. Variances of the random effects and stochastic approximation of the standard errors were selected. The log-likelihood was estimated by linearization and fisher-matrix estimation was selected to generate standard errors of parameter estimates.

Since the available data had only single dose level, further model evaluation was performed by simulating a new random data set using the final model and fitting the simulated data set to the model to compare the parameter estimates. Monte Carlo simulations (n=1000 per group) was performed to evaluate the 90% population target attainment rate when time of drug concentration above MIC (T>MIC) at least 25% or 50% of dosing intervals for 500, 400, 300, and 250 mg doses. In addition, 2 hour infusion versus 1 hour infusion for the 500 and 400 mg dose levels were also evaluated.

Results

The diagnostic plots for the final model are shown in Figures 7-2 to 7-7. The population predicted versus observed values (Figure 7-2) shows that for each tissue, the values were evenly spread alone the line of unity. The distribution alone the line of unity decreased for individual predictions in all three tissues (Figure 7-3). No systemic bias was observed when comparing the weighted residual population means versus the population predicted values (Figure 7-4). The visual predictive checks showed that the majority of the observations from all three tissues were evenly distributed within the predicted 90^{th} percentiles with the predicted median centering the observation distributions (Figures 7-5 to 7-7).

The diagnostic plots from modeling the simulated data are shown in Figures 7-8 to 7-13. The simulated data contain a wider distribution compared to that of the original data set. This resulted in a larger spread of data variability compared to that of the original dataset. As expected, the ω and σ were larger when modeling simulated data compared to observed data. Nonetheless, the VPCs showed a reasonable model prediction in all three tissues (Figures 7-11 to 7-13). In addition, model parameter estimates between the two approaches were similar (Table 7-5).

The current dataset consists of small sample size with minimal age and body weight distributions. Hence, no covariate analysis was added to the model. Nonetheless the effects of demographics on PBPK parameters were plotted for visual inspections in Figure 7-14.

Monte Carlo simulations (n=1000 per group) were performed to evaluate target attainment rates. Time of ceftobiprole concentrations above MIC for at least 25% of dosing interval has been shown to achieve desirable clinical outcome. For immune compromised subjects, a stricter criterion was recommended (T>MIC at 50% of dosing interval). Using the criterion of 90% population target attainment rate, Figure 7-15 plots the outcome in all three tissues for doses ranging from 500 mg to 250 mg. To simulate the effects of resistance development on the target attainment rate, scenarios at which the MIC increased from 1 µg/mL to 2 or 4 µg/mL were evaluated. When MIC = 1 µg/mL, it appeared that 500 mg, the standard dose, achieved the target for all three tissues. Reducing the dose to 400 mg was borderline sufficient in the adipose tissue compartment using the T>MIC 50% of dosing interval criteria. If the MIC increased to 2 µg/mL, the desired target attainment for 90% of population would only be reached for 500 and 400 mg doses using the T>MIC of 25% criteria. If the MIC increased to 4 µg/mL, target attainment would not be reached for any of the dose groups in adipose tissues, even though it would be achieved in plasma tissue.

Reducing the intravenous infusion time from 2 hours to 1 hour was also evaluated for target attainment. Figure 7-16 shows that without resistant development (MIC = 1 µg/mL), 500 and 400 mg dose groups can achieve the 90% population target using the T>MIC 25% criteria. However, at T>MIC 50% criteria, only the 500 mg dose was

sufficient. If increased in MIC occurred, insufficient free drug concentrations would be available to adipose tissue.

Figure 7-17 shows the diagram of combing the PBPK model with the mechanism-based PD model developed for emergence of resistance. The drug concentration profiles of Ceftobiprole in plasma, muscle, and adipose tissues were simulated to evaluate the PD profiles in case of resistance development. The growth (k_s) and degradation (k_d) rate constants and drug effects (S_{max}, SC_{50}) of Ceftobiprole in *MRSA* were obtained from[86]. The PD profiles in these three tissues without resistance development are shown in Figures 7-18. Alteration of dose levels and inoculation levels are shown in Figure 7-19. In case of resistance development, the PD profiles are simulated to evaluate various degrees of doses, inoculations, and resistance development (Figure 7-20).

Conclusions/Discussions

The drug concentration time course of ceftobiprole collected from tissue sites using microdialysis techniques in human provided a unique opportunity for clinical population PBPK modeling. The final model described the unbound drug concentrations in the plasma, skeletal muscle and subcutaneous adipose tissues reasonably well. Diagnostics plots and visual predicted checks were used to select the appropriate final model with inter-subject variability (ω). The clearance from the kidneys estimated from the PBPK model was similar to that of plasma clearance from the noncompartmental analysis, confirming ceftobiprole is eliminated mainly by the kidneys (5.46 L/hr from PBPK model versus 5.15 L/hr from noncompartmental analysis). The high partition coefficient of ceftobiprole to kidneys also contributed to the similarity. In addition, the partition coefficient values for muscle and adipose tissues estimated from

the PBPK model correlated well with the unbound tissue-plasma ratios (0.70 and 0.44 for muscle and adipose tissue from PBPK model versus 0.69 and 0.49 from $fAUC_{tissue}/fAUC_{plasma}$).

The model revealed that if resistance occurs (MIC increased from 1 to 4 µg/mL), unbound drug concentrations at the site of action would be insufficient with the standard dose of 500 mg administered by intravenous infusion over 2 hours. A higher or more frequent dose may be needed to achieve the desired dose levels at the relevant tissue sites.

In summary, using microdialysis probes in human tissues allows direct measurement of free drug concentrations in relevant tissue sites. In the majority of the clinical cases, where only plasma samples were collected, a false conclusion may be drawn for optimal dosing scheme. If tolerable, one hour instead of two hour IV infusion may be used for the standard dose of 500 mg. In the case of resistance development, a higher or more frequent dose may be needed. The PBPK model combined with mechanism-based PD model further provided insights into the drug effects in case of resistance emergence. These simulations provided insightful PKPD relationships and allowed adjustment of dosing strategies in case of resistant development.

Table 7-1. Mean and standard deviation (n=12) of noncompartmental parameters of ceftobiprole in healthy volunteers.

PK Parameter	Plasma (total)	Muscle	S.C. Adipose
Cmax (mg/L)	25.8 ± 2.96	14.0 ± 3.22	9.61 ± 4.74
Tmax (hr)	1.92 ± 0.15	2.25 ± 0.14	2.25 ± 0.21
t1/2 (hr)	2.61 ± 0.33	2.61 ± 0.52	2.56 ± 0.39
AUCt (hr*mg/L)	97.1 ± 10.3	50.6 ± 10.9	34.3 ± 19.0
AUCinf (hr*mg/L)	98.0 ± 10.5	53.2 ± 11.5	36.5 ± 19.4
CL (L/hr)	5.15 ± 3.61	na	na
Vss (L)	14.6 ± 2.17	na	na
AUC,tissue/AUC,plasma	na	0.69 ± 0.13	0.49 ± 0.28

Note: Values are mean ± SD from noncompartmental anlaysis

Table 7-2. Gender-specific plasma flow rate and tissue weights obtain from literature for the PBPK model.[144]

	Plasma Flow Rate		Tissue Weight	
	Male (mL/kg/min)	Female (mL/kg/min)	Male (kg)	Female (kg)
Muscle	38	38	30	18
Adipose Fat	28	28	12.5	17.5
Kidney	4000	3500	0.31	0.275
Muscle	38	38	30	18
Remainder	2634	2234	30.19	24.2
CO	6700	5800	na	na

Table 7-3. Individual plasma flow rate calculated based on proportion of body surface area to standard values presented in Table 7-2.

Subject ID	Total Body Weight (kg)	Gender	Height (cm)	Q Fat (L/hr)	Q Kidney (L/hr)	Q Muscle (L/hr)	Q remainder (L/hr)	QCO (L/hr)
1	80.1	M	179.1	22.2	78.8	72.4	5051	426
2	68.2	F	171.2	32.6	64.1	45.6	3606	386
3	75.3	M	177.8	21.5	76.3	70.2	4894	412
4	64	F	169.7	31.6	62.0	44.1	3487	374
6	59.9	F	171.5	30.9	60.8	43.2	3417	366
7	76.3	M	180.3	21.9	77.5	71.3	4972	419
8	72.8	F	162.6	32.3	63.5	45.1	3571	383
9	76.9	F	167.6	33.8	66.5	47.2	3736	400
10	76.9	M	170.2	21.1	74.6	68.6	4784	403
12	63.5	M	179.8	20.2	71.6	65.8	4589	387
14	56.7	F	160.0	28.7	56.4	40.1	3174	340
15	78.4	M	184.4	22.5	79.7	73.3	5112	431
Mean	70.8	6m/6f	173	26.6	69.3	57.2	4199	394
SD	7.96	na	7.51	5.44	8.02	13.8	755	26.5

Table 7-4. Individual tissue volume calculated based on proportion of body surface area to standard values presented in Table 7-2.

BSA (m^2)	Fat Volume (L)	Kidney Volume (L)	Muscule Volume (L)	Remainder Volume (L)	Plasma Volume (L)
1.99	13.2	0.328	31.8	32.0	7.09
1.80	19.4	0.305	20.0	26.9	6.44
1.93	12.8	0.318	30.8	31.0	6.87
1.74	18.8	0.295	19.3	26.0	6.23
1.70	18.4	0.289	18.9	25.5	6.10
1.96	13.0	0.323	31.3	31.5	6.98
1.78	19.2	0.302	19.8	26.6	6.38
1.86	20.1	0.316	20.7	27.9	6.67
1.89	12.5	0.311	30.1	30.3	6.72
1.81	12.0	0.298	28.9	29.0	6.44
1.58	17.1	0.269	17.6	23.7	5.67
2.01	13.4	0.332	32.1	32.3	7.18

Note: BSA calculated using DuBois formula: BSA (m^2) = 0.20247 x Height(m)$^{0.725}$ x Weight(kg)$^{0.425}$

Table 7-5. Population PBPK parameter estimates.

Model Estimates		
Parameter Description	Observed Data (%RSE)	Simulated Data (%RSE)
K_{PM}, Muscle Partition Coefficient	0.703 (5%)	0.733 (5%)
K_{PF}, Fat Partition Coefficient	0.436 (18%)	0.264 (19%)
K_{PR}, Remainder Partition Coefficient	0.505	0.569
K_{PK}, Kidney Partition Coefficient	0.604	0.393
Plasma Clearance (L/hr)	5.46 (41%)	6.42
$\omega_{Plasma\ Volume}$	0.0118 (47%)	0.0171 (63%)
$\omega_{Muscle\ Volume}$	0.430 (50%)	0.485 (51%)
$\omega_{Fat\ Volume}$	0.328 (64%)	0.103 (249%)
$\omega_{Kidney\ Volume}$	0.205 (52%)	0.0425 (127%)
ω_{KPM}	0.0270 (73%)	0.0214 (75%)
ω_{KPF}	0.365 (44%)	0.403 (41%)
ω_{KPR}	0.185 (85%)	0.0299 (84%)
ω_{KPK}	0.0724 (186%)	0.0251
ω_{CL}	0.316	0.0905 (218%)
$\sigma_{Plasma\ Proportional\ Error}$	0.198 (18%)	0.326 (7%)
$\sigma_{Muscle\ Proportional\ Error}$	0.119 (9%)	0.356 (4%)
$\sigma_{Fat\ Proportional\ Error}$	0.145 (6%)	0.271 (4%)

%RES = percent relative standard error; ω is the intersubject variability, σ is he proportional error variance.

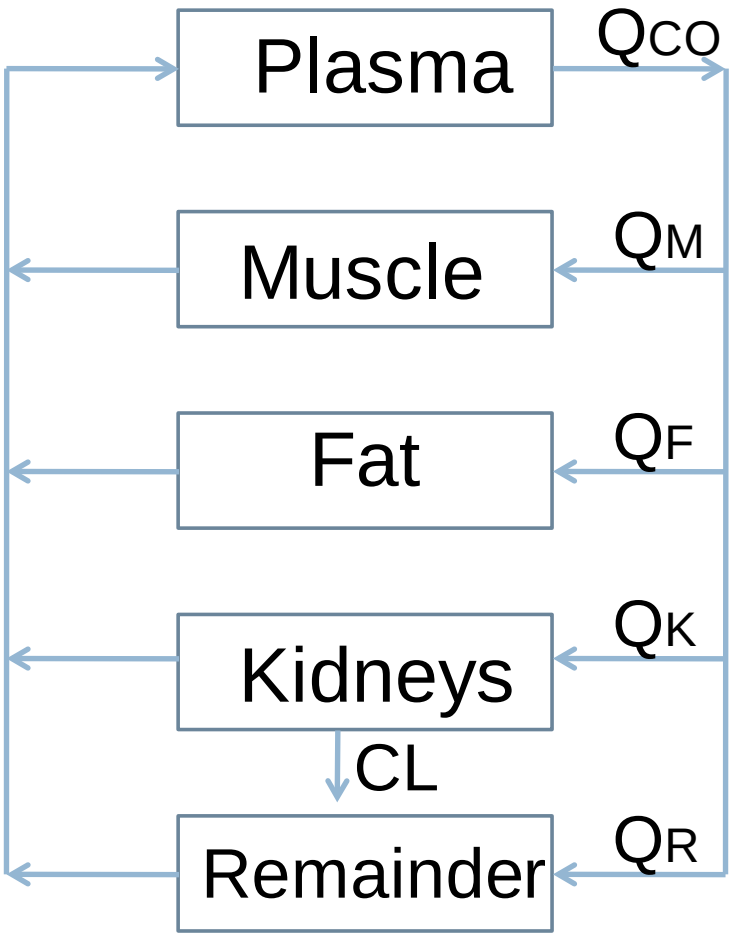

Figure 7-1. Physiologically-Based Pharmacokinetic (PBPK) model. Co = plasma cardio output; M = muscle; F = fat; K=kidney; R = remainder; FP = free plasma; Q = plasma flow; K_P = tissue partition coefficient; CL = clearance; V = volume.

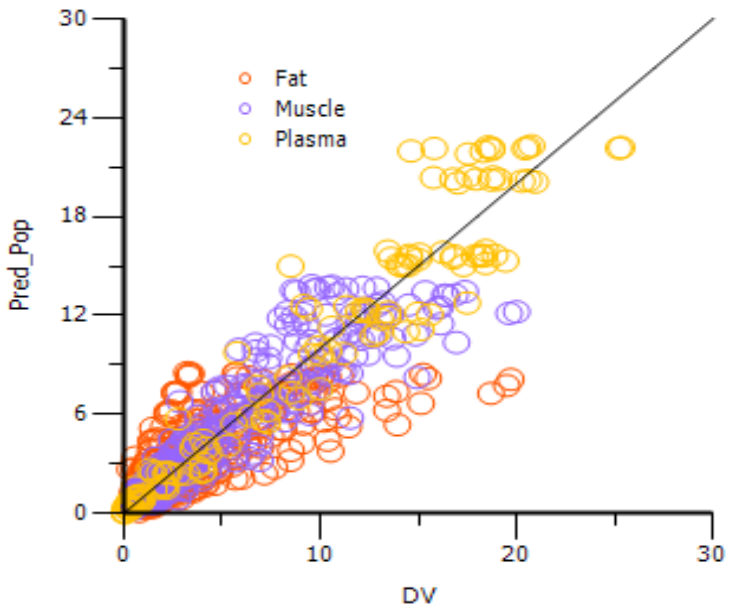

Figure 7-2. Diagnostic plot of modeling the observed data: Population predicted versus observed (DV) values for plasma (yellow), muscle (blue) and fat (red).

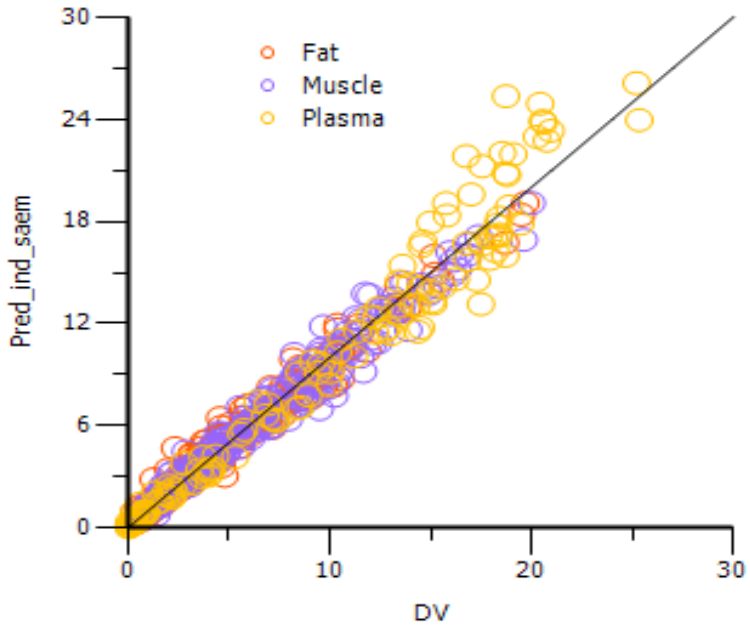

Figure 7-3. Diagnostic plot of modeling the observed data: Individual predicted versus observed (DV) values for plasma (yellow), muscle (blue) and fat (red).

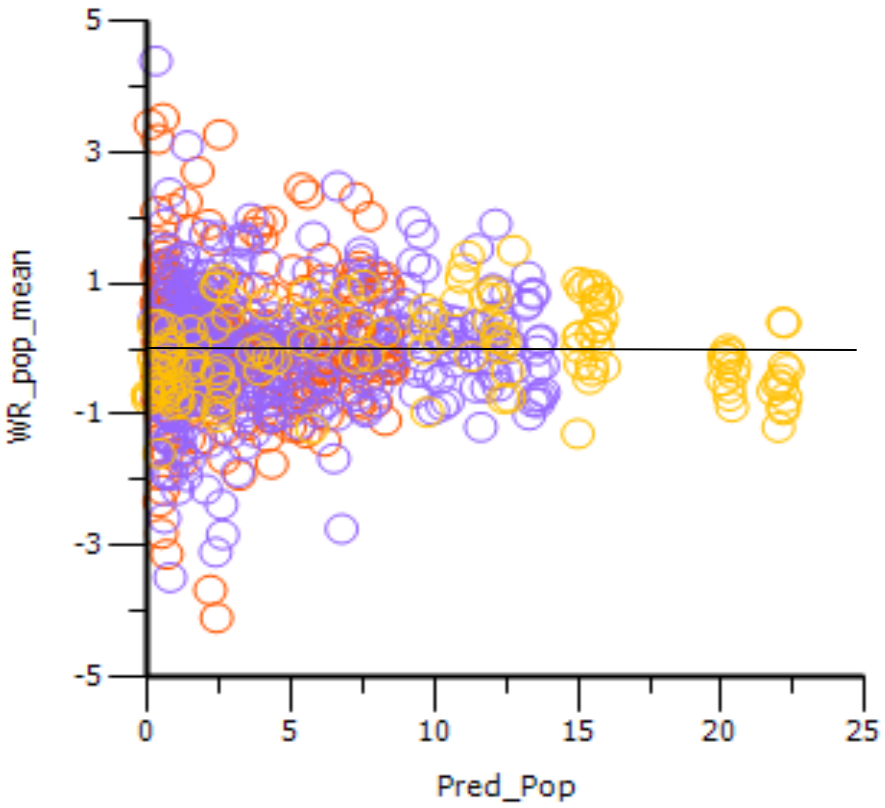

Figure 7-4. Diagnostic plot of modeling the observed data: Weighted residual of population mean versus population predicted values for plasma (yellow), muscle (blue) and fat (red).

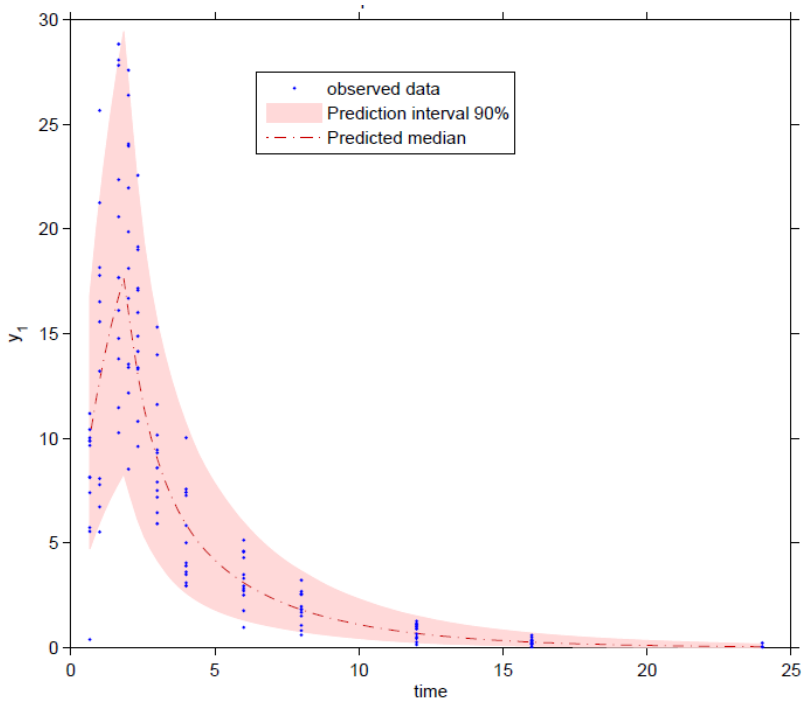

Figure 7-5. Diagnostic plot of modeling the observed data: Visual predictive checks of unbound ceftobiprole concentrations in plasma.

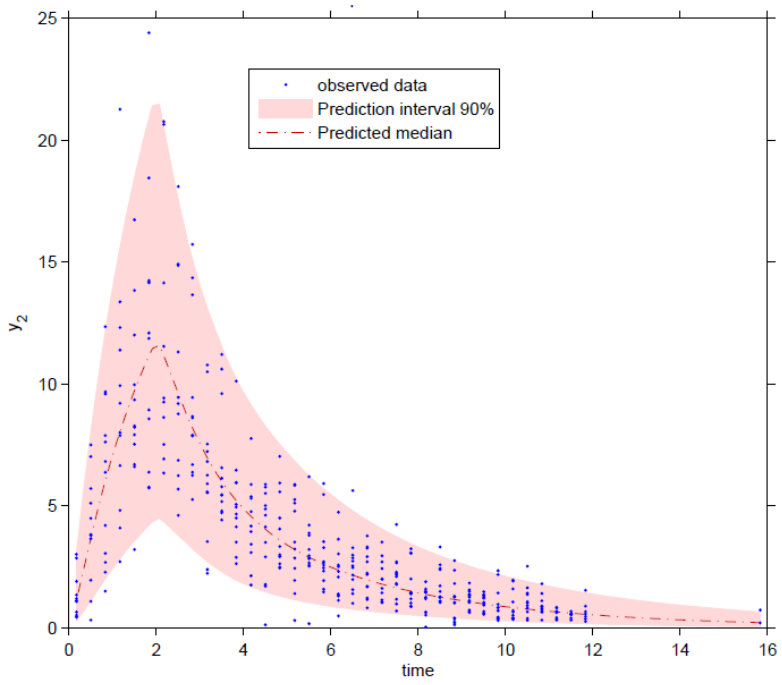

Figure 7-6. Diagnostic plot of modeling the observed data: Visual predictive checks of unbound ceftobiprole concentrations in skeletal muscle.

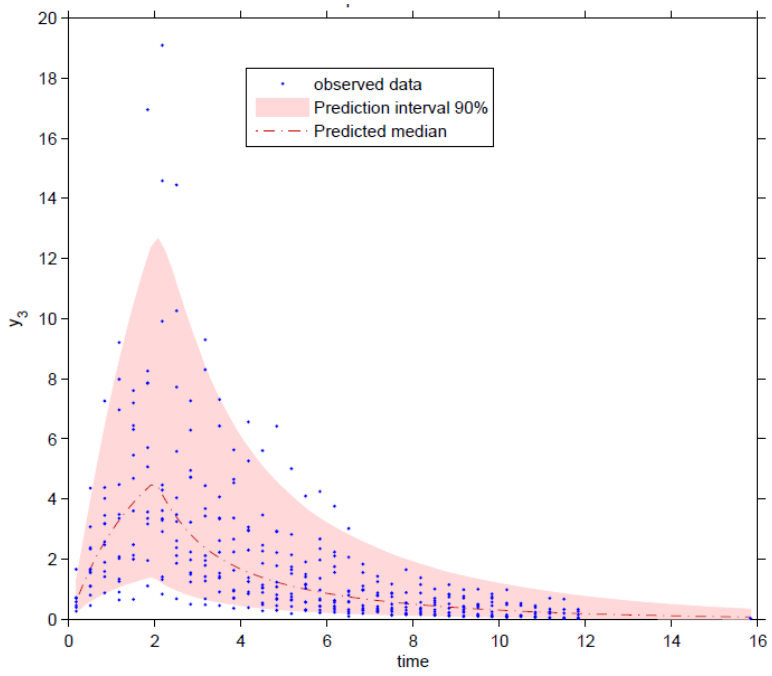

Figure 7-7. Diagnostic plot of modeling the observed data: Visual predictive checks of unbound ceftobiprole concentrations in subcutaneous adipose fat.

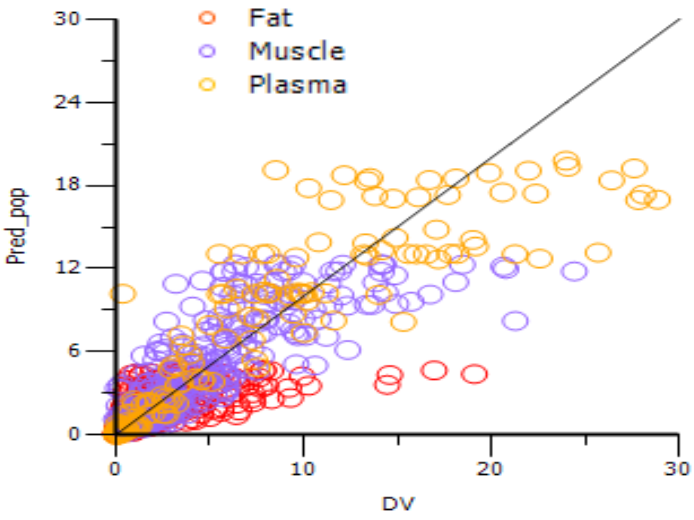

Figure 7-8. Diagnostic plot of modeling the simulated data: Population predicted versus observed (DV) values for plasma (yellow), muscle (blue) and fat (red).

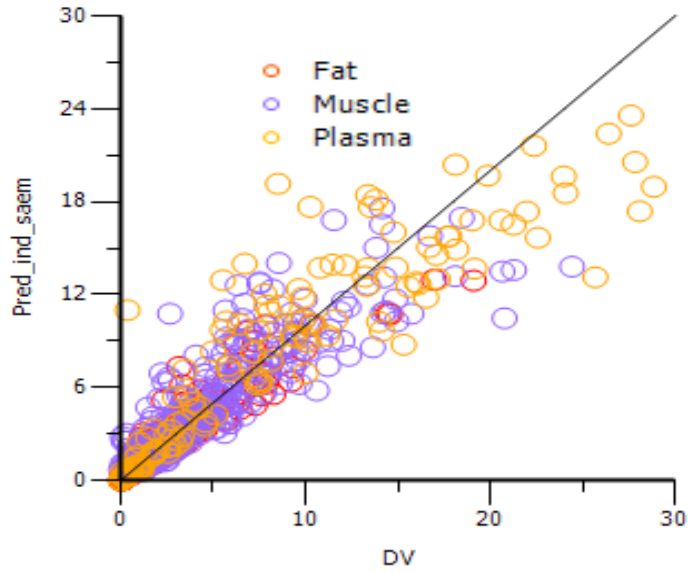

Figure 7-9. Diagnostic plot of modeling the simulated data: Individual predicted versus observed (DV) values for plasma (yellow), muscle (blue) and fat (red).

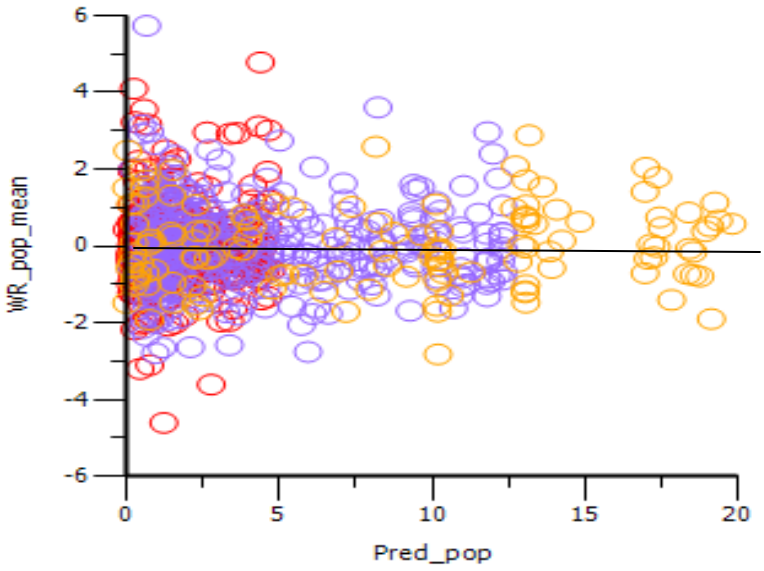

Figure 7-10. Diagnostic plot of modeling the simulated data: Weighted residual of population mean versus population predicted values for plasma (yellow), muscle (blue) and fat (red).

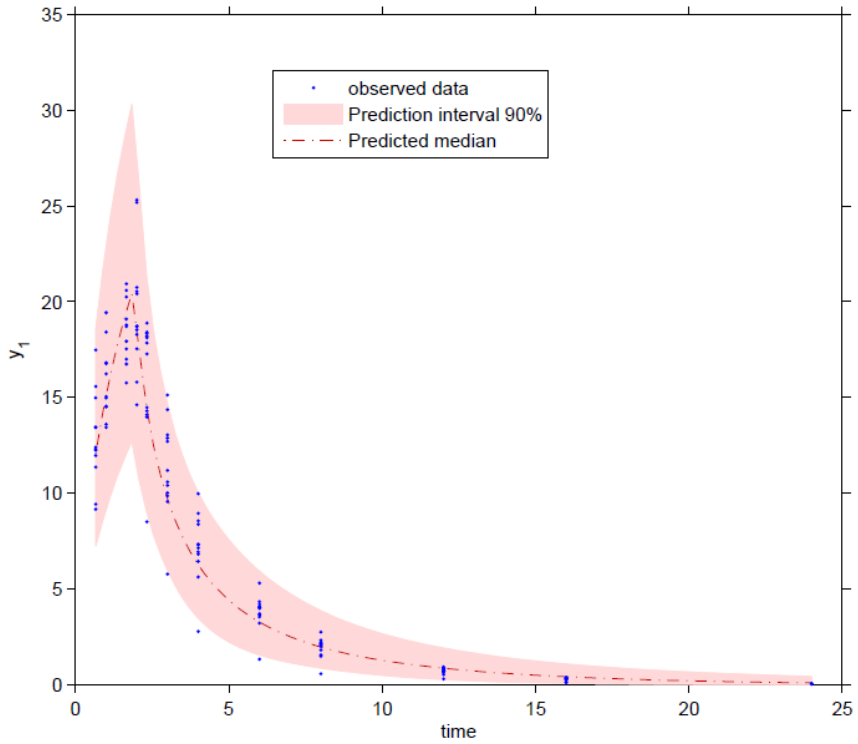

Figure 7-11. Diagnostic plot of modeling the simulated data: Visual predictive checks of unbound ceftobiprole concentrations in plasma.

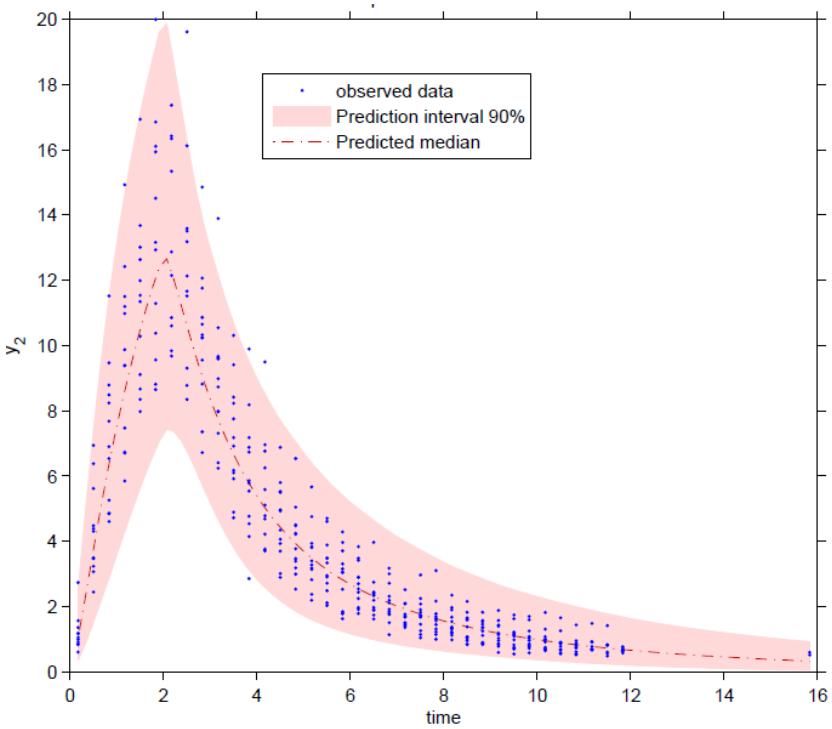

Figure 7-12. Diagnostic plot of modeling the simulated data: Visual predictive checks of unbound ceftobiprole concentrations in skeletal muscle.

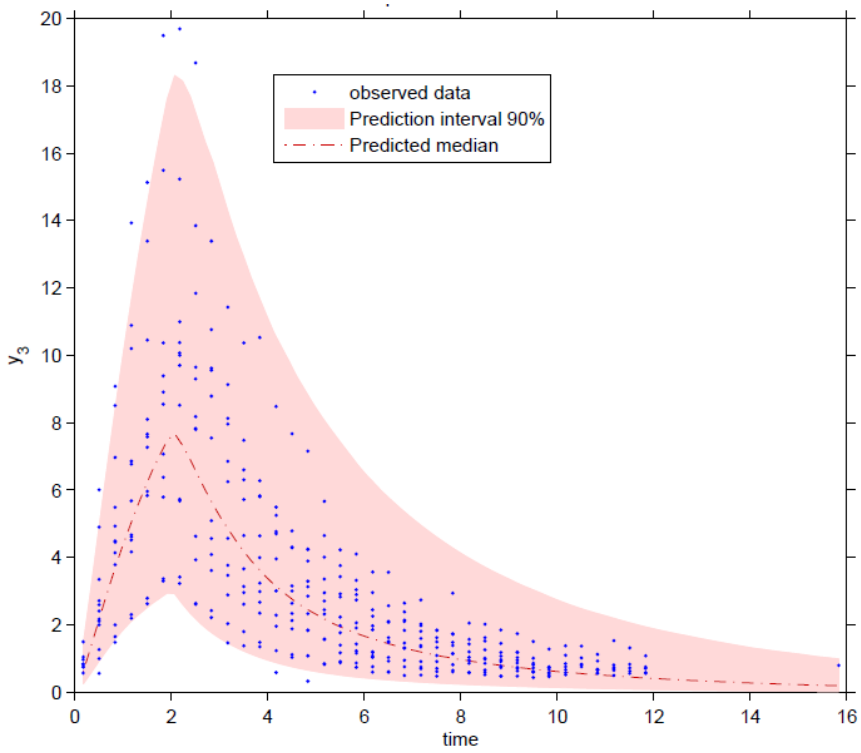

Figure 7-13. Diagnostic plot of modeling the simulated data: Visual predictive checks of unbound ceftobiprole concentrations in subcutaneous adipose fat.

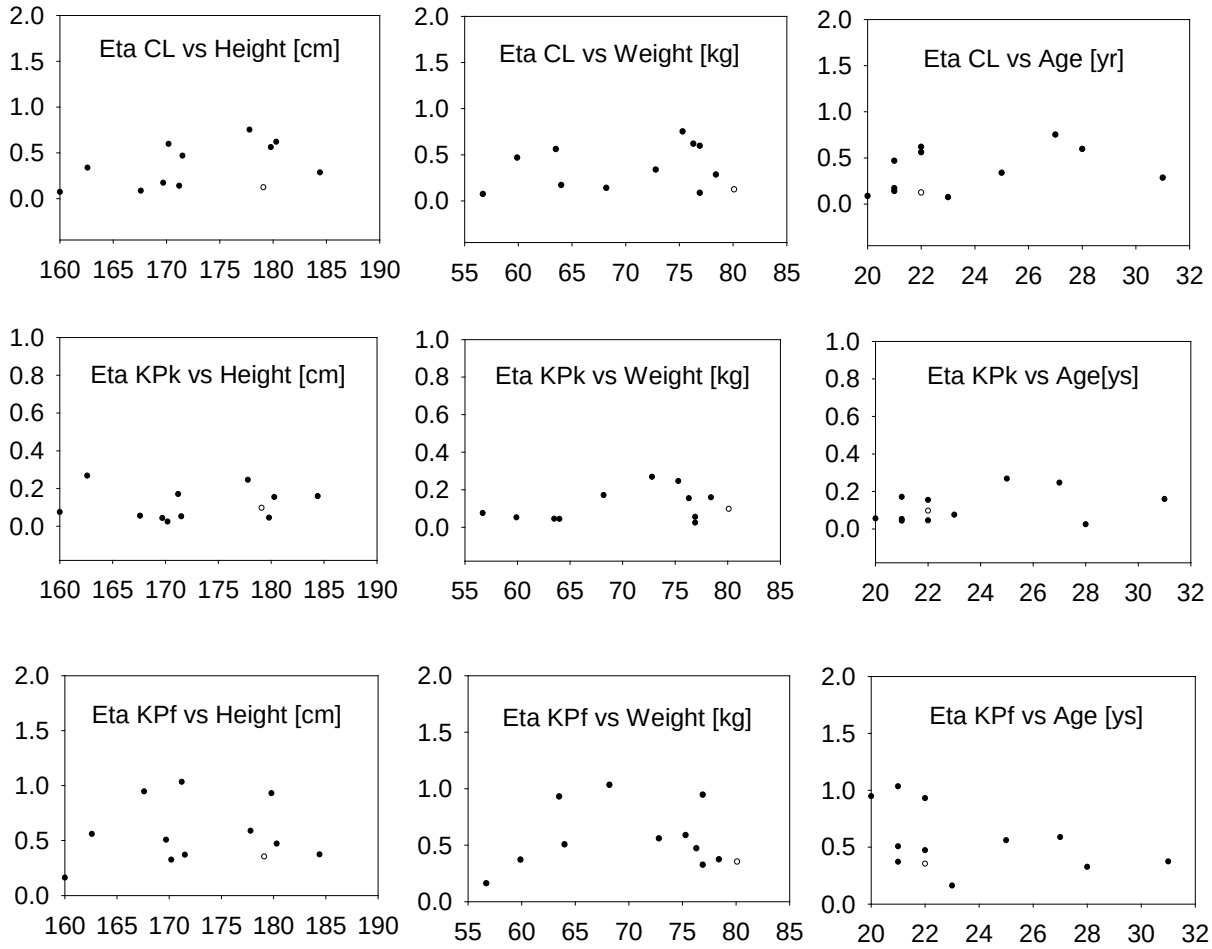

Figure 7-14. Visual plots of covariate analysis of various demographic parameters. No covariate was building in the final PBPK model due to lack of demographic distribution in the 12 healthy volunteers.

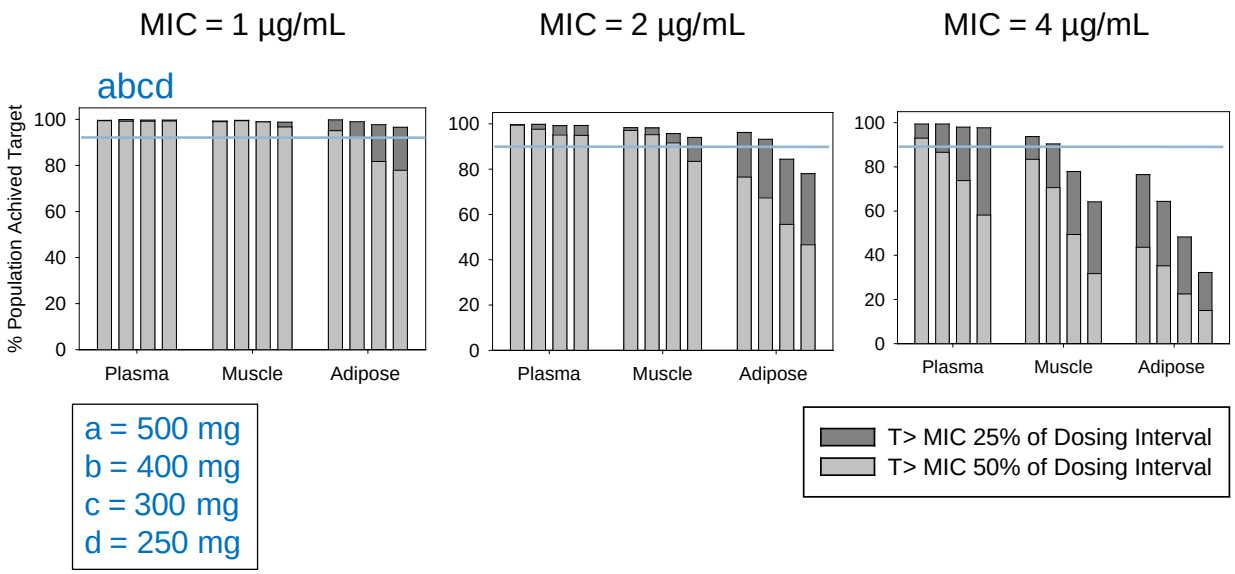

Figure 7-15. Probability of target attainment rates of ceftobiprole for 90% of population (solid line) based on 1000 Monte Carlo simulation following 2 hour intravenous infusion ceftobiprole. Dark and light grapy bars were simulated based on time of drug concentration above MIC 25% and 50% of dosing interval. Four doses and three MIC profiles were simulated.

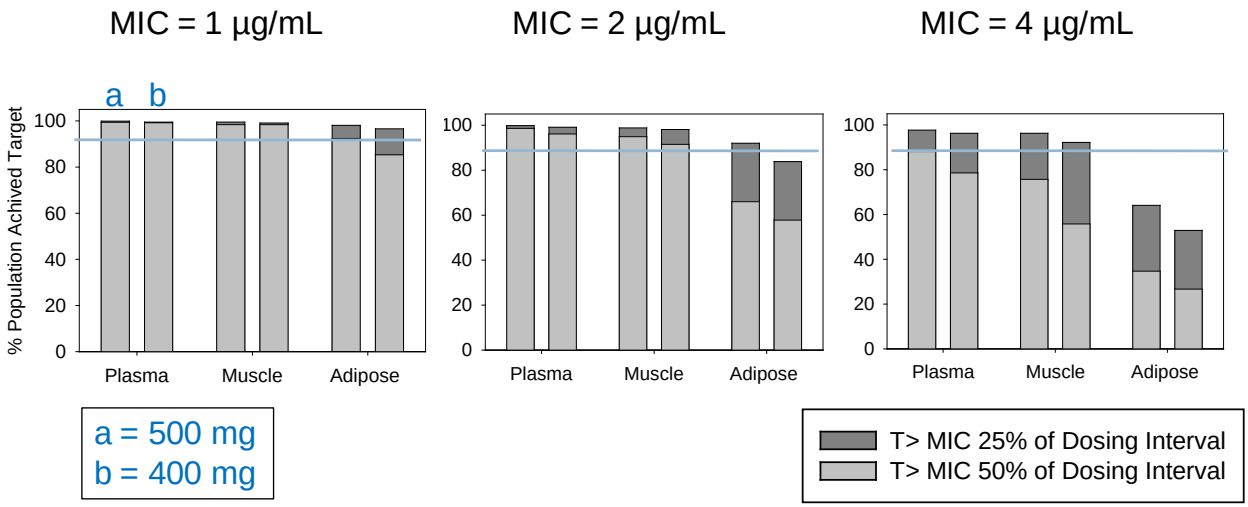

Figure 7-16. Probability of target attainment rates of ceftobiprole for 90% of population (solid line) based on 1000 Monte Carlo simulation following 1 hour intravenous infusion ceftobiprole. Dark and light grapy bars were simulated based on time of drug concentration above MIC 25% and 50% of dosing interval. Two doses and three MIC profiles were simulated.

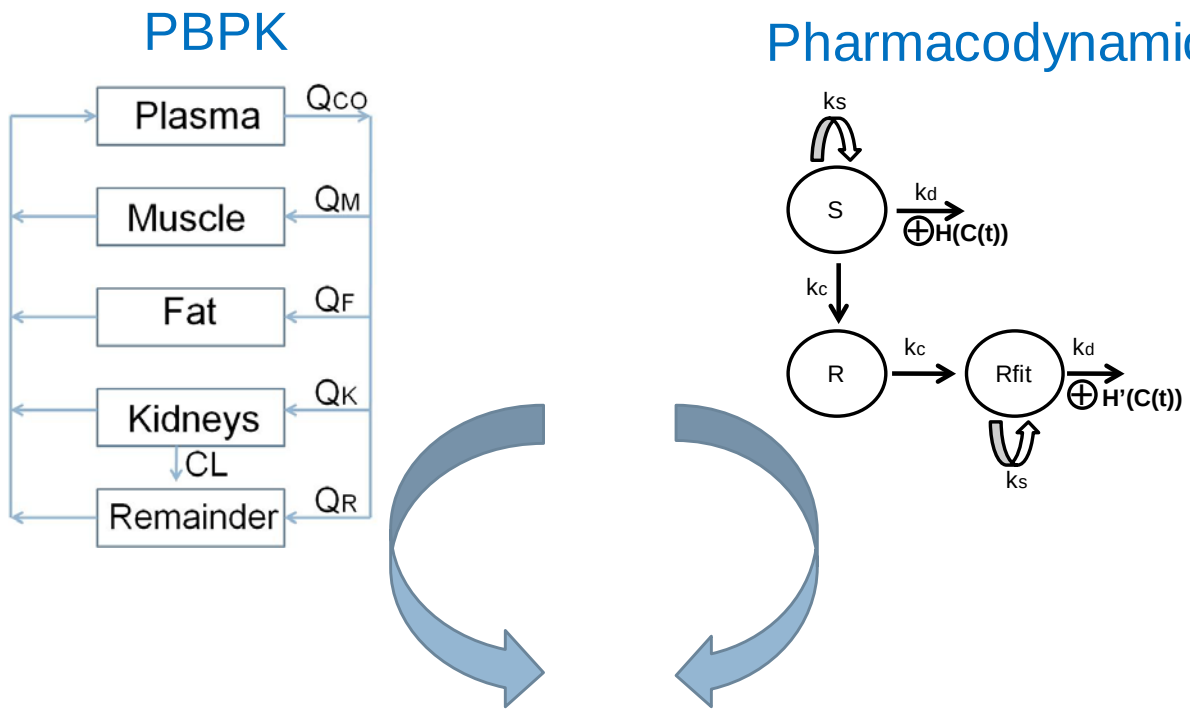

Figure 7-17. Integration of ceftobiprole pharmacokinetics described by the PBPK model with the Compensatory Mutation PD model for resistance evaluations.

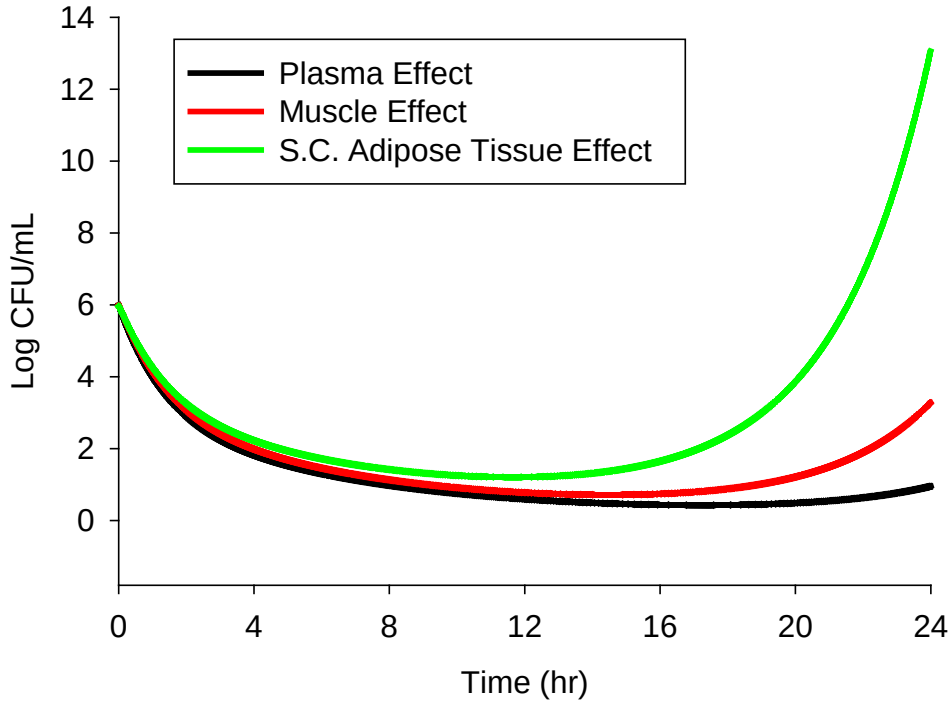

Figure 7-18. Simulation of ceftobiprole pharmacodynamic profiles: *MRSA* in tissues without the emergence of drug resistance.

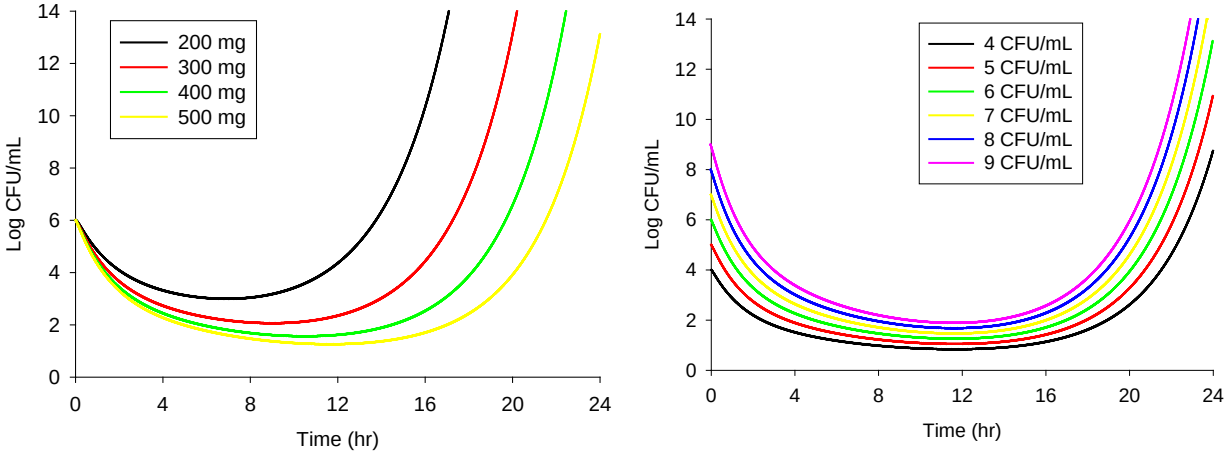

Figure 7-19. Simulation of ceftobiprole pharmacodynamic profiles: *MRSA* in subcutaneous adipose tissue without the emergence of drug resistance after various doses and inoculation levels.

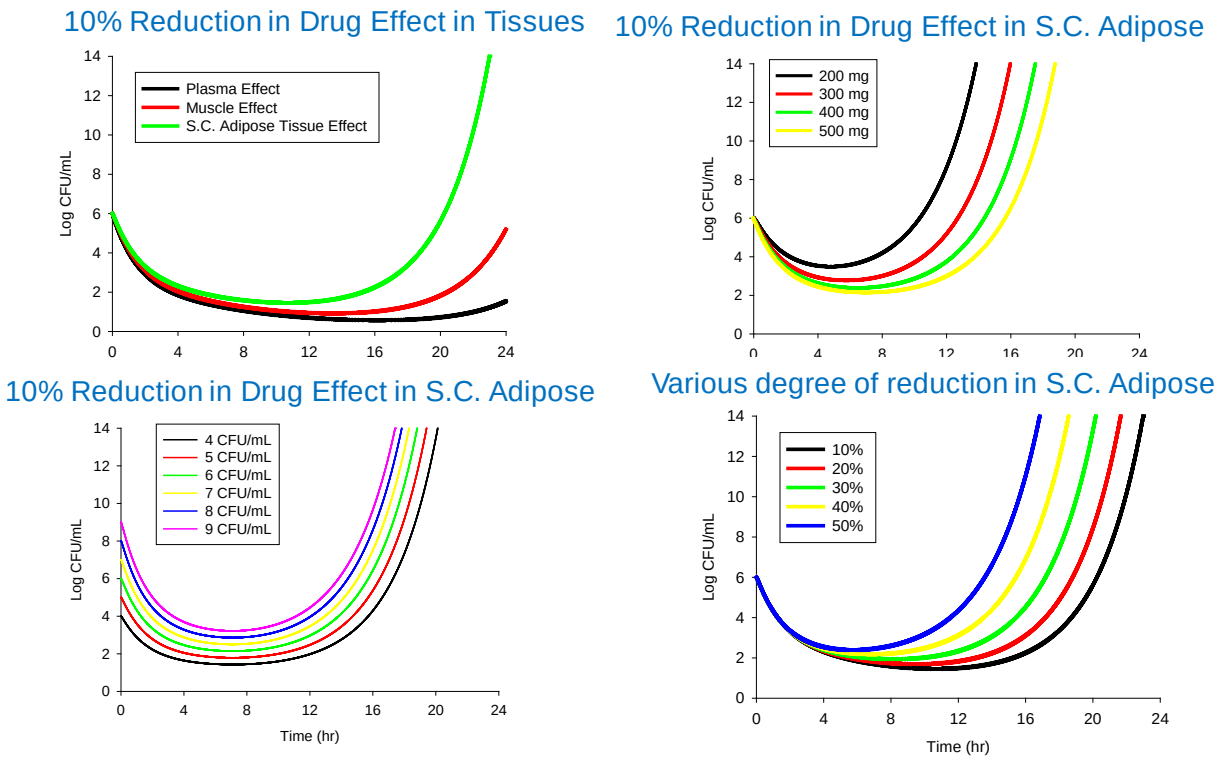

Figure 7-20. Simulation of ceftobiprole pharmacodynamic profiles: *MRSA* with the emergence of drug resistance.

CHAPTER 8
CONCLUSIONS

The emergence of antimicrobial resistance poses a critical challenge to public health. The current practice to treat microbes is less than optimal. Relying on single MIC data to define clinical dose disregards the adaptive nature of microbial response, which leads to fostering of drug resistance microbes over time. In order to overcome antimicrobial resistance, the time course relationships of drug and microbial behavior must first be delineated. In this dissertation, the development of novel mechanism-based PKPD models was described using new molecular and genetic findings. The resulting mathematical models provide insight into the complex PKPD relationships necessary to optimize antimicrobial treatments.

Within recent years, several hypotheses claim to explain the main mechanisms of antimicrobial resistance were published. The two most well accepted hypotheses are the dormant and compensatory mutation hypotheses. Dormant hypothesis describes the ability of microbes to induce a dormant phenotypic variant upon sensing environmental challenge. It does so by upregulating endogenous toxins to temporarily disable DNA replications and translations. Since antimicrobial agents only target dividing cells, the dormant microbes safely escape drug killings. Once the environment improves (decreased drug concentration), microbes can upregulate antitoxins to reinitiate microbial cell divisions.

The Compensatory Mutation hypothesis on the other hand proposes a genetic variant model. When microbes undergo random mutations to develop drug resistance characteristics, a fitness cost is imposed on the new strain. In order to be a clinically relevant strain, these mutated strains need compensatory mutations to restore microbial

fitness. These new strains would be able to grow at the same rate as the susceptible strains but with increased MICs.

Mathematical models describing each of the new hypotheses independently and in combination as well as a common literature model were developed to using extensive in vitro dynamic kill-curve data. Each model fitted control, suboptimal and lethal doses of ciprofloxacin against E. coli (totaling 11 dose groups) simultaneously. The models describing each resistance hypothesis underwent rigorous testing in order to select the best model to describe the kill-cuves. The model selection criteria consisted of performance in terms of (1) having fewest possible parameters to describe the hypotheses (2) bootstrap statistics of 1000 new dataset (3) visual predictive check of 1000 simulation (4) observe versus predicted plots (5) agreement of model fitting with ADAPT II versus median, mean and 90% confidence interval of bootstrap statistics with NONMEM VI (6) subcompartmental profile evaluation (7) multiple dose simulation (8) literature comparisons and (9) in-house kill-curve experimental data.

After thorough evaluations of these models, the Compensatory Mutation Model best describes the dynamics of antimicrobial resistance. The model was used to simulate anticipated results prior to the laboratory work which helped guide the study design of new multiple dose experiments. The first experiment confirmed the absence of pre-resistance strains of a clinical isolate of P. aeruginosa to ciprofloxacin. This information supports the development of a new model capturing the emergence of resistance, rather than using the literature model where a small percentage of resistance strain was included to model the susceptible and resistance population independently. The dynamic kill-curve evaluated the changing unbound drug

concentration versus microbial response over time. The MIC during and post antimicrobial treatments were evaluated. The dynamic kill-curve of P. aeruginosa confirmed the model prediction of loss of drug effects after the second exposure of 200 mg ciprofloxacin at 12 hours. The MIC increased several folds within six hours of ciprofloxacin dose and remain significantly high throughout the treatment period. The post antimicrobial effects indicated that despite the overall return to the predose MIC level three days after drug exposure, the microbial population was not homogenous; the E-strip test revealed that visible individual colonies were growing throughout the high ciprofloxacin concentration zone, indicating a wide range of MIC distribution formed post ciprofloxacin treatment.

Once P. aeruginosa developed resistance to ciprofloxacin, a three-fold drug dose increase was still inadequate to induce significant killing effects, supporting the highly adaptive nature of microbial response. In this stage, it would be necessary to switch to a new treatment with different mechanism of actions. However, our findings revealed that arbitrarily switching to a new class of antimicrobial agent does not guarantee successful outcome due to cross-resistance potential. The first alternative drug (ceftriaxone) used to treat the emerged resistance strain was ineffective. This was further confirmed by susceptibility analysis with microscan that the particular clinical isolate of P. aeruginosa was intermediate resistance to ceftriaxone prior to ciprofloxacin treatment and was advanced to full resistance after ciprofloxacin treatment. The microscan analysis of drug susceptibility across a large panel of antimicrobial agents revealed that mainly the aminoglycosides retained their drug effects after ciprofloxacin exposure. This ability to suppress ciprofloxacin-resistant strains was confirmed in

another dynamic kill-curve study using gentamicin. The drug-induced resistance phenomenon was not specific to ciprofloxacin treatment. A β-lactam, aztreonam, was also capable of inducing emergence of resistance. The exact mechanisms of resistance development in such a timely fashion warrant further investigations.

The in vitro PKPD and dynamic MIC profiles revealed important drug-microbe relationships. However, the translational interpretation needs to consider the lack of immune system involvement. The immune system may play an important role in eradicating the bacteria infection from the system147, thereby creating a temporal differences in the emergence of resistance in clinical settings. From statistics we know that antimicrobial drug effects reduce over time. However, the ability to predict this clinical observation remains a challenge in this field. Nonetheless, understanding these PKPD relationships is crucial to achieving the ultimate goal of predicting clinical resistance. It confirms the inadequate traditional dosing approach of using exposure-MIC relationship where the PKPD depends on a single PD time point. It would be necessary to consider the adaptive nature of microbes over the course of antimicrobial treatment to optimize effective dosing strategies against emerged resistance populations. While exposure-MIC dosing approaches still provide useful pharmacology guidelines, incorporation of a resistance emergence component would be informative.

To integrate a resistance emergence model to a clinical scenario, a novel population physiologically-based PK model for ceftobiprole against MRSA was developed as the PK input for PD simulations. The population PBPK model estimated the partition coefficients of drugs to relevant tissue sites, plasma clearance and inter- and intra- subject variabilities which are important for clinical predictions. Monte Carlo

simulations were used to predict target attainment rate with and without ceftobiprole resistance development. The PBPK model combined with the mechanism-based PD model for resistance further provided insights into different scenarios of pharmacodynamic profiles at tissue sites. The PBPK model reaffirmed that 500 mg ceftobiprole infused intravenously over 1 or 2 hours is sufficient to achieve the pharmacological target. However, an MIC increase from 1 to 4 μg/mL will require a more frequent dosing or higher dose levels of ceftobiprole.

In conclusion, the dynamics of microbes in response to drug treatments are extremely complex, involving the drug, microbes, and host. Currently, the best system to study drug-microbes relationship is to use in vitro dynamic kill-curve models. The immune system may potentiate the killings of drug actions and prolong the regrowth time of resistance strains. One of the most important findings that disregards the traditional exposure-MIC approach is that the MIC is not stationary during the treatment period. In order to ensure successful treatment over time, the dosing strategy should consider susceptible and the newly emerged populations.

The findings presented in this dissertation serve as a foundation to further explore the emergence of antimicrobial resistance. Specifically for P. aeruginosa, it would be informative to evaluate the dose- and inoculation-dependency on the emergence resistance. It is possible that a higher initial dose of ciprofloxacin (i.e. 600 mg starting dose instead of 200 mg) may reduce the development of resistance. The current study only tested the emergence of resistance at a low clinical dose. Evaluation of a range of initial inoculation concentrations (4 to 9 CFU/mL) will further characterize the adaptive nature of microbes. In summary, the mechanism-based PKPD model improved the

understanding of antimicrobial resistance and was used to explore new dosing strategies for the resistant populations. The clinical utilities of the resistance model were presented for a novel population PBPK model of ceftobiprole against MRSA.

LIST OF REFERENCES

1. Geddes A. 80th Anniversary of the discovery of penicillin An appreciation of Sir Alexander Fleming. *Int J Antimicrob Agents* 2008;**32**:373.

2. Palumbi SR. Humans as the world's greatest evolutionary force. *Science* 2001;**293**:1786-90.

3. Gerrits MM, van Vliet AH, Kuipers EJ, Kusters JG. Helicobacter pylori and antimicrobial resistance: molecular mechanisms and clinical implications. *Lancet Infect Dis* 2006;**6**:699-709.

4. Kraus D, Peschel A. Molecular mechanisms of bacterial resistance to antimicrobial peptides. *Curr Top Microbiol Immunol* 2006;**306**:231-50.

5. Livermore DM. Multiple mechanisms of antimicrobial resistance in Pseudomonas aeruginosa: our worst nightmare? *Clin Infect Dis* 2002;**34**:634-40.

6. McManus MC. Mechanisms of bacterial resistance to antimicrobial agents. *Am J Health Syst Pharm* 1997;**54**:1420-33; quiz 44-6.

7. Sefton AM. Mechanisms of antimicrobial resistance: their clinical relevance in the new millennium. *Drugs* 2002;**62**:557-66.

8. Skold O. Evolution and mechanisms for spread of antimicrobial resistance. *Acta Vet Scand Suppl* 2000;**93**:23-7; discussion 8-36.

9. Stratton CW. Mechanisms of bacterial resistance to antimicrobial agents. *J Med Liban* 2000;**48**:186-98.

10. Tenover FC. Mechanisms of antimicrobial resistance in bacteria. *Am J Med* 2006;**119**:S3-10; discussion S62-70.

11. Woods CR. Antimicrobial resistance: mechanisms and strategies. *Paediatr Respir Rev* 2006;**7** Suppl 1:S128-9.

12. Yeaman MR, Yount NY. Mechanisms of antimicrobial peptide action and resistance. *Pharmacol Rev* 2003;**55**:27-55.

13. Lipsitch M. The rise and fall of antimicrobial resistance. *Trends Microbiol* 2001;**9**:438-44.

14. Bradford PA. Extended-spectrum beta-lactamases in the 21st century: characterization, epidemiology, and detection of this important resistance threat. *Clin Microbiol Rev* 2001;**14**:933-51, table of contents.

15. Chopra I, Roberts M. Tetracycline antibiotics: mode of action, applications, molecular biology, and epidemiology of bacterial resistance. *Microbiol Mol Biol Rev* 2001;**65**:232-60 ; second page, table of contents.

16. Fluit AC, Visser MR, Schmitz FJ. Molecular detection of antimicrobial resistance. *Clin Microbiol Rev* 2001;**14**:836-71, table of contents.

17. Ouellette M, Kundig C. Microbial multidrug resistance. *Int J Antimicrob Agents* 1997;**8**:179-87.

18. Mlynarczyk B, Mlynarczyk A, Kmera-Muszynska M, Majewski S, Mlynarczyk G. Mechanisms of Resistance to Antimicrobial Drugs in Pathogenic Gram-Positive Cocci. *Mini Rev Med Chem.*

19. Tenover FC. Mechanisms of antimicrobial resistance in bacteria. *Am J Infect Control* 2006;**34**:S3-10; discussion S64-73.

20. Nizet V. Antimicrobial peptide resistance mechanisms of human bacterial pathogens. *Curr Issues Mol Biol* 2006;**8**:11-26.

21. Novotna G, Adamkova V, Janata J, Melter O, Spizek J. Prevalence of resistance mechanisms against macrolides and lincosamides in methicillin-resistant coagulase-negative staphylococci in the Czech Republic and occurrence of an undefined mechanism of resistance to lincosamides. *Antimicrob Agents Chemother* 2005;**49**:3586-9.

22. Poole K. Multidrug resistance in Gram-negative bacteria. *Curr Opin Microbiol* 2001;**4**:500-8.

23. Wientjes FB, Woldringh CL, Nanninga N. Amount of peptidoglycan in cell walls of gram-negative bacteria. *Journal of bacteriology* 1991;**173**:7684-91.

24. Storm DR. Mechanism of bacitracin action: a specific lipid-peptide interaction. *Ann N Y Acad Sci* 1974;**235**:387-98.

25. Frere JM. Mechanism of action of beta-lactam antibiotics at the molecular level. *Biochem Pharmacol* 1977;**26**:2203-10.

26. Sandanayaka VP, Prashad AS. Resistance to beta-lactam antibiotics: structure and mechanism based design of beta-lactamase inhibitors. *Curr Med Chem* 2002;**9**:1145-65.

27. Rake JB, Gerber R, Mehta RJ, Newman DJ, Oh YK, Phelen C, Shearer MC, Sitrin RD, Nisbet LJ. Glycopeptide antibiotics: a mechanism-based screen employing a bacterial cell wall receptor mimetic. *J Antibiot (Tokyo)* 1986;**39**:58-67.

28. Schouten MA, Willems RJ, Kraak WA, Top J, Hoogkamp-Korstanje JA, Voss A. Molecular analysis of Tn1546-like elements in vancomycin-resistant enterococci isolated from patients in Europe shows geographic transposon type clustering. *Antimicrob Agents Chemother* 2001;**45**:986-9.

29. Trenin AS, Olsuf'eva EN. [Glycopeptide antibiotics resistance mechanism as the basis for novel derivatives development capable to overcome resistance]. *Bioorg Khim* 1997;**23**:851-67.

30. Cocito C. The ribosomal cycle in bacteria treated with an inhibitor of protein synthesis. *Biochimie* 1973;**55**:309-16.

31. Tanaka N. [Aminoglycoside antibodies: mechanism of action and resistance]. *Nippon Saikingaku Zasshi* 1986;**41**:587-601.

32. Gomazkov OA. Mechanism of Action of Tetracycline Antibiotics. *Fed Proc Transl Suppl* 1964;**23**:876-8.

33. Gregory ST, Carr JF, Dahlberg AE. A mutation in the decoding center of Thermus thermophilus 16S rRNA suggests a novel mechanism of streptomycin resistance. *Journal of bacteriology* 2005;**187**:2200-2.

34. Suzuki Y. Mode of Action of Streptomycin and Mechanism of Resistance to the Drug in Bacteria. *Jpn J Med Sci Biol* 1963;**16**:235-9.

35. Wright GD, Thompson PR. Aminoglycoside phosphotransferases: proteins, structure, and mechanism. *Front Biosci* 1999;**4**:D9-21.

36. Bissonnette L, Champetier S, Buisson JP, Roy PH. Characterization of the nonenzymatic chloramphenicol resistance (cmlA) gene of the In4 integron of Tn1696: similarity of the product to transmembrane transport proteins. *Journal of bacteriology* 1991;**173**:4493-502.

37. Zhong P, Shortridge VD. The role of efflux in macrolide resistance. *Drug Resist Updat* 2000;**3**:325-9.

38. Kobayashi N, Nishino K, Yamaguchi A. Novel macrolide-specific ABC-type efflux transporter in Escherichia coli. J*ournal of bacteriology* 2001;**183**:5639-44.

39. Prystowsky J, Siddiqui F, Chosay J, Shinabarger DL, Millichap J, Peterson LR, Noskin GA. Resistance to linezolid: characterization of mutations in rRNA and comparison of their occurrences in vancomycin-resistant enterococci. *Antimicrob Agents Chemother* 2001;**45**:2154-6.

40. Tschesche R. [Mechanism of the antibacterial action of sulfonamides.]. *Arzneimittelforschung* 1951;**1**:335-9.

41. Sevag MG, Steers E, Forbes M. The mechanism of resistance of sulfonamides; a comparative study of the resistance to sulfathiazole of the metabolism of glucose and pyruvate by Staphylococcus aureus. *Arch Biochem* 1950;**25**:185-90.

42. Chen S, Zhao S, White DG, Schroeder CM, Lu R, Yang H, McDermott PF, Ayers S, Meng J. Characterization of multiple-antimicrobial-resistant salmonella serovars isolated from retail meats. *Appl Environ Microbiol* 2004;**70**:1-7.

43. Zhao S, White DG, Ge B, Ayers S, Friedman S, English L, Wagner D, Gaines S, Meng J. Identification and characterization of integron-mediated antibiotic resistance among Shiga toxin-producing Escherichia coli isolates. *Appl Environ Microbiol* 2001;**67**:1558-64.

44. Bryan LE, Bedard J, Wong S, Chamberland S. Quinolone antimicrobial agents: mechanism of action and resistance development. *Clin Invest Med* 1989;**12**:14-9.

45. Xu KY, Wang YS. [A primary study on the mechanism of action of benzothiazole-rifamycin]. Yao xue xue bao = *Acta pharmaceutica Sinica* 1984;**19**:881-7.

46. Abramycheva N, Govorun VM. [The participation of the transport-barrier functions of the plasma membrane in the development of fluoroquinolone (ciprofloxacin) resistance in Acholeplasma laidlawii]. *Antibiot Khimioter* 2000;**45**:14-9.

47. Gootz TD, Brighty KE. Fluoroquinolone antibacterials: SAR mechanism of action, resistance, and clinical aspects. *Med Res Rev* 1996;**16**:433-86.

48. Drlica K, Zhao X. DNA gyrase, topoisomerase IV, and the 4-quinolones. *Microbiol Mol Biol Rev* 1997;**61**:377-92.

49. Harrison JJ, Ceri H, Roper NJ, Badry EA, Sproule KM, Turner RJ. Persister cells mediate tolerance to metal oxyanions in Escherichia coli. Microbiology 2005;**151**:3181-95.

50. Keren I, Kaldalu N, Spoering A, Wang Y, Lewis K. Persister cells and tolerance to antimicrobials. *FEMS microbiology letters* 2004;**230**:13-8.

51. Keren I, Shah D, Spoering A, Kaldalu N, Lewis K. Specialized persister cells and the mechanism of multidrug tolerance in Escherichia coli. *Journal of bacteriology* 2004;**186**:8172-80.

52. Korch SB, Hill TM. Ectopic overexpression of wild-type and mutant hipA genes in Escherichia coli: effects on macromolecular synthesis and persister formation. *Journal of bacteriology* 2006;**188**:3826-36.

53. Lewis K. Persister cells, dormancy and infectious disease. *Nature reviews* 2007;**5**:48-56.

54. Bjorkman J, Nagaev I, Berg OG, Hughes D, Andersson DI. Effects of environment on compensatory mutations to ameliorate costs of antibiotic resistance. *Science* 2000;**287**:1479-82.

55. Levin BR, Perrot V, Walker N. Compensatory mutations, antibiotic resistance and the population genetics of adaptive evolution in bacteria. *Genetics* 2000;**154**:985-97.

56. Nagaev I, Bjorkman J, Andersson DI, Hughes D. Biological cost and compensatory evolution in fusidic acid-resistant Staphylococcus aureus. *Mol Microbiol* 2001;**40**:433-9.

57. Marcusson LL, Frimodt-Moller N, Hughes D. Interplay in the selection of fluoroquinolone resistance and bacterial fitness. *PLoS Pathog* 2009;**5**:e1000541.

58. Neuhauser MM, Weinstein RA, Rydman R, Danziger LH, Karam G, Quinn JP. Antibiotic resistance among gram-negative bacilli in US intensive care units: implications for fluoroquinolone use. *JAMA* 2003;**289**:885-8.

59. Spellberg B, Powers JH, Brass EP, Miller LG, Edwards JE, Jr. Trends in antimicrobial drug development: implications for the future. *Clin Infect Dis* 2004;**38**:1279-86.

60. Falla TJ, Chopra I. Joint tolerance to beta-lactam and fluoroquinolone antibiotics in Escherichia coli results from overexpression of hipA. *Antimicrob Agents Chemother* 1998;**42**:3282-4.

61. Craig WA. Choosing an antibiotic on the basis of pharmacodynamics. E*ar Nose Throat J* 1998;**77**:7-11; discussion -2.

62. Ambrose PG, Bhavnani SM, Rubino CM, Louie A, Gumbo T, Forrest A, Drusano GL. Pharmacokinetics-pharmacodynamics of antimicrobial therapy: it's not just for mice anymore. *Clin Infect Dis* 2007;**44**:79-86.

63. Craig WA, Redington J, Ebert SC. Pharmacodynamics of amikacin in vitro and in mouse thigh and lung infections. *J Antimicrob Chemother* 1991;**27** Suppl C:29-40.

64. Drusano GL. Human pharmacodynamics of beta-lactams, aminoglycosides and their combination. *Scand J Infect Dis Suppl* 1990;**74**:235-48.

65. Turnidge JD. The pharmacodynamics of beta-lactams. *Clin Infect Dis* 1998;**27**:10-22.

66. Vogelman B, Gudmundsson S, Leggett J, Turnidge J, Ebert S, Craig WA. Correlation of antimicrobial pharmacokinetic parameters with therapeutic efficacy in an animal model. *J Infect Dis* 1988;**158**:831-47.

67. Leggett JE, Fantin B, Ebert S, Totsuka K, Vogelman B, Calame W, Mattie H, Craig WA. Comparative antibiotic dose-effect relations at several dosing intervals in murine pneumonitis and thigh-infection models. *J Infect Dis* 1989;**159**:281-92.

68. Moise PA, Schentag JJ. Pharmacokinetic and pharmacodynamic modelling of antibiotic therapy. *Curr Opin Infect Dis* 1998;**11**:673-80.

69. Dasgupta A. Usefulness of monitoring free (unbound) concentrations of therapeutic drugs in patient management. *Clin Chim Acta* 2007;**377**:1-13.

70. Mouton JW, Theuretzbacher U, Craig WA, Tulkens PM, Derendorf H, Cars O. Tissue concentrations: do we ever learn? *J Antimicrob Chemother* 2008;**61**:235-7.

71. Treyaprasert W, Schmidt S, Rand KH, Suvanakoot U, Derendorf H. Pharmacokinetic/pharmacodynamic modeling of in vitro activity of azithromycin against four different bacterial strains. *Int J Antimicrob Agents* 2007;**29**:263-70.

72. Barbour A, Schmidt S, Sabarinath SN, Grant M, Seubert C, Skee D, Murthy B, Derendorf H. Soft-tissue penetration of ceftobiprole in healthy volunteers determined by in vivo microdialysis. *Antimicrob Agents Chemother* 2009;**53**:2773-6.

73. Hoffman A, Stepensky D. Pharmacodynamic aspects of modes of drug administration for optimization of drug therapy. *Crit Rev Ther Drug Carrier Syst* 1999;**16**:571-639.

74. Garrett ER, Miller GH, Brown MR. Kinetics and mechanisms of action of antibiotics on microorganisms. V. Chloramphenicol and tetracycline affected Escherichia coli generation rates. *J Pharm Sci* 1966;**55**:593-600.

75. Garrett ER, Nolte H. Kinetics and mechanisms of drug action on microorganisms. XIV. The action of fluorouracil, other uracils and derived nucleosides on the microbial kinetics of Escherichia coli. *Chemotherapy* 1972;**17**:81-108.

76. Mielck JB, Garrett ER. Kinetics and mechanisms of drug action on microorganisms. IX. Inhibitory action of lincomycin on Escherichia coli by microbial kinetics. *Chemotherapy* 1969;**14**:337-55.

77. Grasso S, Meinardi G, de Carneri I, Tamassia V. New in vitro model to study the effect of antibiotic concentration and rate of elimination on antibacterial activity. *Antimicrob Agents Chemother* 1978;**13**:570-6.

78. Sanfilippo A, Morvillo E. An experimental model for the study of the antibacterial activity of the sulfonamides. *Chemotherapy* 1968;**13**:54-60.

79. Sanfilippo A, Schioppacassi G. New approach to the evaluation of antibacterial activity of aminosidine. *Chemotherapy* 1973;**18**:297-303.

80. Craig WA. Pharmacokinetic/pharmacodynamic parameters: rationale for antibacterial dosing of mice and men. *Clin Infect Dis* 1998;**26**:1-10; quiz 1-2.

81. Jumbe N, Louie A, Leary R, Liu W, Deziel MR, Tam VH, Bachhawat R, Freeman C, Kahn JB, Bush K, Dudley MN, Miller MH, Drusano GL. Application of a mathematical model to prevent in vivo amplification of antibiotic-resistant bacterial populations during therapy. *J Clin Invest* 2003;**112**:275-85.

82. Liu P, Rand KH, Obermann B, Derendorf H. Pharmacokinetic-pharmacodynamic modelling of antibacterial activity of cefpodoxime and cefixime in in vitro kinetic models. *Int J Antimicrob Agents* 2005;**25**:120-9.

83. Mueller M, de la Pena A, Derendorf H. Issues in pharmacokinetics and pharmacodynamics of anti-infective agents: kill curves versus MIC. *Antimicrob Agents Chemother* 2004;**48**:369-77.

84. Campion JJ, McNamara PJ, Evans ME. Evolution of ciprofloxacin-resistant Staphylococcus aureus in in vitro pharmacokinetic environments. *Antimicrob Agents Chemother* 2004;**48**:4733-44.

85. Bulitta JB, Ly NS, Yang JC, Forrest A, Jusko WJ, Tsuji BT. Development and qualification of a pharmacodynamic model for the pronounced inoculum effect of ceftazidime against Pseudomonas aeruginosa. *Antimicrob Agents Chemother* 2009;**53**:46-56.

86. Barbour A, Schmidt S, Rand KH, Derendorf H. Ceftobiprole: a novel cephalosporin with activity against Gram-positive and Gram-negative pathogens, including methicillin-resistant Staphylococcus aureus (MRSA). *Int J Antimicrob Agents* 2009;**34**:1-7.

87. de la Pena A, Grabe A, Rand KH, Rehak E, Gross J, Thyroff-Friesinger U, Muller M, Derendorf H. PK-PD modelling of the effect of cefaclor on four different bacterial strains. *Int J Antimicrob Agents* 2004;**23**:218-25.

88. Schmidt S, Sabarinath SN, Barbour A, Abbanat D, Manitpisitkul P, Sha S, Derendorf H. Pharmacokinetic-pharmacodynamic modeling of the in vitro activities of oxazolidinone antimicrobial agents against methicillin-resistant Staphylococcus aureus. *Antimicrob Agents Chemother* 2009;**53**:5039-45.

89. Drusano GL, D'Argenio DZ, Preston SL, Barone C, Symonds W, LaFon S, Rogers M, Prince W, Bye A, Bilello JA. Use of drug effect interaction modeling with Monte Carlo simulation to examine the impact of dosing interval on the projected antiviral activity of the combination of abacavir and amprenavir. *Antimicrob Agents Chemother* 2000;**44**:1655-9.

90. Owens RC, Jr., Bhavnani SM, Ambrose PG. Assessment of pharmacokinetic-pharmacodynamic target attainment of gemifloxacin against Streptococcus pneumoniae. *Diagn Microbiol Infect Dis* 2005;**51**:45-9.

91. Schuck EL, Derendorf H. Pharmacokinetic/pharmacodynamic evaluation of anti-infective agents. *Expert Rev Anti Infect Ther* 2005;**3**:361-73.

92. Liu P, Muller M, Grant M, Obermann B, Derendorf H. Tissue penetration of cefpodoxime and cefixime in healthy subjects. *Journal of clinical pharmacology* 2005;**45**:564-9.

93. Andersson DI. Persistence of antibiotic resistant bacteria. *Curr Opin Microbiol* 2003;**6**:452-6.

94. Hayes F. Toxins-antitoxins: plasmid maintenance, programmed cell death, and cell cycle arrest. *Science* 2003;**301**:1496-9.

95. Opperman T, Murli S, Smith BT, Walker GC. A model for a umuDC-dependent prokaryotic DNA damage checkpoint. *Proc Natl Acad Sci U S A 1*999;**96**:9218-23.

96. Andersson DI. The biological cost of mutational antibiotic resistance: any practical conclusions? *Curr Opin Microbiol* 2006;**9**:461-5.

97. Bjorkholm B, Sjolund M, Falk PG, Berg OG, Engstrand L, Andersson DI. Mutation frequency and biological cost of antibiotic resistance in Helicobacter pylori. *Proc Natl Acad Sci U S A* 2001;**98**:14607-12.

98. Gustafsson I, Cars O, Andersson DI. Fitness of antibiotic resistant Staphylococcus epidermidis assessed by competition on the skin of human volunteers. *J Antimicrob Chemother* 2003;**52**:258-63.

99. Johnson CN, Briles DE, Benjamin WH, Jr., Hollingshead SK, Waites KB. Relative fitness of fluoroquinolone-resistant Streptococcus pneumoniae. *Emerg Infect Dis* 2005;**11**:814-20.

100. Kugelberg E, Lofmark S, Wretlind B, Andersson DI. Reduction of the fitness burden of quinolone resistance in Pseudomonas aeruginosa. *J Antimicrob Chemother* 2005;**55**:22-30.

101. Lofmark S, Jernberg C, Billstrom H, Andersson DI, Edlund C. Restored fitness leads to long-term persistence of resistant Bacteroides strains in the human intestine. *Anaerobe* 2008;**14**:157-60.

102. Martinez JL, Baquero F. Mutation frequencies and antibiotic resistance. *Antimicrob Agents Chemother* 2000;**44**:1771-7.

103. Firsov AA, Vostrov SN, Shevchenko AA, Zinner SH, Cornaglia G, Portnoy YA. MIC-based interspecies prediction of the antimicrobial effects of ciprofloxacin on bacteria of different susceptibilities in an in vitro dynamic model. *Antimicrob Agents Chemother* 1998;**42**:2848-52.

104. Campion JJ, McNamara PJ, Evans ME. Pharmacodynamic modeling of ciprofloxacin resistance in Staphylococcus aureus. *Antimicrob Agents Chemother* 2005;**49**:209-19.

105. D'Argenio DZ, Schumitzky A. A program package for simulation and parameter estimation in pharmacokinetic systems. *Comput Programs Biomed* 1979;**9**:115-34.

106. Dudley MN, Mandler HD, Gilbert D, Ericson J, Mayer KH, Zinner SH. Pharmacokinetics and pharmacodynamics of intravenous ciprofloxacin. Studies in vivo and in an in vitro dynamic model. *Am J Med* 1987;**82**:363-8.

107. Kaatz GW, Seo SM, Ruble CA. Mechanisms of fluoroquinolone resistance in Staphylococcus aureus. *J Infect Dis* 1991;**163**:1080-6.

108. Austin DJ, Kristinsson KG, Anderson RM. The relationship between the volume of antimicrobial consumption in human communities and the frequency of resistance. *Proc Natl Acad Sci U S A* 1999;**96**:1152-6.

109. Muller M, Brunner M, Hollenstein U, Joukhadar C, Schmid R, Minar E, Ehringer H, Eichler HG. Penetration of ciprofloxacin into the interstitial space of inflamed foot lesions in non-insulin-dependent diabetes mellitus patients. *Antimicrob Agents Chemother* 1999;**43**:2056-8.

110. Schmidt S, Barbour A, Sahre M, Rand KH, Derendorf H. PK/PD: new insights for antibacterial and antiviral applications. *Curr Opin Pharmacol* 2008;**8**:549-56.

111. Andersson DI, Levin BR. The biological cost of antibiotic resistance. *Curr Opin Microbiol 1999*;**2**:489-93.

112. Gerrish PJ, Garcia-Lerma JG. Mutation rate and the efficacy of antimicrobial drug treatment. *Lancet Infect Dis* 2003;**3**:28-32.

113. Rozen DE, McGee L, Levin BR, Klugman KP. Fitness costs of fluoroquinolone resistance in Streptococcus pneumoniae. *Antimicrob Agents Chemother* 2007;**51**:412-6.

114. Firsov AA, Vostrov SN, Shevchenko AA, Cornaglia G. Parameters of bacterial killing and regrowth kinetics and antimicrobial effect examined in terms of area under the concentration-time curve relationships: action of ciprofloxacin against Escherichia coli in an in vitro dynamic model. *Antimicrob Agents Chemother* 1997;**41**:1281-7.

115. Earp J, Krzyzanski W, Chakraborty A, Zamacona MK, Jusko WJ. Assessment of drug interactions relevant to pharmacodynamic indirect response models. *J Pharmacokinet Pharmacodyn* 2004;**31**:345-80.

116. Lambert PA. Mechanisms of antibiotic resistance in Pseudomonas aeruginosa. *J R Soc Med* 2002;**95** Suppl 41:22-6.

117. Poole K. Multidrug efflux pumps and antimicrobial resistance in Pseudomonas aeruginosa and related organisms. *J Mol Microbiol Biotechnol* 2001;**3**:255-64.

118. Poole K. Aminoglycoside resistance in Pseudomonas aeruginosa. *Antimicrob Agents Chemother* 2005;**49**:479-87.

119. Piddock LJ. Mechanisms of fluoroquinolone resistance: an update 1994-1998. *Drugs* 1999;**58** Suppl 2:11-8.

120. Zilberberg MD, Chen J, Mody SH, Ramsey AM, Shorr AF. Imipenem resistance of Pseudomonas in pneumonia: a systematic literature review. *BMC Pulm Med*;**10**:45.

121. Lister PD, Wolter DJ, Hanson ND. Antibacterial-resistant Pseudomonas aeruginosa: clinical impact and complex regulation of chromosomally encoded resistance mechanisms. *Clin Microbiol Rev* 2009;**22**:582-610.

122. Strateva T, Yordanov D. Pseudomonas aeruginosa - a phenomenon of bacterial resistance. *J Med Microbiol* 2009;**58**:1133-48.

123. Sacha P, Wieczorek P, Hauschild T, Zorawski M, Olszanska D, Tryniszewska E. Metallo-beta-lactamases of Pseudomonas aeruginosa--a novel mechanism resistance to beta-lactam antibiotics. *Folia Histochem Cytobiol* 2008;**46**:137-42.

124. Jeannot K, Elsen S, Kohler T, Attree I, van Delden C, Plesiat P. Resistance and virulence of Pseudomonas aeruginosa clinical strains overproducing the MexCD-OprJ efflux pump. *Antimicrob Agents Chemother* 2008;**52**:2455-62.

125. Mariani-Kurkdjian P, Bingen E. [Pseudomonas aeruginosa: resistance to antibiotics]. *Arch Pediatr* 2006;**13** Suppl 1:S5-9.

126. Zhanel GG, Hoban DJ, Schurek K, Karlowsky JA. Role of efflux mechanisms on fluoroquinolone resistance in Streptococcus pneumoniae and Pseudomonas aeruginosa. *Int J Antimicrob Agents* 2004;**24**:529-35.

127. Ong CT, Kuti JL, Nightingale CH, Nicolau DP. Emerging Pseudomonas aeruginosa resistance: implications in clinical practice. Conn Med 2004;**68**:11-5.

128. Schweizer HP. Efflux as a mechanism of resistance to antimicrobials in Pseudomonas aeruginosa and related bacteria: unanswered questions. *Genet Mol Res* 2003;**2**:48-62.

129. Nordmann P. [Mechanisms of resistance to betalactam antibiotics in Pseudomonas aeruginosa]. *Ann Fr Anesth Reanim* 2003;**22**:527-30.

130. Cunha BA. Pseudomonas aeruginosa: resistance and therapy. *Semin Respir Infect* 2002;**17**:231-9.

131. Gilleland LB, Gilleland HE, Gibson JA, Champlin FR. Adaptive resistance to aminoglycoside antibiotics in Pseudomonas aeruginosa. *J Med Microbiol* 1989;**29**:41-50.

132. Bidwell JL, Reeves DS. Resistance of Pseudomonas species to beta-lactam antibiotics. *Scand J Infect Dis Suppl* 1981;**29**:20-6.

133. Cogen AL, Yamasaki K, Muto J, Sanchez KM, Crotty Alexander L, Tanios J, Lai Y, Kim JE, Nizet V, Gallo RL. Staphylococcus epidermidis antimicrobial delta-toxin (phenol-soluble modulin-gamma) cooperates with host antimicrobial peptides to kill group A Streptococcus. *PLoS One*;**5**:e8557.

134. Nannini E, Murray BE, Arias CA. Resistance or decreased susceptibility to glycopeptides, daptomycin, and linezolid in methicillin-resistant Staphylococcus aureus. *Curr Opin Pharmacol.*

135. Steinkraus G, White R, Friedrich L. Vancomycin MIC creep in non-vancomycin-intermediate Staphylococcus aureus (VISA), vancomycin-susceptible clinical methicillin-resistant S. aureus (MRSA) blood isolates from 2001-05. *J Antimicrob Chemother* 2007;**60**:788-94.

136. Tsiodras S, Gold HS, Sakoulas G, Eliopoulos GM, Wennersten C, Venkataraman L, Moellering RC, Ferraro MJ. Linezolid resistance in a clinical isolate of Staphylococcus aureus. *Lancet* 2001;**358**:207-8.

137. Betriu C, Culebras E, Gomez M, Lopez-Fabal F, Rodriguez-Avial I, Picazo JJ. Comparative in vitro activity of ceftobiprole against Gram-positive cocci. *Int J Antimicrob Agents*;**36**:111-3.

138. Hebeisen P, Heinze-Krauss I, Angehrn P, Hohl P, Page MG, Then RL. In vitro and in vivo properties of Ro 63-9141, a novel broad-spectrum cephalosporin with activity against methicillin-resistant staphylococci. *Antimicrob Agents Chemother* 2001;**45**:825-36.

139. Walkty A, Decorby M, Nichol K, Karlowsky JA, Hoban DJ, Zhanel GG. In vitro activity of ceftobiprole against clinical isolates of Pseudomonas aeruginosa obtained from Canadian intensive care unit (ICU) patients as part of the CAN-ICU Study. *J Antimicrob Chemother* 2008;**62**:206-8.

140. Schmitt-Hoffmann A, Nyman L, Roos B, Schleimer M, Sauer J, Nashed N, Brown T, Man A, Weidekamm E. Multiple-dose pharmacokinetics and safety of a novel broad-spectrum cephalosporin (BAL5788) in healthy volunteers. *Antimicrob Agents Chemother* 2004;**48**:2576-80.

141. Schmitt-Hoffmann A, Roos B, Schleimer M, Sauer J, Man A, Nashed N, Brown T, Perez A, Weidekamm E, Kovacs P. Single-dose pharmacokinetics and safety of a novel broad-spectrum cephalosporin (BAL5788) in healthy volunteers. *Antimicrob Agents Chemother* 2004;**48**:2570-5.

142. Stahl M, Bouw R, Jackson A, Pay V. Human microdialysis. *Curr Pharm Biotechnol* 2002;**3**:165-78.

143. Stahle L, Arner P, Ungerstedt U. Drug distribution studies with microdialysis. III: Extracellular concentration of caffeine in adipose tissue in man. *Life Sci* 1991;**49**:1853-8.

144. Williams LR, Leggett RW. Reference values for resting blood flow to organs of man. *Clin Phys Physiol Meas* 1989;**10**:187-217.

145. Burmeister W, Bingert A. [The body surface formula of DuBois and DuBois as a representative of the body cell mass in men between the ages of 21 and 51 years]. *Klin Wochenschr* 1966;**44**:901-2.

146. Lodise TP, Patel N, Renaud-Mutart A, Gorodecky E, Fritsche TR, Jones RN. Pharmacokinetic and pharmacodynamic profile of ceftobiprole. *Diagn Microbiol Infect Dis* 2008;**61**:96-102.

147. Krieg AM. An innate immune defense mechanism based on the recognition of CpG motifs in microbial DNA. *J Lab Clin Med* 1996;**128**:128-33.

BIOGRAPHICAL SKETCH

Benjamin M Wu received his bachelor's degree in molecular cellular developmental biology from University of California of Satan Cruz with Honors in thesis research in environmental toxicology. Post bachelor's, he started out working as a biochemist at Stanford Research Institute where he was awarded as an Honorary Member of the United States Medical Regimen by Surgeon Ronald Blank for his contribution work on the Gulf-War Syndrome. He then worked at Chiron Corporation and Genentech Inc. in the clinical pharmacokinetic/pharmacodynamic department for over five years running clinical and nonclinical studies, analyzing data, writing reports and supporting filings of protein therapeutics. A bioengineered drug for psoriasis (efalizumab) he was heavily involved in at Genentech was approved by the FDA in 2003. Benjamin received his master's from University of Buffalo and joined Dr. Hartmut Derendorf's lab for the PhD work on mathematical modeling of antimicrobial resistance. He received his doctor of philosophy in pharmaceutics in December 2010.